MARS TELESCOPIC OBSERVATIONS WORKSHOP II

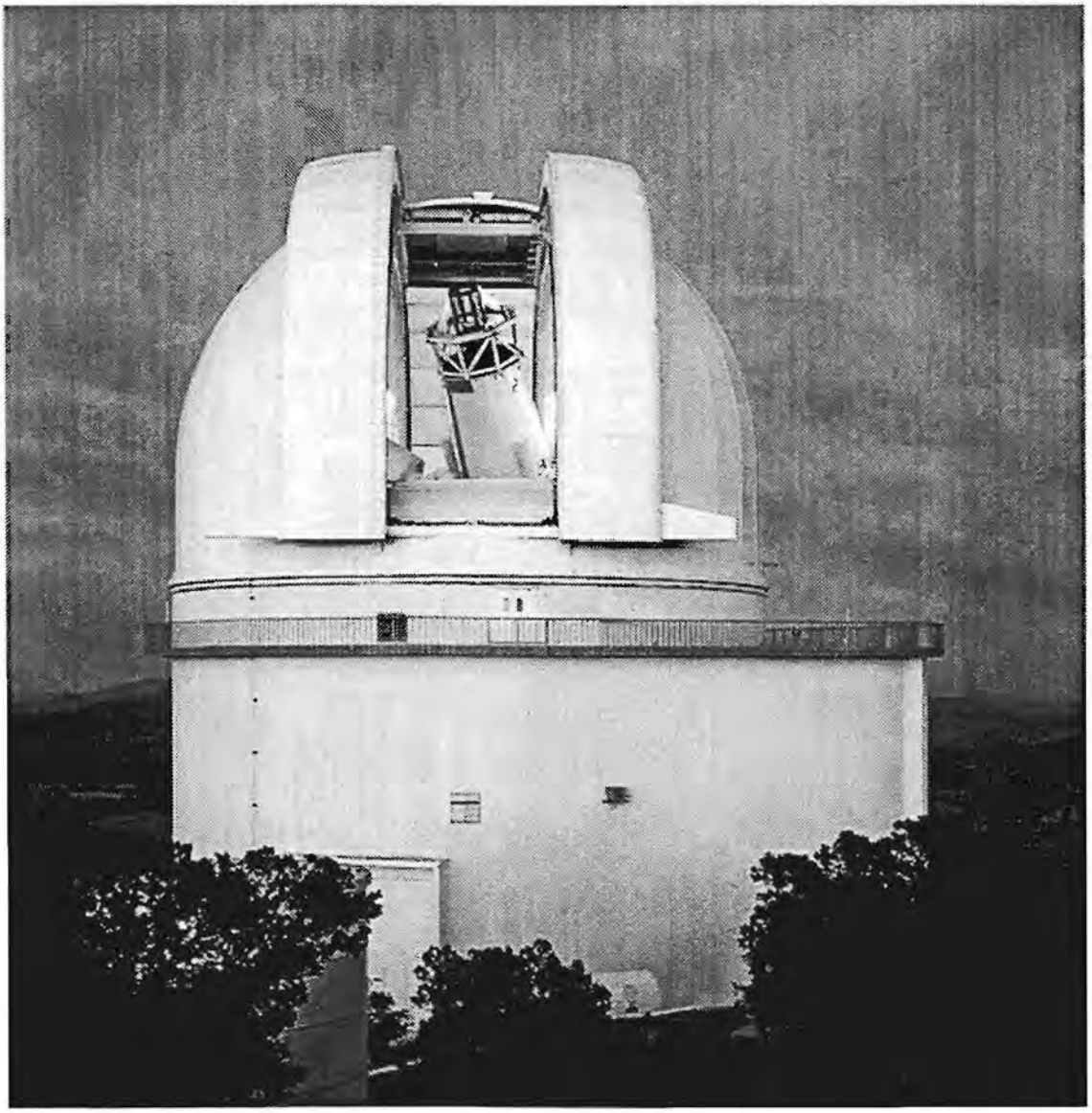

LPI Technical Report Number 97-03

Lunar and Planetary Institute 3600 Bay Area Boulevard Houston TX 77058-1113

LPI/TR--97-03

MARS TELESCOPIC OBSERVATIONS

WORKSHOP II

Edited by

A. L. Sprague and J. F. Bell III

Held at
Tucson, Arizona

October 2–3, 1997

Sponsored by
Lunar and Planetary Laboratory, University of Arizona
Lunar and Planetary Institute
National Aeronautics and Space Administration

Lunar and Planetary Institute 3600 Bay Area Boulevard Houston TX 77058-1113

LPI Technical Report Number 97-03
LPI/TR--97-03

Compiled in 1997 by
LUNAR AND PLANETARY INSTITUTE

The Institute is operated by the Universities Space Research Association under Contract No. NASW-4574 with the National Aeronautics and Space Administration.

This report may be cited as

Sprague A. L. and Bell J. F. III, eds. (1997) *Mars Telescopic Observations Workshop II*. LPI Tech. Rpt. 97-03, Lunar and Planetary Institute, Houston. 41 pp.

This report is distributed by

ORDER DEPARTMENT
Lunar and Planetary Institute
3600 Bay Area Boulevard
Houston TX 77058-1113

Mail order requestors will be invoiced for the cost of shipping and handling.

Cover: The dome pictured on the cover houses the 107-inch Harlan J. Smith Telescope at McDonald Observatory near Fort Davis, Texas. Although it was the third largest telescope in the world when dedicated in 1969, the Harlan Smith is dwarfed by McDonald Observatory's recently completed Hobby-Eberly Telescope, which has a light-gathering surface spanning 433 inches.

In Memory of Leonard Martin (1930–1997)

This meeting was dedicated to the memory of Leonard Martin, a long-time member of the planetary sciences community who passed away April 7, 1997.

Martin was involved in groundbased observations of Mars from 1969 until his retirement in 1997. He also studied martian clouds as part of the Viking Orbiter Imaging Team and was an active member of the Hubble Space Telescope Mars program. Martin emphasized the value of the historical record in many papers. He stressed that Mars is a changing, dynamic system, and that observations of a small range of years, however detailed, do not reveal its entire nature. He liked to savor and assimilate new observations and was happiest professionally when he was poring over Viking images or sets of telescopic photos. His quiet but persistent voice lent a tone of reality to many scientific discussions, and his contributions invariably helped advance our understanding of Mars. His encouragement and mentoring of younger colleagues started many scientists on their way to careers in Mars research.

Martin's familiarity with diverse groups of Mars data was unmatched, and his role in the community will not be easily filled. He was the last in a prestigious line of telescopic observers of Mars at Lowell Observatory, and his like will not soon be seen again. Leonard Martin will be deeply missed by all who were privileged to know and work with him.

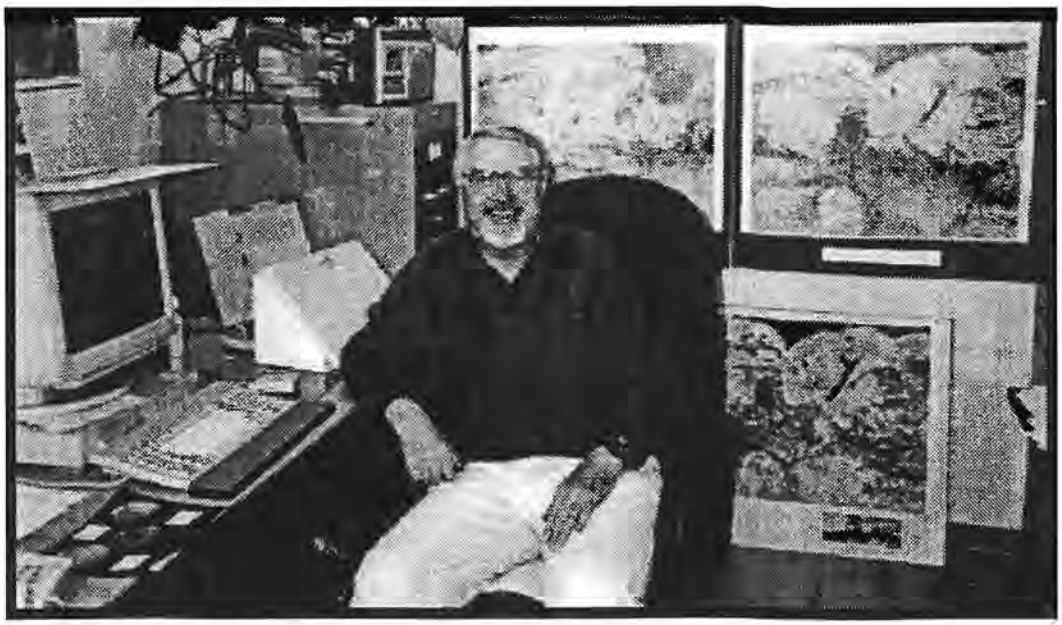

Preface

Mars Telescopic Observations Workshop II convened in Tucson, Arizona, in October 1997 by popular demand slightly over two years following the first successful Mars Telescopic Observations Workshop, held in Ithaca, New York, in August 1995. Experts on Mars from the United Kingdom, Japan, Germany, and the United States were present. Twenty-eight oral presentations were made and generous time allotted for useful discussions among participants. The goals of the workshop were to (1) summarize active groundbased observing programs and evaluate them in the context of current and future space missions to Mars, (2) discuss new technologies and instrumentation in the context of changing emphasis of observations and theory useful for groundbased observing, and (3) more fully understand capabilities of current and planned Mars missions to better judge which groundbased observations are and will continue to be of importance to our overall Mars program. In addition, the exciting new discoveries presented from the Pathfinder experiments and the progress report from the Mars Global Surveyor infused the participants with satisfaction for the successes achieved in the early stages of these missions. Just as exciting was the enthusiasm for new groundbased programs designed to address new challenges resulting from mission science results.

We would like to thank the National Aeronautics and Space Administration as well as Dr. David Black, director of the Lunar and Planetary Institute, and the staff of the Institute's Publications and Program Services Department for providing logistical, administrative, and publication support services for this workshop.

Program

Thursday Morning, October 2, 1997

8:00–8:30 a.m. Welcome

DUST

8:30 a.m. *Martian Dust and Apparent CO_2 Abundance*
Hunten D. M.* Sprague A. L.

9:00 a.m. *Telescopic Martian Dust Storm Activity, 1971 to 1993*
McKim R. J.*

9:30 a.m. *Telescopic Observations of Mars, 1996–1997: Results of the Marswatch Program I: Surface and Dust*
Troiani D. M.* Joyce D. P.* Parker D. C. Hernandez C. E. Beish J. D.

10:00–10:15 a.m. ***Coffee Break***

10:15 a.m. *Hubble Space Telescope Observations of Martian North Polar Cap: 1990–1997*
James P. B.* Cantor B. A. Wolff M. J. Lee S. W. Clancy R. T. Bell J. F. III Martin L. J.

10:45 a.m. *Pathfinder Imaging*
Smith P. H.*

11:15 a.m. *Mars Global Surveyor Overview*
Bougher S. W.*

11:45 a.m. *Thermal Effects of the North Polar Hood of Mars*
Narumi Y.*

12:15 p.m. ***Announcements***

12:30–1:45 p.m. ***Lunch***

Thursday Afternoon, October 2, 1997

THERMAL INFRARED

1:45 p.m. *What Happened to Cerberus? Telescopically-observed Thermophysical Properties of the Martian Surface*
Moersch J. E.* Bell J. III Carter L. Hayward T. Nicholson P. Squyres S. Van Cleve J.

2:15 p.m. *Thermal Emission Spectra of Mars Using SC-10 in 1997*
Blaney D. L.*

2:45 p.m. *Thermal Emission Spectrograph on MGS*
Christensen P.*

3:15–3:30 p.m. ***Coffee Break***

---

* Denotes speaker

3:30 p.m. *Detectability Limits of Volatile-bearing Minerals on Mars: Laboratory and Theoretical Constraints*
Roush T. L.* Orenberg J. B. Banin A. White S.

4:00 p.m. *IR-Spectroscopy of Minerals: What Could Our Lab Contribute to the Interpretation of Martian Spectra?*
Wagner C.*

4:30 p.m. *Spectral Irradiance Standards for Observations from 3 to 30 Microns*
Witteborn F. C.* Cohen M.

5:00–5:30 p.m. ***Discussion***

Friday Morning, October 3, 1997

8:00–8:15 a.m. ***Announcements***

VOLATILES

8:15 a.m. *Martian Atmospheric Water Vapor: The 1996–1997 Apparition*
Barker E. S.*

8:45 a.m. *Spectroscopic Measurements of Water Vapor in Mars Atmosphere*
Sprague A. L.* Hill R. E. Hunten D. M. Rizk B.

9:15 a.m. *Mars CO_2 and H_2O Clouds in the Context of 1996–97 Microwave Spectral Line Observations and HST UV Spectroscopy*
Clancy R. T.* Wolff M. J. James P. B. Sandor B. J. Butler B.

9:45–10:00 a.m. ***Coffee Break***

10:00 a.m. *The Atmospheric Temperature Structure and Water Abundance on Mars*
Gurwell M. A.* Muhleman D. O.

10:30 a.m. *Coordinated Analysis of Surface-Atmosphere Interactions from MGS*
Jakosky B.*

11:00 a.m. *Mars Pathfinder Observations of Water on Mars*
Lemmon M. T.* Tomasko M. G. Smith P. H. Doose L. R.

11:30 a.m. *Preliminary Results from the Mars Pathfinder ASI/MET Experiment*
Haberle R. M.* Schofield J. T. Crisp D. Barnes J. R. Magalhaes J. A. Murphy J. R. Seiff A. Wilson G. Larsen S.

12:00–1:15 p.m. ***Lunch***

Friday Afternoon, October 3, 1997

CLOUDS

1:15 p.m. *Telescopic Observations of Mars, 1996–1997: Results of the Marswatch Program II: Clouds*
Parker D. C.* Troiani D. M. Joyce D. P. Hernandez C. E. Beish J. D.

1:45 p.m. *Martian Dust and Condensate Clouds: 1996–1997 Hubble Space Telescope Observations*
Lee S. W.* James P. B. Wolff M. J. Clancy R. T. Bell J. F. III

2:15 p.m. *Diurnal Variation of Morning and Afternoon Clouds in Tharsis-Amazonis Area in 1995 and 1997*
Akabane T.* Iwasaki K. Saito S.

Regression of Martian North Polar Cap 1996–1997
Iwasaki K.* Parker D. C. Larson S. Akabane T.

2:45–3:00 p.m. ***Coffee Break***

SURFACE

3:00 p.m. *Mineralogy of Unweathered Mars Surface Materials from HST Multispectral Imaging*
Bell J. F. III* Wolff M. J. Thomas P. C. James P. B. Cloutis E. A.

3:30 p.m. *Volatile Searches in Martian NIR Spectral Images from the 1995 Opposition*
Klassen D. R.* Bell J. F. III Howell R. R. Johnson P. E.

4:00–5:00 p.m. ***Discussion***

Contents

Summary of Technical Sessions

—by D. Klassen with contributions from A. Sprague and J. Bell

The Mars Telescopic Observations Workshop II convened on October 2–3, 1997, in Tucson, Arizona to bring together Mars observers to present and discuss their most recent results. Observers from the United States, Japan, Germany, and the United Kingdom were in attendance and 28 oral presentations were made with generous time between talks and sessions for useful discussion.

The goals of the workshop were to (1) summarize groundbased observations especially in reference to current and future Mars space missions, (2) discuss new instrumentation and technologies in reference to changing emphasis of observations and theory useful for groundbased observing, and (3) more fully understand current and planned Mars missions to better judge which groundbased techniques will continue to be of importance in the overall Mars program. In addition, updates and preliminary results of the Mars Pathfinder and Mars Global Surveyor missions were presented.

The workshop presentations were divided into groups based on the area of martian study. This provided participants a cohesive framework for more fruitful discussions. The topics discussed were: dust, compositional infrared measurements, laboratory spectroscopy, spacecraft updates, polar caps, water vapor, and clouds. The presentations within each topic are summarized below.

DUST

D. Hunten (University of Arizona) began the session with a discussion of some historical Mars spectra used to measure the surface pressure of CO_2. Hunten mentioned that, although the groundbased results were measured first, spacecraft results from Mariner 4 and then Mariner 9 were published first. The moral, he said, is that groundbased observers should not be in the game of trying to race or compete with spacecraft missions, but rather should make complimentary observations. Since one strength of groundbased work lies in frequency, time-dependent measurements are a good place to work. It was with these measurements that dust storms can be (and have been) discovered. He also described the successful use of the CO_2 bands to monitor dust opacity and to discern dust storms. An anomalous low pressure indicates a shorter atmospheric pathlength (i.e., something stopping the reflected light from reaching the ground level).

R. McKim (British Astronomical Association) continued along the historical thread by discussing dust storm statistics from an archive he compiled. The archive spans the years 1659(!)–1993. Based on the observations, dust storm activity peaks during southern spring/summer and tends to affect mostly the southern hemisphere.

D. Troiani (Association of Lunar and Planetary Observers) and D. Joyce (Triton College) then presented a summary of the 1996–1997 MarsWatch program that monitors dust activity. The program has received, to date, more than 2748 observations from 70 observers in 14 countries. A full 41% of these observations are CCD images through standard filters from 330 to 820 nm. Compiling the data and dust activity into a statistical form similar to financial statistics, they presented some predictions for dust activity that would be seen by the MGS: (1) 2/1/98, peak of dust activity; (2) 6/1/98, dust activity drops off; and (3) 11/1/98, look for Rima Tenuis. Dust activity during the 1996–1997 apparition showed up in the north polar regions as well as in dust in the white clouds over Chryse and Solis Lacus. The Cerberus feature was visible, but was not very distinct (it has been fading since 1992).

COMPOSITIONAL INFRARED MEASUREMENTS

The afternoon session began with a presentation of midinfrared work on Cerberus, the classic dark albedo region, by J. Moersch (Cornell University). This feature has been fading in the past few oppositions, and one idea is that it is being covered by dust. However, in Moersch's midinfrared work, Cerberus is still seen as a high thermal inertia region. The main focus of the work is to use Viking albedo and thermal measurements to create a model of the observed thermal radiance, and then use current thermal and albedo measurements to calculate how much dust is covering Cerberus.

D. Blaney (Jet Propulsion Laboratory) presented midinfrared spectra of Mars that she obtained to look for 8.7 and 9.8 μm sulfate/bisulfate absorption features. She pointed out that spectroscopy in this region is difficult because there is not enough work on standard stars at these wavelengths. She thus presented her spectra as one part of Mars ratioed to a standard area of Mars. There are a few features seen, but as yet no interpretations of them.

T. Martin's (JPL) midinfrared work is in imaging of Mars at discrete wavebands to establish the shape and depth of the silicate band. This band arises from airborne dust over a warmer surface. These measurements are used to calculate atmospheric dust opacities. Again he brought up the problem of lack of standard star measurements.

F. Witteborn addressed the problem of the infrared standards in the 3–30 μm range. The problem is that blackbody extrapolation or interpolation from midinfrared broadband measurements will not work. This is true not only because of molecular absorption features but also because the stellar

atmosphere opacity is dominated by H^- free-free transitions so that different wavelength observations are seeing to different depths in the stellar atmosphere (i.e., different effective temperatures). A network of standard stars is being built so that measurements relative to one of these stars can be turned into flux units. The stellar spectra are even available via ftp (from sites listed in the abstract reference).

Shifting to shorter wavelengths but still examining surface composition, J. Bell (Cornell University) presented mineralogical studies of Hubble Space Telescope (HST), multiple-wavelength image sets. The dark region surrounding the north polar cap shows a deep feature at 953 nm, so a band-depth map and a ratio map of this wavelength to the local continuum was made to study the spatial limits. The band depths are considerably deeper than other dark areas (25–40%; cf. Acidalia/Syrtis at 5–15%). This could indicate higher pyroxene content or perhaps less alteration of the pyroxene.

LABORATORY SPECTROSCOPY

T. Roush's (NASA Ames Research Center) work on laboratory mineral spectroscopy is attempting to determine the detection feasibility of sulfates and carbonates on Mars. The reflectance spectra of various physical and chemical mixtures of relevant minerals with a soil analog are measured over the 0.25–2.5 μm range and the 2–25 μm range. There are no distinctive features in the VIS-NIR region but there are some minor features seen for sulfates and carbonates at even low levels of concentration in the NIR-midinfrared range. No diagnostic spectral features for nitrates or phosphates were found.

C. Wagner (DLR) also presented laboratory work on mineral spectroscopy. His work is in measuring the emissivity of several mineral types for use in comparison to acquired reflectance/emission spectra of Mars. He shows that adding carbonates and/or sulfates to a palagonite causes the emissivity in the 3–4 μm range to increase.

SPACECRAFT UPDATES

P. Smith (University of Arizona) presented an update on the Imager for Mars Pathfinder (IMP) results. The IMP was used to image the Sun as a function of airmass through four different filters. The atmospheric extinction does not appear to be a function of wavelength (i.e., the color of the Sun is constant over airmass). Morning ice clouds were also seen as early as 2 hr before sunrise. These clouds must be quite high and cause an overall brightening of the morning sky due to multiple scattering of sunlight. These clouds burn off by noon and sunsets are cloudless. The ratio of diffuse to direct light comes out to be fairly red, although it becomes bluer nearer the Sun. This, combined with the strong phase function of the soil, means that illumination conditions of rocks must be known and accounted for before any real rock spectra interpretations can proceed.

Continuing with spacecraft updates, S. Bougher (University of Arizona) presented some news on the Mars Global Surveyor. The spacecraft is currently in an elliptical orbit and performing its aerobraking maneuvers. This phase will continue for the next four months until the orbit is circularized in a 2 a.m.–2 p.m. Sun-synchronous orbit. There are no real science plans during this phase, but all the instruments are turned on. The TES is looking toward the nadir and measuring the 15-μm brightness to measure atmospheric temperatures and dust opacities. Continued groundbased observations are necessary to keep track of dust as the dust can change the effective atmospheric density by a factor of 2, and this will adjust the aerobraking maneuvers. The MAG/ER is measuring the local e^- density as well as mapping the crustal magnetic fields it discovered.

Preliminary Pathfinder water observations were presented by M. Lemmon (University of Arizona). Using the solar images from the IMP and calculating the excess extinction (i.e., that not caused by dust) within the water band at 0.935 μm relative to two nearby water continuum bands (where dust extinction would be similar across all three bands) the column abundances can be measured. There is a difference between a.m. and p.m. opacities and the a.m. opacity is nonlinear with airmass. There are also thick clouds being illuminated before sunrise, presumably by multiple scattering in the martian atmosphere.

R. Haberle (NASA Ames Research Center) presented preliminary results from the Pathfinder ASI/MET experiments, both during descent and on the ground. The atmospheric density profile is less than Viking by a factor of 10 at high altitudes. The temperature profile at about 80 km is less than the CO_2 condensation, but there is general agreement with Viking below 50 km with the exception of an inversion between 9–16 km not seen at all by Viking (which could be due to clouds). At the ground the wind direction rotates due to local slope. Winds downslope at night and upslope in the day, with stronger winds at night. The local pressure was steadily declining to a minimum (corresponding to the maximum extent of the south polar cap) and then started rising as the south cap retreated. The temperatures show expected and highly repeatable diurnal effects. The average is about 10 K warmer than the Viking measurements. Spikes in the pressure data correlating with wind measurements and temperature dips appear to suggest the passage of dust devils. The passage takes about a minute and the sizes are on the order of a couple hundred meters in diameter.

POLAR CAPS

Hubble Space Telescope observations of the north polar cap were presented by P. James (University of Toledo). These

data cover four full polar cap recessions from 1990–1991 to 1996–1997. The recession rate over all four of these years was the same, within the errors. There is some amount of scatter in the size of the cap before $L_s = 0$ due mainly to the polar hood and clouds that can be difficult to distinguish at violet wavelengths. Some notable observations include (1) in October 1996, cap was large with cloud activity at the edge and (2) in January 1997, residual cap had a distinctly hexagonal shape.

Y. Narumi (Kyushu-Takai University) presented an investigation of the thermal effects of dust and hood clouds on the north polar cap. He presented models of dust-only clouds with optical depths of 0, 1, 3, 10 and polar-hood-only models with water ice cloud optical depths of 0, 1, 3, 10. The dust model found that the surface daytime temperatures decrease with increasing opacity as less solar radiation reaches the surface. In the polar-hood model it was found that the daytime surface temperatures show very little change with increasing opacity, but that the nighttime temperatures increase with increasing hood opacity due to a greenhouse effect. Thus, the north polar hood may serve to retard the growth of the north polar cap itself.

WATER VAPOR

E. Barker (University of Texas) presented the results of the McDonald Observatory survey of Mars water vapor. This survey is a long-term monitoring program going back to 1967. The 1996–1997 results were presented. The study uses the water vapor absorption feature at 8197.704 Å, Doppler shifted, to calculate abundances from the line equivalent width. The data show a diurnal effect where the vapor is low in the morning and higher later in the day.

A. Sprague (University of Arizona) also presented water vapor measurements made in collaboration with Hunten, Hill, and Rizk. The technique is to measure the Doppler-shifted water vapor lines in the NIR, measure their equivalent widths, then backward-interpolate from a curve of growth to calculate column abundance. Results from Barker, Sprague, et al. are in good agreement. Water vapor is at a maximum around martian noon and shows typical seasonal variations.

T. Clancy (Space Science Institute) presented submillimeter to centimeter observations of water vapor profiles and temperatures in the martian atmosphere. The temperatures at perihelion are in general agreement with Viking measurements but the controversy comes at $L_s = 0°–180°$, where the microwave measurements show an atmosphere 15–20 K cooler than the Viking IRTM measurements. Measurements of the water-vapor emission lines show no features above 10 km, implying a low level of water vapor saturation. There is indication that the higher-level temperatures approach or reach the CO_2 condensation value, and thus the twilight clouds seen by Pathfinder could be thin high-level CO_2 clouds instead of water ice clouds lit by multiple scattering of sunlight.

M. Gurwell (Harvard-Smithsonian Astrophysics) also presented millimeter data on water abundances in the martian atmosphere. These data were gathered using an array of telescopes and thus have a beam smaller than the disk size of Mars in the sky, allowing some spatial information to be gathered. Measured temperatures and water-vapor abundances match well with Clancy's disk integrated results. The water is concentrated over the north polar region and at the morning and evening limbs.

B. Jakosky (University of Colorado) reviewed current water vapor models in the context of measurements of the interannual variability being seen. The data and models do not always match, so there remains much modeling work to perform.

CLOUDS

M. Wolff (Space Science Institute) presented on measurements of the water ice cloud opacities of Mars from HST images. There is a belt of clouds seen best in 410-nm images in the 1993, 1995, and 1997 apparitions, but this belt is absent in the 1992 and early 1993 images. This belt encircles the planet from a latitude of 10°S to 30°N. The belt opacity is greatest at 20°N latitude. The clouds in general increase in opacity at aphelion and are estimated to be at an altitude of 10–15 km.

K. Iwasaki (University of Arizona) presented results of the north polar cap regression in 1996–1997 as part of an ongoing study of the interannual variability. The latitude of the polar cap edge is measured for many points, and a latitudinal average is then recorded. The recession rates do show some amount of variation. In 1963 the cap was systematically larger than previous years. The measurements from this groundbased work agree with similar work from HST data.

D. Parker (ALPO) presented the volatile cloud results of the MarsWatch program in comparison to cloud models constructed from data as far back as 1965 to 1996–1997. In comparison, clouds over Tharsis formed early and clouds over Elysium formed late. Chryse was quite cloudy until about July 1997. The north-tropic cloud band during the northern spring/summer was thicker over Syrtis Major, and the pole-to-pole limb hazes are very bright in blue, indicating a volatile composition. They are also somewhat bright in yellow and orange, which would indicate a partial dust composition.

Hubble Space Telescope cloud results from 1997 were presented by S. Lee (University of Colorado). The HST coverage is from $L_s = 11°–186°$ and a dust cloud is seen in all polar images during the cap recession as well as an extensive dust cloud in Valles Marineris one week before the Pathfinder landing. Condensate clouds are persistent across the disk and highly variable in both space and time.

T. Akebane (Kyoto University) presented observations of variations in condensate clouds. In March 1995 images there are strong morning clouds that break up in the afternoon. Morning cloud opacities range from 0.8 to 0.4 as they break up. In April 1995 images, a single cloud can be traced from about 8:40–10:00 Mars local time. It is quite thick (opacity about 1.5) and again breaks up in the afternoon.

D. Klassen (Cornell University) closed the final session by presenting an innovative and effective method to identify and discriminate between CO_2 and H_2O clouds in groundbased spectral images of Mars. Band-depth maps at 3.33-μm trace CO_2 ices, and the images show no detectable CO_2 clouds at the time of the observations. Evidence for the seasonal polar cap is seen in some of these images. Band-depth maps at 2.25 and 3.69 μm trace H_2O and show fine water frosts at the north polar region and along morning and evening limbs, indicating water ice clouds. These results are used to confirm results of Principal Components Analysis and Linear Mixture Modeling, which also show fine water frosts in the same regions. The PCA/LMM technique traces the clouds better than the band-depth maps, as there appears to be no correlation with respect to albedo features like in the band-depth maps.

Abstracts

DIURNAL VARIATION OF MORNING AND AFTERNOON CLOUDS IN THE THARSIS-AMAZONIS AREA IN 1995 AND 1997. T. Akabane[1], K. Iwasaki[2], and S. Saito[3], [1]Hida Observatory, Kyoto University, Kamitakara, Gifu 506-13, Japan, [2]Kyoto Gakuen University, Sogabe-Cho, Kameoka, Kyoto 621, Japan (visiting Lunar and Planetary Laboratory, University of Arizona, Tucson AZ, USA, until March 1998), [3]Noda 3-9-14, Takatsuki, Osaka 569, Japan.

In the northern late spring to midsummer season on Mars, the equatorial region is surrounded with a wide cloud belt extending from 10°S to 30°N [1]. It is bright in the morning and evening (morning and evening clouds), and reduces in midday. In late morning to evening, bright cloud masses appear in Tharsis and Elysium (afternoon clouds). In northern early spring, the equatorial clouds appear as discrete morning, afternoon, or evening clouds. Their brightness increases gradually, and they grow to form the equatorial cloud belt. In the mature stage of the equatorial cloud belt during late spring to midsummer, it does not disappear completely even in midday (Fig. 1).

The equatorial clouds in the Tharsis-Amazonis area are bright and conspicuous. A morning cloud centered at 120°W and 10°N is interesting and remarkable (Figs. 2a and 2b). The morning cloud reduces drastically around 11h MLT (Martian Local Time), and then afternoon cloud masses appear near east and west of the morning cloud as seen in Fig. 2c. Their locations correspond to the huge mountains Olympus Mons and Ascroeus Mons. Comparing Fig. 2b with Fig. 2c, one can see a change of brightness in the morning and afternoon clouds. The features of the morning cloud (120°W, 10°N) in early morning are shown in Fig. 2d. The bright morning cloud is surrounded by the high mountains Olympus Mons, Ascroeus Mons, and Nodus Mons, which are seen as dark spots. Those features suggest that the level of the cloud is lower than the mountains [2].

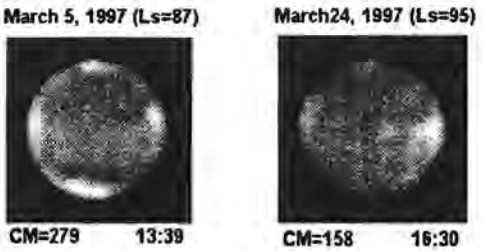

Fig. 1. Equatorial cloud belt in March of 1997 (blue).

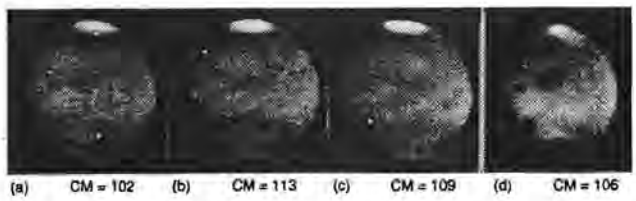

Fig. 2. Morning cloud in blue centered at 120°W and 10°N in 1995. Figures 2a, 2b, and 2c were exposed on March 6, 1995, and 2d was exposed on April 13, 1995. Local time was 9.6h (2a), 10.3h (2b), 11.3h (2c), and 8.7h (2d).

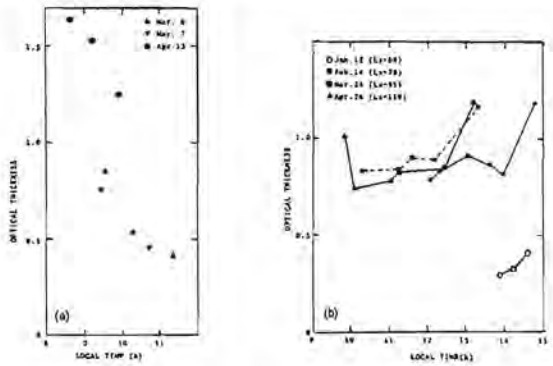

Fig. 3. Diurnal variation of opacity for (3a) morning cloud at 120°W and 10°N in 1995 and (3b) Olympus cloud in 1997.

The afternoon clouds in the Tharsis-Amazonis area are prominent in the equatorial cloud belt. They appear around 11h MLT. Their brightness relative to that of the surroundings increases as evening approaches [3]. However, after 16h MLT, evening clouds become bright, and afternoon clouds are buried in the evening clouds.

The opacity of clouds may be a measure of their activity. Figure 3 shows diurnal variation of optical thickness of the morning cloud centered at 120°W and 10°N in 1995 (Fig. 3a) and the afternoon cloud located at Olympus Mons (Olympus cloud) in 1995 and 1997 (Fig. 3b). The opacity of the morning cloud decreases with local time. However, in its mature state in late spring to midsummer it does not disappear even in midday. Its minimum value of opacity is 0.3 to 0.4. The opacity of the morning cloud on March 6 and 7, 1995 (L_s = 68°), is about 0.7 at 9.5h MLT, while it is 1.6 at 8.7h MLT and 1.2 at 10h MLT on April 13, 1995 (L_s = 84°).

The opacity of the Olympus cloud increases rapidly in the early afternoon and reaches its maximum at 14h to 15h MLT [3]. As Fig. 3b shows, the opacities on March 24, 1997, and April 26, 1997 (L_s = 95°, 110°), are about 1.2 in the afternoon, while the opacity is 0.3–0.4 on January 12, 1997 (L_s = 64°) and about 0.7 on March 6 and 7, 1995 (L_s = 68°). The Olympus cloud in late spring may not have been in the mature state yet.

References: [1] James P. B. et al. (1996) *JGR, 101*, 1883. [2] Clancy R. T. et al. (1996) *Icarus, 122*, 36. [3] Akabane T. et al. (1987) *PASJ, 39*, 343.

MARTIAN ATMOSPHERIC WATER VAPOR: THE 1996–1997 APPARITION. E. S. Barker, McDonald Observatory, University of Texas at Austin, RLM 15.308, Austin TX 78712-1083, USA (esb@pecos.as.utexas.edu).

Introduction: As part of our long-term coverage of the behavior of martian water vapor from late 1996 to late 1997 (hopefully), we obtained high-resolution (R ~225,000) spectra of the water vapor band at 8200 Å. The amounts of martian water vapor have been monitored over 13 seasonal cycles since 1964 [1–3]. In recent years, this monitoring has been augmented by the Arizona group using techniques similar to the current CCD technology used at McDonald [4–6].

The 2DCoude cross-dispersed echelle spectrograph on the 2.7-m telescope at McDonald Observatory was used with a 2048 × 2048 Tektronics CCD with 24-μpixels. The spatial scale along the 2DCoude slit was 0.13 arcsec per pixel, resulting in seeing limited spatial resolution (~1.0–1.5 arcsec). Guidance on the martian disk was accomplished via a television monitor with a RG-850 filter.

Data: Table 1 summarizes the observations either carried out or scheduled. The seasonal coverage in L_s concentrated on the northern spring-summer season, with samples at L_s = 25°, 46°, 67°, 74°, and 83° before opposition and at L_s = 132°, 143°, 166°, 181°, and 212° (scheduled time) after opposition. Each of the spectra noted under the "slit" columns will yield 5–10 spatial samples along the spectrograph slit. The primary water vapor lines included in the region are 8176.975, 8186.371, 8189.272, and 8197.704 Å, but not all of these lines will have usable martian counterparts due to Doppler shifts and blending with solar absorption lines. The slit was placed either in the north-south direction along the central meridian to study the latitudinal distribution or the east-west direction to study the diurnal behavior of the martian water vapor for the dates listed in Table 1.

General Results: During the preopposition period, normal amounts of martian water vapor were observed with increasing amounts toward higher northern latitudes. Most of the north-south samples showed just barely detectable (~2 μ = internal error) amounts at southern latitudes. Measurements made to investigate the diurnal change in atmospheric water vapor at different martian latitudes showed much lower abundances above both the morning and evening terminator regions. Data reduction of the entire dataset is still in progress using the uniform reduction processes for groundbased observations that were agreed upon by Sprague et al. at MTO II in Tucson. Use of common definitions of seeing-disk width and the location of sectors on the seeing disk, line strengths of water lines, effective temperatures, and use of the same computer code (developed by Rizk and Hunten to convert equivalent widths to vertical column abundances) will greatly improve the quality and intercomparability of groundbased datasets.

TABLE 1. Martian water vapor spectra.

Date (UTC)	Slit N-S	Slit E-W	L_s °	Mars long °	Dia (")
1996 Oct 16	6	-	24.8	195–208	5.1
1996 Oct 17	4	-	24.9	184–192	5.1
1996 Dec 3	3	-	46.1	17–46	6.5
1996 Dec 4	5	-	46.6	359–42	6.6
1997 Jan 20	9	-	67.2	258–330	9.5
1997 Jan 21	1	2	67.4	240–271	9.6
1997 Feb 3	1	-	73.3	210–215	10.8
1997 Feb 4	4	7	73.7	88–164	10.9
1997 Feb 5	4	-	74.2	82–117	11.0
1997 Feb 24	-	2	82.2	290–291	12.9
1997 Feb 26	1	2	83.0	274–285	13.1
1997 Feb 27	3	7	83.7	213–271	13.1
1997 Jun 12	4	-	131.5	298–330	8.4
1997 Jun 13	2	7	132.0	257–309	8.3
1997 Jul 5	3	2	142.8	45–97	7.3
1997 Jul 6	4	5	143.3	32–77	7.2
1997 Aug 18	1	-	165.7	334–345	6.0
1997 Sep 15	4	-	181.2	11–78	5.5
1997 Sep 16	2	3	181.7	31–57	5.4
1997 Nov 5	tbo	tbo	211.8	tbo	4.8
1997 Nov 6	tbo	tbo	212.2	tbo	

Pathfinder Abundances: The remainder of the paper will be devoted to the measurements made on July 5 and 6, 1997, Universal Time (Sols 1 and 2). Each north-south echelle spectrum (36 CCD lines) was collapsed into nine individual spectra. Each spectrum or sector corresponded to about 1 arcsec on the 9-arcsec seeing disk of Mars. Equivalent widths were measured for the 8197 Å line and converted to vertical abundances using the Rizk and Hunten program (colabundh2.f). This program also calculates the average martian airmass and the average longitude/latitude for the relevant sector on the seeing disk. The effective temperature at 8 km (1 scale height) was estimated by adding 47 K to the temperatures derived from the Viking 15-μ IRTM channel [see 5,6].

The north-south or meridional abundances are shown in Fig. 1. On July 6, one of these meridional spectra sampled the longitude/latitude of the Pathfinder site (32.5°W, 19.5°N). In Fig. 2 this meridional dataset is plotted against the average of all the meridional samples taken on July 5–6, showing that the Pathfinder site has a similar abundance to adjacent longitudes. Actually, the average latitudes (27°, 15°N) of the sectors encompass the Pathfinder latitude, so it is appropriate to average those two sector abundances (15.9, 11.2 μ) to give a mean abundance of 13.6 μ, which is plotted in Fig. 4 at a local time of 2.9 hr, time of central meridian (phase angle = 40.5°).

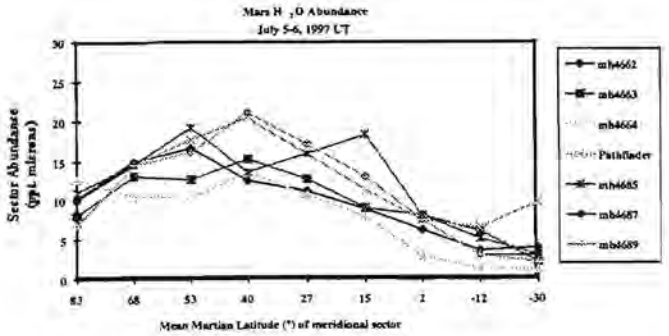

Fig. 1

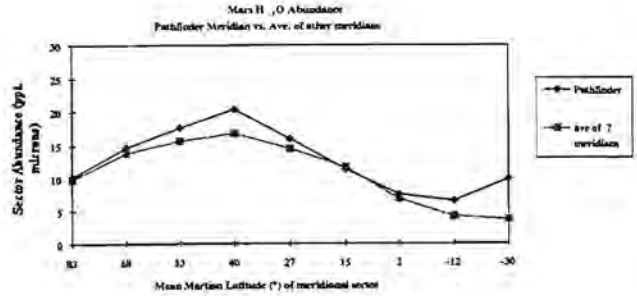

Fig. 2

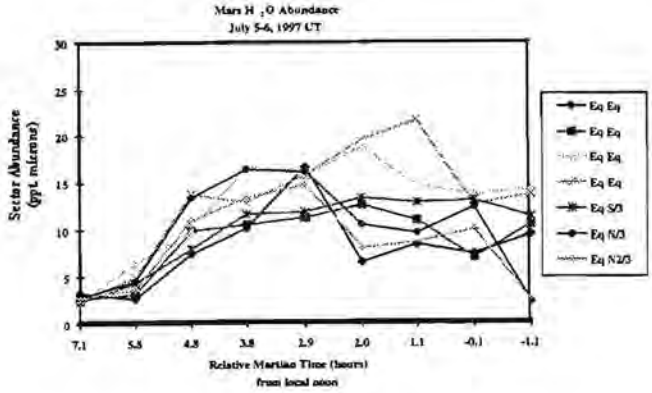

Fig. 3

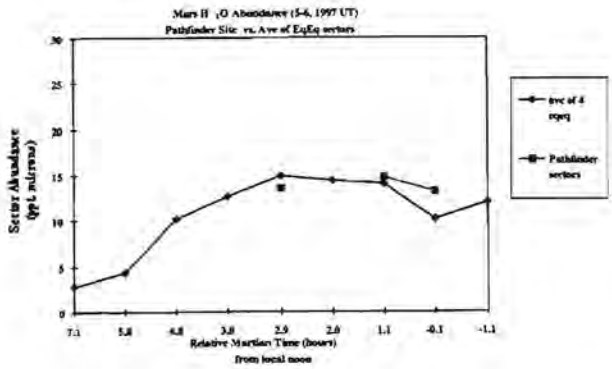

Fig. 4

All east-west sector abundances taken with the slit parallel to the martian equator at various latitudes are presented in Fig. 3 and correspond to different longitudes from the subsolar longitude or time from local noon. The east-west sectors also covered the Pathfinder site at different times of the martian day and are shown in Fig. 4 along with the average of the equatorial sectors (actually about 25°N latitude). This average shows the diurnal behavior at this latitude. A constant atmospheric temperature of 234 K was used in these east-west reductions. The decrease at the evening terminator would have been 20% greater, if a realistic temperature change with time of day had been used. Further study of the vertical structure of the water abundance and diurnal temperatures is needed.

Summary: Our early afternoon, Pathfinder site abundances (13–15 μ) are smaller than those obtained by Sprague et al. [6] on July 12 by about 3–15 μ, for as yet undetermined reasons. Our afternoon abundances are generally consistent with the *in situ* measurement of 8 μ [7] made later in the martian afternoon and season.

References: [1] Barker E. et al. (1970) *Science, 170,* 1308–1310. [2] Barker E. (1976) *Icarus, 28,* 247–268. [3] Jakosky B. and Barker E. (1984) *Icarus, 57,* 322–334. [4] Rizk B. et al. (1988) *Icarus, 90,* 205–213. [5] Sprague A. et al. (1996) *JGR, 101,* 23229–23241. [6] Sprague A. et al., this volume. [7] Lemmon M. et al., this volume.

MINERALOGY OF UNWEATHERED MARS SURFACE MATERIALS FROM HUBBLE SPACE TELESCOPE MULTISPECTRAL IMAGING.

J. F. Bell III[1], M. J. Wolff[2], P. C. Thomas[1], P. B. James[3], and E. A. Cloutis[4], [1]Department of Astronomy, 424 Space Sciences Building, Cornell University, Ithaca NY 14853-6801, USA (jimbo@marswatch.tn.cornell.edu), [2]Space Science Institute, Boulder CO, USA, [3]University of Toledo, Toledo OH, USA, [4]University of Winnipeg, Manitoba, Canada.

The chemistry and mineralogy of unweathered martian volcanic rocks is of great interest for modeling the planet's interior composition as well as understanding martian volcanic/magmatic processes and the subsequent weathering and alteration history of materials deposited on the surface. Knowledge of the composition of the unweathered or "pristine" martian surface materials, when combined with compositional and mineralogical information on the highly oxidized and ubiquitous weathered surface materials known to exist there, can constrain models of physical and chemical mineral alteration processes and thus provide possibly unique data on past climate and climatic variations on Mars [e.g., 1–3]. Iron-bearing minerals are the most detectable and geologically relevant materials studied by remote sensing observations of Mars because of the relatively high abundance of Fe in the martian crust and mantle [4,5] and the very spec-

troscopically active nature of Fe within the crystal lattices of many common rock- and soil-forming minerals [6,7]. In fact, most of the (limited) current information that exists on the mineralogy of the martian surface concerns the detection, distribution, and abundance of the anhydrous ferric (Fe^{3+}) iron oxide hematite (α-Fe_2O_3) and the ferrous (Fe^{2+}) Fe-bearing volcanic mineral pyroxene ($Ca[Fe,Mg]Si_2O_6$–$[Mg,Fe]SiO_3$), both of which have been unequivocally detected on Mars based on data from the past several decades of groundbased and spacecraft remote sensing [1,8,9].

We are expanding upon these remote sensing efforts by using HST to obtain images of regions of Mars at ultraviolet to NIR wavelengths not previously measured by Mars spacecraft and at spatial resolutions much better than earlier telescopic multispectral investigations. The data discussed here were obtained using the Wide Field/Planetary Camera 2 (WFPC2) instrument [10]. WFPC2 can obtain images at many hundreds of narrowband filter wavelengths, but for the data discussed here we were limited to a set of only nine filters in order to fit each set of observations into a single HST orbit. The wavelengths for imaging were carefully chosen to maximize the potential detectability and spectral contrast of surface ferric and ferrous minerals. Images were taken in midmartian summer ($L_s = 122°$) during three HST orbits in July 1995, and the orbits were timed so that there was ≈120° separation in the martian central meridians between each set of observations. The data underwent standard HST reduction procedures, were calibrated to radiance factor (I/F), and were projected into polar stereographic maps [10–12]. Analyses were performed by assembling the mapped images into an image cube and performing spectrum extraction, color ratios, and band-depth mapping [11].

The nine-color HST spectra of classical bright, dark, and polar cap regions show excellent agreement with previously measured groundbased and spacecraft visible to NIR spectra of Mars, and the accuracy of the calibrated data most likely exceeds the accuracy of any previous Mars spectra obtained at these wavelengths. We quickly noticed that spectra extracted from the dark circumpolar annulus (the north polar sand sea [18,19]) exhibited anomalous behavior, having a low albedo and a strong drop in I/F at 953 nm. In order to assess better the spatial distribution of this 953-nm absorption, we generated band-depth maps using two different continuum techniques: the traditional cross-band continuum method [13,14] and the single-sided band depth ($SSBD_{953} = R_{740}/R_{953}$) method [14]. The results of the $SSBD_{953}$ map show a region surrounding the residual polar cap that displays the highest $SSBD_{953}$ values of any region measured on the martian surface, with band depths ranging from 25% to 40%. For comparison, the $SSBD_{953}$ values of the classical dark regions Acidalia and Syrtis Major range from 5% to 15%, while values in classical bright regions like Tharsis and Isidis range from 0% to 10%.

We interpret the origin of the 953-nm band as an absorption feature from the ferrous mineral pyroxene occurring in dark martian volcanic rocks [15–17]. Other possibilities that we considered include ferric oxides and oxyhydroxides like hematite and goethite, poorly crystalline ferric phases like ferrihydrite, ferric sulfates like jarosite, and olivine. None of these materials, though, have the 800–1100-nm NIR spectral characteristics similar to those seen in the dark circumpolar region of Mars. The shape and position of the 953-nm absorption feature in the martian north polar annulus spectra are perhaps more consistent with the spectra of low-Ca orthopyroxene than higher-Ca clinopyroxene; however, the spectral sampling of these data is not high enough to make this chemical distinction with confidence. In addition, it is known that there is a substantial overlap in possible pyroxene Ca and Fe compositions interpreted from the occurrence of a band center near 950 nm [15,16].

The increased strength of the 953-nm absorption feature relative to that in other, nonpolar dark regions, may have several causes: (1) increased pyroxene abundance in this region; (2) variations in pyroxene chemistry, such as increased Fe content, that can lead to increased band strength; (3) a lower degree of alteration of the pyroxenes, leading to increased band depth because of the removal of the spectral muting effects of poorly crystalline ferric phases; and (4) coarser particle sizes, possibly accompanied by a narrower particle size distribution, leading to increased band depth because of the increased role of volume scattering in larger particles.

An intriguing possibility can be considered for option 3 to explain why the pyroxene in the north polar sand sea shows an increased band depth relative to that in other dark, nonpolar regions. The north polar sand sea is covered each martian winter by probably up to several meters of seasonal CO_2 ice. The weight of this ice cover compacts the surface fines, and the ice likely occupies pore space between individual sand-sized or larger particles. In spring, the surface is heated by sunlight and acts in many ways like a comet, with CO_2 (and H_2O) ice subliming back into the atmosphere. The action of the subliming ice escaping from pore spaces may serve to jostle or even abrade particles in a process that we refer to as "sublimation gardening." Unweathered facets of pyroxene grains, which yield much deeper NIR absorption bands than weathered grains, could thus be continually exposed in these polar regions.

This mechanism may be testable by multispectral imaging and other experiments on the 1998 Mars Surveyor lander, which will land at high southern polar latitude and will operate through at least some of the polar winter and may survive until polar spring. Alternately, it could be tested by focused groundbased or Mars orbital NIR spectroscopic studies of the time-evolution of ice deposition and surface spectral properties at high latitudes.

References: [1] Bell J. F. III (1996) in *Mineral Spectroscopy: A Tribute to Roger G. Burns*, Geochemical Society Special Publication 5 (M. D. Dyar et al., eds.), pp. 359–380. [2] Burns R. G. (1993) *GCA*, *57*, 4555–4574.

[3] Banin A. et al. (1997) *JGR, 102,* 13341–13356. [4] Clark B. C. et al. (1982) *JGR, 87,* 10059–10067. [5] Dreibus G. and Wänke H. (1985) *Meteoritics, 20,* 367–382. [6] Sherman D. M. and Waite T. D. (1985) *Amer. Mineral., 70,* 1262–1269. [7] Morris R. V. et al. (1985) *JGR, 90,* 3126–3144. [8] Roush T. L. et al. (1993) in *Remote Geochemical Analysis: Elemental and Mineralogical Composition* (C. Pieters and P. Englert, eds.), pp. 367–393, Cambridge Univ. [9] Soderblom L. A. (1992) in *Mars* (H. Kieffer et al., eds.), pp. 557–593, Univ. of Arizona. [10] Holtzman J. A. et al. (1995) *Pub. Astron. Soc. Pac. 107,* 156–178. [11] Bell J. F. III et al. (1997) *JGR, 102,* 9109–9123. [12] Wolff M. J. et al. (1997) *JGR, 102,* 1679–1692. [13] Clark R. N. and Roush T. L. (1984) *JGR, 89,* 6329–6240. [14] Bell J. F. III and Crisp D. (1993) *Icarus, 104,* 2–19. [15] Adams J. B. (1974) *JGR, 79,* 4829–4836. [16] Cloutis E. A. and Gaffey M. J. (1991) *JGR, 96,* 22809–22826. [17] Mustard J. F. et al. (1993) *JGR, 98,* 3387–3400. [18] Thomas P. and Weitz C. (1989) *Icarus, 81,* 185–215. [19] Lancaster N. and Greeley R. (1990) *JGR, 95,* 10921–10927.

THERMAL EMISSION SPECTRA OF MARS USING SC-10 IN 1997.

D. L. Blaney, Jet Propulsion Laboratory, MS 183-501, 4800 Oak Grove Drive, Pasadena CA 91109, USA (blaney@scn1.jpl.nasa.gov).

Data: Data were collected at the 200-in Hale telescope at Palomar Mountain, California, using Spectro-Cam 10 in both high and low spectral resolution modes on April 19, 1997, and May 15, 1997. Low-resolution observations covered the entire 8–13 μm range to measure dust opacity, surface temperature, and broad mineral absorption features. Pollack et al. [1] showed that when limb and center of the disk spectra were ratioed, mineralogic absorption features were detected at 8.7 and 9.8 μm that were attributable to sulfates or bisulfates. Observations were made centered around the 8.7 sulfate feature at high spectral resolution (R = 2000) using five grating positions to try to define the spectral shape of this feature. Alpha Boo was used as the primary standard and was measured in both the high- and low-resolution grating modes with the same grating positions used on Mars. Additionally, the spectra were reduced to the center of the Mars disk to minimize uncertainties in the spectral shape of Alpha Boo and telluric atmospheric removal. Spectra are shown in Fig. 1 for six locations along a north-south slit at a longitude of 137°W with latitudes ranging from 80°N to 42°S ratioed to a spot at 24°N. These "ratio" spectra are useful in the identification of regions with different spectral features.

Atmospheric Features: The most notable spectral features occur in the spectrum labeled 80°N. Their origin is almost certainly atmospheric. These features are being investigated using a class of radiative modeling methods called Spectral Mapping Transformations (SMT). A simple extension to the original SMT approach, called "backmapping," substantially improves its versatility without compromising its accuracy or efficiency. In addition, the backmapping approach offers an efficient, rigorous method for including the combined effects of several gases and aerosols within a given broad spectral interval; provides a simple exact means for including wavelength-dependent variations in the solar flux; allows for variable surface temperatures; and provides for a wavelength-dependent surface albedo/emissivity. The SMT method has recently been implemented in a radiative transfer model based on the discrete ordinate method and has been provided by Dave Crisp. We are investigating the possibility that these features are due to unique chemical atmosphereric components in the martian north polar region or are caused by atmospheric thermal structure.

Surface Features: Pollack et al. (1990) showed that when limb and center of the disk spectra were ratioed, mineralogic absorption features were detected at 8.7 and 9.8 μm, which were interpreted as sulfates and bisulfate in atmospheric dust. The ratioed spectra in Fig. 1 do not show these features. This is most likely due to the relatively "clear" nature of the martian atmosphere. Additionally, the spectra do not show dramatic surface emissivity variations when ratioed. The interpretation of these spectra requires detailed modeling.

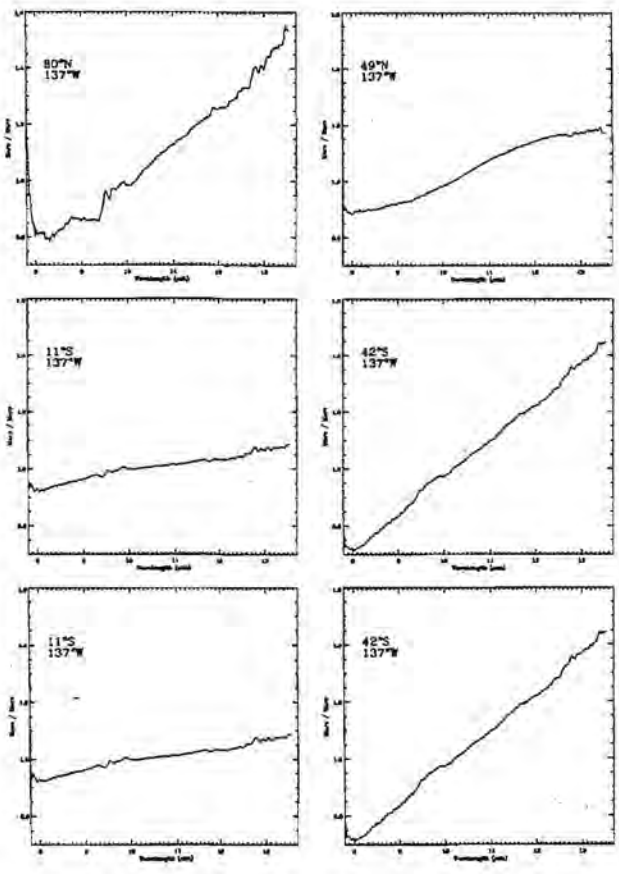

Fig. 1.

Acknowledgments: The author would like to thank Tom Hayward (Cornell), Martha Hanner, Padma Yanamandra-Fisher, and Terry Martin (JPL) for their assistance in making these observations. Thanks also go to Dave Crisp and Vikki Meadows for their help in running SMART.

This work was performed at JPL/CALTECH under contract by NASA.

References: [1] Pollack et al. (1990).

MARS GLOBAL SURVEYOR OVERVIEW. S. W. Bougher, Lunar and Planetary Laboratory, Space Science Building, University of Arizona, Tucson AZ 85721, USA (sbougher@lpl.arizona.edu).

Mars Global Surveyor (MGS) is the first of a new, decade-long program of Mars robotic exploration known as the Mars Surveyor program. The MGS mission is composed of a polar-orbiting spacecraft that is designed to survey the planet's topography, magnetism, mineral composition, and atmosphere. The MGS spacecraft will enter Mars orbit on September 11, 1997, and thereafter will undergo aerobraking for roughly four months prior to the beginning of mapping operations in March 1998. The final mapping orbit to be achieved is Sun-synchronous (2 p.m./2 a.m.). An aerobraking strategy will be implemented that not only will provide the "walk-in" capability needed to achieve this required orbit safely, but also will provide a careful monitoring of the atmospheric structure. Aerobraking is a technique that uses atmospheric drag to slow the spacecraft into its final mapping orbit while minimizing the amount of fuel required. Such an aerobraking exercise was recently successful at Venus; a successful Mars aerobraking campaign by MGS will pave the way for the rest of the Mars Surveyor program.

MGS carries six instruments that will acquire data from Mars during its mapping operations over a full martian year. These instruments include the (1) Magnetometer and Electron Reflectometer (MAG/ER), (2) Mars Orbital Laser Altimeter (MOLA), (3) Mars Orbital Camera (MOC), (4) Thermal Emission Spectrometer (TES), and (5) Radio Science (RS). The MGS spacecraft 2 p.m./2 a.m. orbit will place the Sun at a fixed angle above the horizon in each image, thereby allowing the midafternoon lighting to cast shadows sufficient to study surface features. The primary geoscience objectives of the MGS mission include the global definition of the topography and the gravitational field, the global determination of the mineralogical character of the surface materials, and the determination of the nature of the magnetic field. The primary climatological objectives are the determination of the time and space distribution, abundances, and sources/sinks of volatile material and dust over a seasonal cycle. In addition, a careful delineation of the atmospheric structure and dynamics will be made. The capabilities of these six instruments and their role in meeting these scientific objectives will be described.

At the completion of the MGS primary mission, the spacecraft will be available to serve as a data relay station for U.S. and international spacecraft landers and low-altitude probes over the next three years.

MARS CARBON DIOXIDE AND WATER CLOUDS IN THE CONTEXT OF 1996–1997 MICROWAVE SPECTRAL LINE OBSERVATIONS AND HUBBLE SPACE TELESCOPE ULTRAVIOLET SPECTROSCOPY. R. T. Clancy[1], M. J. Wolff[1], P. B. James[2], B. J. Sandor[3], and B. Butler[4], [1]Space Science Institute, 1234 Innovation Drive, Boulder CO 80303, USA (clancy@isidis.colorado.edu), [2]University of Toledo, Department of Physics and Astronomy, Toledo OH 43609, USA, [3]Jet Propulsion Laboratory, MS 183-701, 4800 Oak Grove Drive, Pasadena CA 91109, USA, [4]National Radio Astronomy Observatory, Very Large Array, P.O. Box 0, Socorro NM 87801, USA.

Submillimeter to centimeter wave spectral line observations of Mars allow retrievals of Mars atmospheric temperature and water vapor profiles, without interference from aerosol scattering or terrestrial absorptions [1]. Seasonal and interannual (since 1988) coverages of Mars atmospheric temperatures are obtained from submillimeter (346, 451 GHz) and millimeter (115, 230 GHz) spectra of the first four rotation transitions of the optically thick Mars ^{12}CO lines. The CO mixing ratio is determined from 220 and 341 GHz spectra of the optically thin ^{13}CO lines. Profiles of Mars atmospheric water vapor are constrained by centimeter (22 GHz) H_2O and millimeter HDO (226 GHz) spectral line observations. The CO and HDO observations are observed most often from the NRAO 12-m telescope at Kitt Peak, although key submillimeter CO measurements are taken at the James Clerk Maxwell Telescope (JCMT) on Mauna Kea. In both cases, the spatial resolution corresponds to whole disk-averaged measurements of Mars atmospheric temperatures. In contrast, centimeter mapping of Mars H_2O from the NRAO Very Large Array (VLA) can provide latitudinal and diurnal distributions of Mars atmospheric water profiles [2].

The combined microwave water vapor and temperature measurements consistently indicate low altitudes of water vapor saturation for the global Mars atmosphere around aphelion ($L_s = 0°–140°$) in 1991, 1993, 1995, and 1997. The predicted water 100% supersaturation altitude descends to altitudes below 10 km at aphelion, as compared to altitudes above 25 km for warmer, Viking-like atmospheric temperatures (Fig. 1). A highly nonlinear interaction between Mars dust and water ice aerosols has been proposed to clear dust from the aphelion northern spring/summer half of the Mars orbit, and so create an orbital dichotomy between dust and cloud loading, and hemispheric transport of atmospheric water in the current Mars climate [3]. The potential efficacy of such a nonlinear temperature dependence between dust heating, cloud formation on dust nucleation centers, and

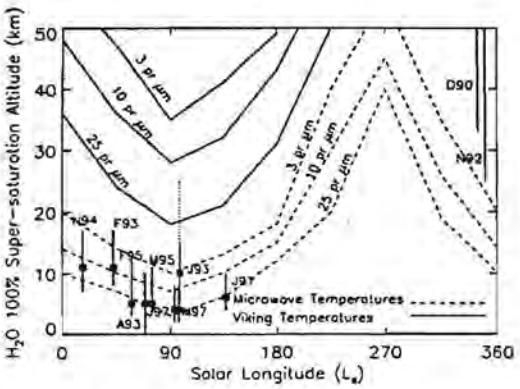

Fig. 1. Altitude of water vapor supersaturation.

dust removal/albedo changes has been shown through detailed microphysical/vertical transport/radiative balance models [4].

Hubble Space Telescope (HST) ultraviolet observations of the Mars atmosphere with the Faint Object Spectrograph (FOS) in September 1996 and January 1997 (L_s = 10° and 60°, respectively) specifically determine low levels of dust loading relative to the Viking 1 lander dust opacity measurements for this season (see Fig. 2, similar result for L_s = 60°). The presence of globally distributed water ice clouds at low altitudes becomes more dominant toward aphelion (L_s = 70°), with the development of the northern summer Hadley circulation [3]. Extensive clouds of opacities 0.1–0.4 are observed in HST Mars images at aphelions in 1991, 1993, 1995, and 1997 [3,5].

Carbon monoxide temperature retrievals for the L_s = 100°–150° northern summer season in 1997 exhibit a series of 10–15 K increases in lower atmospheric temperatures that decay on rapid timescales (1–2 weeks), as compared to dust settling times. These changes are seen to correlate with dust and cloud behaviors, as observed in early and late March HST imaging [6]. Carbon monoxide temperature retrievals during July 1997 show some evidence of regional atmospheric heating by dust, as does HST imaging [7]. But they do not indicate the dusty, warm conditions implied by Viking observations in this season. In this sense we are in direct conflict with the Viking-like atmospheric conditions espoused by the Pathfinder imaging and meteorology science teams [8,9]. On the other hand, the 15-km-altitude clouds identified in Pathfinder IMP imaging are very likely related to the low-altitude water ice clouds inferred from the microwave temperature/water vapor retrievals and imaged by HST.

The JCMT high-frequency CO line observations permit Mars atmospheric temperature measurements at altitudes of 50–80 km, which is a largely unexplored region of the Mars atmosphere. These upper-altitude temperature retrievals exist for September 1996 (L_s = 8°), March 1997 (L_s = 90°), and July 1997 (L_s = 150°); and are compared to Viking, Pathfinder, 1994 dust storm microwave, and CO_2 condensation temperature profiles in Fig. 3. The 1976 Viking descent temperatures are 10–20 K warmer than the JCMT 1996–1997 retrieved temperatures and 30 K warmer than the Pathfinder descent temperatures, on average. The 1994 microwave temperatures were obtained during a perihelion dust storm in 1994 [10], and clearly show that significant dust heating can ascend to high altitudes during global dust storms. The warm temperatures of the Viking period also suggest upper altitude dust heating at this time.

The Pathfinder and 1996–1997 microwave temperatures imply cold, dust-free conditions for this upper altitude region. As noted by Clancy and Sandor [6], the cold temperatures returned for the dayside average atmosphere of Mars from the 1996–1997 JCMT CO observations are only 10–15 K warmer than CO_2 saturation conditions at 70–80 km altitudes, such that local regions of CO_2 cloud formation are

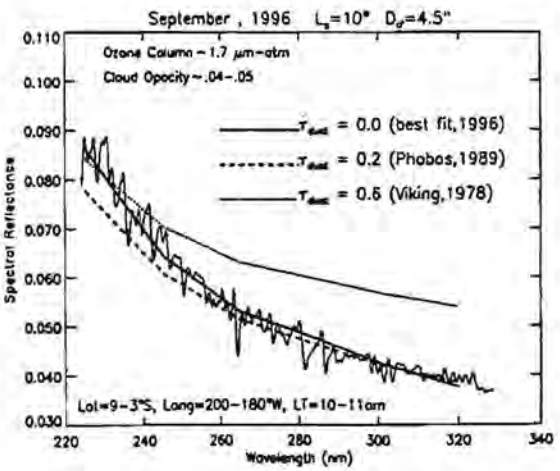

Fig. 2. 1996 HST UV spectra of Mars.

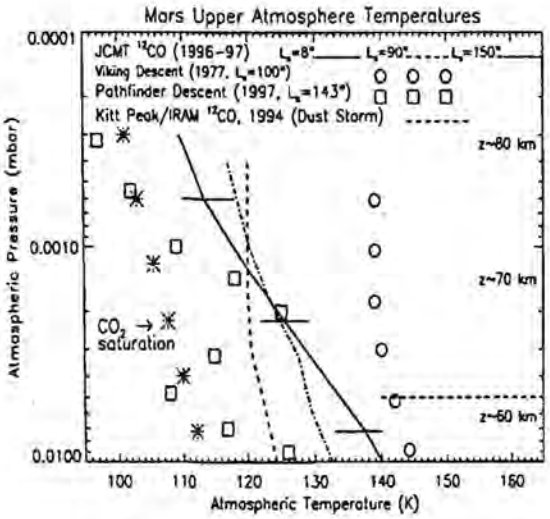

Fig. 3. Temperatures in the Mars mesospheres.

possible. Clancy and Sandor [6] also pointed out that the Pathfinder descent profiling in this region clearly exhibits temperatures below CO_2 saturation conditions.

More recently, the Pathfinder IMP imaged blue clouds with wave structures some 35–40 min before sunrise (Sol 39) [12]. Although the NASA Pathfinder Web site describes these clouds as very fine water ice aerosols at low altitudes (15 km), Clancy and Sandor [11] argue that these are in fact the high altitude (60–100 km altitudes) CO_2 ice clouds predicted from the JCMT CO line and Pathfinder entry measurements of very cold atmospheric temperatures. Furthermore, Clancy and Sandor [6,11] argue that these high-altitude CO_2 clouds and the very cold atmospheric temperatures measured during the 3 a.m. Pathfinder entry *do not imply* a large (30 K) diurnal variation in atmospheric temperatures over the 60–90 km altitude region, as maintained by the Pathfinder meteorology science team [9,12]. Instead, they are day and nighttime phenomena, based on the facts that (1) the JCMT temperatures are dayside observations and (2) these clouds are very likely the CO_2 ice, 4.3-μm line features revealed in Mariner 6 and Mariner 7 infrared spectral observations of the Mars atmospheric limb [13,14]. These Mariner 6 and 7 observations (L_s = 200°) are also daytime (11 a.m.–noon) measurements. Although the limb tangent for pointing of these measurements is ~25 km [13], they would include CO_2 cloud signatures at higher altitudes, within the foreground or background of the limb-viewed pathlengths [14].

References: [1] Clancy et al. (1990) *JGR, 95*, 14543–14554. [2] Clancy et al. (1992) *Icarus, 100*, 48–59. [3] Clancy et al. (1996) *Icarus, 122*, 36–62, 1996. [4] Rodin et al. (1997) *Bull. AAS, 29*, 966. [5] James et al. (1997) *JGR, 101*, 18883–18890. [6] Clancy and Sandor (1997) *Bull. AAS, 29*, 962. [7] Wolff et al. (1997) *Bull. AAS, 29*, 961. [8] Smith (1997) *Bull. AAS, 29*, 958. [9] Haberle (1997), personal communication. [10] Clancy et al. (1994) *Bull. AAS, 26*, 1130. [11] Clancy and Sandor, in preparation. [12] *Mars Pathfinder Project Information* (1997) http://nssdc.gsfc.nasa.gov/planetary/mesur.html. [13] Herr and Pimental (1970) *Science, 167*, 47–49. [14] Calvin (1996) *Bull. AAS, 28*, 1059–1060. [14] Pearl J. (1997), personal communication.

THE ATMOSPHERIC TEMPERATURE STRUCTURE AND WATER ABUNDANCE ON MARS. M. A. Gurwell[1] and D. O. Muhleman[2], [1]Harvard-Smithsonian Center for Astrophysics, Mail Stop 42, 60 Garden Street, Cambridge MA 02138, USA (mgurwell@cfa.harvard.edu), [2]California Institute of Technology, Mail Stop 170-25, Pasadena CA 91125, USA (dom@venus1.gps.caltech.edu).

Mars continues to be a major focus for planetary exploration, and as we await the arrival of the Mars Global Surveyor it is important to realize that groundbased observations of Mars will continue to have a vital role. Microwave, millimeter, and submillimeter observations of rotational lines from molecular species in the atmosphere can provide critical information about the abundance of certain species as well as the temperature structure, circulation, and variability of the atmosphere over time.

Rotational transitions are isolated and easily resolved, allowing accurate measurement of the lineshapes. The lineshape provides information of the vertical profiles of temperature and species abundance. This process is made considerably easier since the source function is nearly linear with temperature (the Rayleigh-Jeans limit), and scattering by suspended dust is unimportant.

Here we present results from our recent campaign to observe the temperature and distribution of water vapor in the atmosphere of Mars. Observations were performed on March 1 and March 5, 1997, with the Owens Valley Radio Observatory Millimeter Array, an interferometer consisting of six 10.4-m diameter antennas. At the time, Mars was approximately 13.5 arcsec in diameter, the season was near summer solstice (L_s = 85), and the subearth latitude was 22.8°N, providing a good view of the northern polar regions.

Spectroscopic measurements of the HDO (312–221) transition near 225.9 GHz were obtained on both days, and on March 5 simultaneous measurements of the CO (1–0) transition near 115.3 GHz were also obtained. Carbon monoxide has a well-determined abundance [1] and was used to measure the spatially resolved atmospheric temperature profile from 0 to 45 km at ~5–10 km resolution. With the temperature profile determined, the HDO observations were used to measure the local water vapor column and the altitude of saturation, using $HDO/H_2O = 2D/H = 1.6 \times 10^{-3}$. These observations provide the horizontal and vertical structure of the atmospheric temperature field and the distribution of water vapor.

The synthesized resolution of these observations was ~2.3 arcsec for HDO and 4.4 arcsec for CO. Observations of the bright QSO 3c273, located <2° from Mars at the time, were made roughly every 20 min to provide time-variable gain calibration of the data, and the pointing of the antennas was also checked against 3c273 every hour. Passband calibration was determined from 3c273 and Mars itself.

Temperature Field: The atmosphere of Mars was significantly cooler at the time of these observations than during the Viking era. The observed spectra are relatively deep and broad, indicating temperatures are ~20 K cooler above 10 km compared with the Viking descent profile models, as seen in Fig. 1.

Here a CO spectrum from the disk center is compared to a best fit model spectrum calculated assuming the cool temperature profile (dotted line) and a model spectrum based upon Viking era measurements (dashed line). These temperatures are indicative of significantly less dust-loading of the atmosphere relative to the Viking period, and have been seen often in single dish millimeter spectra of CO [1,2] since the early 1980s.

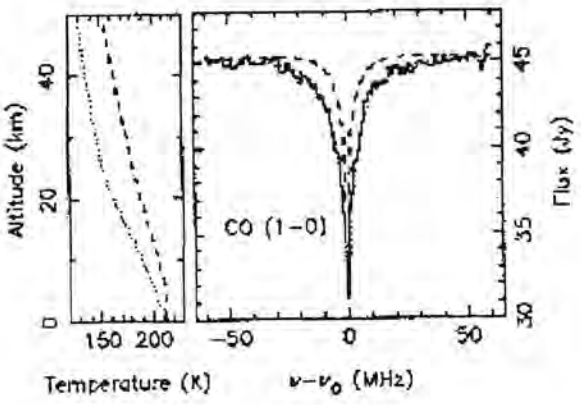

Fig. 1.

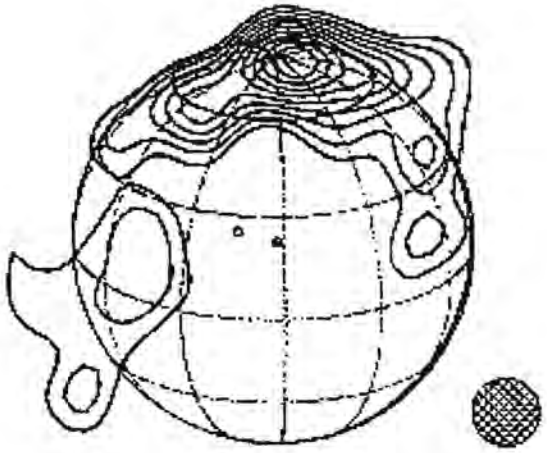

Fig. 3.

The advantage of interferometric observations is the large increase in spatial resolution, allowing resolved measurements of the CO line and, from them, the temperature structure of the atmosphere. Figure 2 shows a cross-section of the temperature field determined from the March 5 CO data.

This cut runs along the sub-Earth meridian and shows significant structure as a function of latitude. In particular, the warmest temperatures are in the northern midlatitudes where the surface altitude is lowest, reflecting a roughly adiabatic increase in temperature with decreasing altititude in the lowest scale height. Temperatures at the most southerly latitudes are significantly cooler, and there is evidence for the atmosphere becoming almost isothermal below 20 km here. Above 20 km, atmospheric structure is not a strong function of latitude. This temperature structure is qualitatively consistent with GCM models [3] for the same season, but the temperatures are generally cooler by 10–20 K, particularly above 10 km.

Water Abundance: The opacity due to HDO is small due to its low abundance, allowing observations from the ground. Due to the low optical depth on Mars as well as the Earth, it is very difficult to measure the lineshape of HDO accurately—at best it represents a broad, ~1.5% spectral feature in emission for ray paths near the planetary limb (where path lengths are maximized).

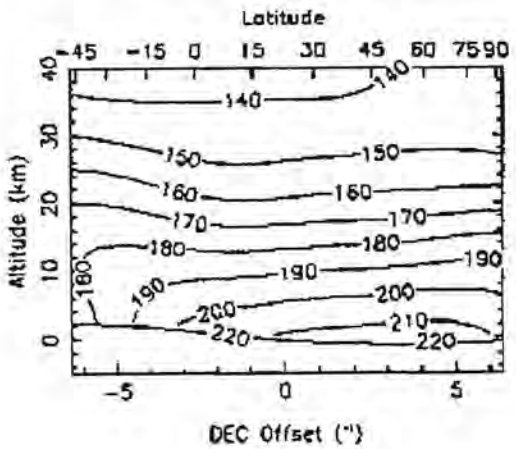

Fig. 2.

The HDO observations from both nights were combined to improve the SNR of individual spectra. A contour map of integrated line-to-continuum emission at 2.3-arcsec resolution is shown in Fig. 3, at 10% steps of the maximum observed value. The line emission is clearly concentrated in the northern polar regions and is minimized in the most southerly regions for any given apparent radius.

These HDO spectra are consistent with a column abundance of 11 ± 3 precipitable μm of water vapor over the north pole, 3 ± 1 precipitable μm at low northern latitudes, and just 1 ± 1 precipitable μm for southern latitudes, where no appreciable line emission was detected. In addition, the spectral shapes of the HDO lines are consistent with a low altitude of saturation, roughly near 10 km, suggesting cooler atmospheric temperatures just as determined from our CO observations. Warm, Viking-like temperatures would cause saturation to occur near 20–25 km, and the spectral shapes of model HDO lines calculated with such profiles do not match the observations.

References: [1] Clancy et al. (1990) *JGR, 95,* 14543. [2] Lellouch et al. (1991) *Planet. Space Sci., 39,* 219. [3] Haberle et al. (1993) *Icarus, 98,* 3093.

PRELIMINARY RESULTS FROM THE MARS PATHFINDER ATMOSPHERIC STRUCTURE INVESTIGATION/METEOROLOGY EXPERIMENT. R. M. Haberle[1], J. T. Schofield[2], D. Crisp[3], J. R. Barnes[4], J. A. Magalhaes[5], J. R. Murphy[6], A. Seiff[6], G. Wilson[7], and S. Larsen[8], [1]Space Science Division, Mail Stop 245-3, NASA Ames Research Center, Moffett Field CA 94035, USA (bhaberle@mail.arc.nasa.gov), [2]Mail Stop 230-235, Jet Propulsion Laboratory, 4800 Oak Grove Drive, Pasadena CA 91109, USA (tim@scn1.jpl.nasa.gov), [3]Mail Stop 169-237, Jet Propulsion Laboratory, 4800 Oak Grove Drive, Pasadena CA 91109,

USA (dc@crispy.jpl.nasa.gov), [4]Department of Atmospheric Science, College of Oceanic and Atmospheric Sciences, Oregon State University, Corvallis OR 97331, USA (barnes@ats.orst.edu), [5]San Francisco State University/Space Science Division, Mail Stop 245-3, NASA Ames Research Center, Moffett Field CA 94035, USA (magalhaes@galileo.arc.nasa.gov), [6]San Jose State University/Space Science Division, Mail Stop 245-3, NASA Ames Research Center, Moffett Field CA 94035, USA (murphy@canali.arc.nasa.gov; aseiff@mail.arc.nasa.gov), [7]Arizona State University/Space Science Division, Mail Stop 245-3, NASA Ames Research Center, Moffett Field CA 94035, USA (gwilson@humbabe.arc.nasa.gov), [8]Risoe National Laboratory, AMV-125, P.O. Box 49, Roskilde, DK-4000, Denmark (metsol@risoe.dk).

Mars Pathfinder successfully landed in the Ares Vallis flood plain (19.3°N, 33.6°W) on July 4, 1997. The spacecraft carried a suite of instruments to record the structure of the atmosphere during the entry, descent, and landing as well as for monitoring meteorological phenomenon while on the surface. Collectively, these instruments are known as the ASI/MET (Atmospheric Structure Investigation/METeorology) experiment. In this paper we present preliminary results from the ASI/MET experiment. As of this writing, the spacecraft is healthy and continues to take daily meteorological measurements. We expect this will continue for almost one more Earth year.

The three science accelerometers aboard Pathfinder began sensing the martian atmosphere at ~160 km above the landing site. Decelerations were recorded throughout the descent, but to date the analysis has focused on data recorded up to parachute release at about 9 km. In the region between 160 km and 90 km, measured atmospheric densities are 5–2.5× lower than that seen by Viking 1. Below 90 km, densities are comparable, though slightly lower, than those measured by Viking, as is expected given that atmospheric mass is near its annual minimum at this season (L_s ~143°). In the upper atmosphere (65–125 km) temperatures are on average about 20 K colder than those measured by Viking 1, and there is a distinct possibility for CO_2 cloud formation near the 80-km level. Below 65 km, temperatures are comparable to those seen by Viking, which is in sharp contrast to those inferred from groundbased microwave observations, which suggest much cooler lower atmosphere temperatures. One interesting feature of Pathfinder's temperature profile is the presence of quite pronounced thermal inversion between 10 km and 16 km, which may provide some altitude information on the predawn clouds seen by Pathfinder's camera.

Pathfinder's surface meteorological measurements show generally warmer temperatures than those seen by Viking 1. Temperatures from the topmast thermocouple at ~1.45 m above the ground range from 200 K just before dawn to 260 K in the early afternoon. During the primary mission, the daily temperature cycle was very repeatable as was the case for Viking at this season. On Sol 25, meteorological data were acquired at 4-s intervals throughout the day. These data clearly mark the onset and decay of turbulence in the lower atmosphere. Temperature fluctuations of 15–20 K, occurring on timescales of seconds to minutes, develop shortly after sunrise and continue into the early afternoon at which time they abruptly subside. Such fluctuations are likely associated with the large temperature gradients measured by the three thermocouples along Pathfinder's meteorology mast.

Calibration of the wind sensor is ongoing. However, some inferences can be made. Winds at the Pathfinder site during the primary mission appear to be controlled by local slopes. In general, they rotate clockwise with time blowing downslope at night (toward the north) and upslope during the day (toward the south). The strongest winds appear to occur in the downslope regime. Wind magnitudes are not yet available, but results from the windsock experiment suggest they are generally light (<10 m/s). Multiple late-night temperature inflections are seen in some of the data, which may be produced by enhanced vertical mixing associated with the strong nighttime winds.

As expected, the pressure data show a secular decline reaching a minimum on or about Sol 20, then rising slowly but steadily thereafter. This minimum signifies that the south polar cap has reached its maximum extent and is now beginning its annual retreat. Unlike the temperature data, however, the pressure data show a remarkable degree of day-to-day variability. In general there are two maxima and two minima each day, which are expressions of the semidiurnal thermal tide. However, some days have three or four maxima and minima, indicating the presence of higher-order harmonics.

The normalized amplitude of the semidiurnal tide varies from 0.005 to 0.010. Modeling results and the Viking experience suggest that such amplitudes can only be produced by a globally and deeply distributed dust haze with visible optical depths on the order of 0.5. Such optical depths are consistent with those observed by the imager. The normalized amplitude of the diurnal tide varies from 0.002 to 0.010 and is in general lower than those observed by Viking at the same season. We have interpreted this in terms of interference effects between eastward and westward traveling tides.

One of the most interesting results of the ASI/MET experiment has been the detection of dust devils. The signature of these events can be found in highly correlated short-term fluctuations in the pressure, temperature, and wind data. To date, 16 dust devils have been detected. They tend to occur between 9 a.m. and 3 p.m. local time. Preliminary analysis suggests that they can be large (200 m in diameter) and quite tall (perhaps 10 km). Given the apparent high frequency of dust devil occurrence, they may be significant contributors to the general high level of background dustiness observed by Pathfinder and Viking at this season.

To date, the meteorology at the Pathfinder site is very similar to that observed 21 years ago by Viking 1. We see no evidence in our data (or in the camera data) for a cold and cloudy, non-Viking-like Mars as has been inferred from groundbased microwave and HST observations [1]. Nor do we see any evidence for rapid climate variability triggered by cloud feedback mechanisms. However, our data have limited coverage in both space and time, and we are moving away from the season such phenomena have been postulated to occur. Thus, it will fall to the Mars Global Surveyor orbiter to better observe the full northern summer season.

References: [1] Clancy et al. (1996) *Icarus, 122.*

MARTIAN DUST AND APPARENT CARBON DIOXIDE ABUNDANCE. D. M. Hunten and A. L. Sprague, Lunar and Planetary Laboratory, University of Arizona, Tucson AZ, USA.

On November 25, 1971, Parkinson and Hunten observed a CO_2 abundance equivalent to a surface pressure of 2.0 mbar; 15 days later it had returned to a near-normal value of 5.8 mbar [1]. We attributed the low value to the presence of a global (or at least hemispheric) dust storm, opaque to a height of 11 km. This same dust storm was present during the early weeks of the Mariner 9 mission, which had entered orbit 12 days earlier. Our detector was a photomultiplier with an S-1 cathode, having a quantum efficiency of around 0.1%; the rather noisy spectrum (shown in Fig. 1) was obtained in 220 min of scanning. The inset to Fig. 1 shows the equivalent widths of the eight observed lines fitted to the martian curve of growth, from which the abundance was obtained. An additional observation was made 15 days later; these points indicated an abundance corresponding to a surface pressure of 5.8 mbar, close to normal. In 1967, Belton et al. [2] had found 5.5 mbar; their equivalent widths plotted inside the irregular curve of the Fig. 1 inset. Figure 2 shows these points, as well as some still earlier ones, with more of the curve of growth. The two versions of this curve

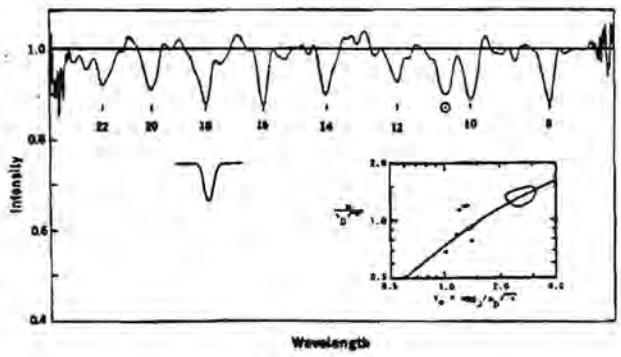

Fig. 1. Spectrum taken by Parkinson and Hunten on Nov. 15, 1971, and fitted curve of growth.

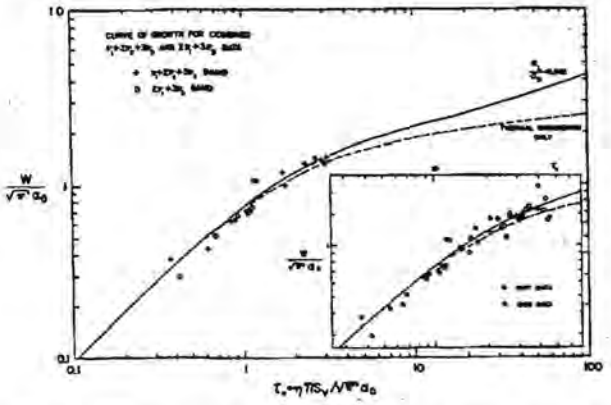

Fig. 2. Curve of growth from Belton et al. (1968) with observed points from 1967 and 1965.

are for Doppler (or thermal) broadening only, and for the actual effective pressure on Mars, half the surface pressure. At the time of the favorable 1971 opposition, we had built a specialized system with a multiple-exit slit to make a pressure, and therefore topographical, map [3]. Integration times were 3–8 min, depending on atmospheric transparency.

We intend to revive this program, with a new emphasis on the time dimension rather than the spatial one. A typical CCD has about 25× better quantum efficiency than the S-1 photomultiplier at the relevant wavelength, 10500 Å, and its multiplex advantage effectively substitutes for the use of a multislit. We estimate that a spectrum of much higher quality than Fig. 1 and seeing-limited spatial resolution can be obtained in 30 min. This estimate is based on prior results with the same telescope and echelle spectrograph that we use for measuring water vapor [4]. We have also used this telescope to observe Mercury as close as 15° to the Sun. The blackout around Mars' superior conjunction is estimated as five months. We therefore have the ability to monitor the atmospheric opacity almost all the way around the orbit. An orbiting spacecraft such as Mars Global Surveyor can provide far better spatial resolution, but a groundbased program can have a much longer time dimension.

References: [1] Parkinson T. D. and Hunten D. M. (1972) *Science, 175,* 323. [2] Belton M. J. S. et al. (1968) *JGR, 73,* 4795–4806. [3] Parkinson T. D. and Hunten D. M. (1973) *Icarus, 18,* 29–53. [4] Sprague A. L. et al. (1996) *JGR, 101,* 23229–23241.

REGRESSION OF MARTIAN NORTH POLAR CAP, 1996–1997. K. Iwasaki[1], D. C. Parker[2], S. Larson[3], and T. Akabane[4], [1]Lunar and Planetary Laboratory, University of Arizona, Tucson AZ 85721, USA (kiwasaki@pirl.lpl.arizona.edu), and Kyoto Gakuen University, Sogabecho, Kameoka, Kyoto 621, Japan, [2]Association of Lunar and Planetary Observers Mars Section, 12911 Lerida Street,

Coral Gables FL 33156, USA, [3]Lunar and Planetary Laboratory, University of Arizona, Tucson AZ 85712, USA, [4]Hida Observatory, Kyoto University, Kamitakara, Gifu 506-13, Japan.

To investigate interannual variability of the regression of the martian north polar cap, the regression of the martian north polar cap during the 1996–1997 apparition is examined with the measurements of the CCD images obtained by Parker.

The regression of the north polar cap of Mars has been examined for a long time. Dollfus [1] studied the north polar cap recession using observations made in 1946, 1948, and 1950 at the Pic du Midi and detected no significant year-to-year variations. Fischbacher et al. [2] found that the recession phase of the cap follows a well-defined curve and repeats itself very closely from one martian year to another. Baum [3] reported the behavior of the north polar cap obtained from the study of the Lowell Observatory plate collection that covers more than 60 yr since 1905 [2], plus more recent data from the patrol films [4]. Baum [3] compared his regression curve with that of Dollfus [1] and pointed out the overall disagreement between the curves is significant; this may arise from the different methods of measurement. However, the possibility that the difference arises from year-to-year variation appears to exist. According to Miyamoto and Nakai [5] and Miyamoto [6], the size of the north polar cap in 1963 was systematically a little larger than in 1960. Capen and Capen's measurements of the observations in 1962–1963, 1964–1965, and 1966–1967 at the Table Mountain Observatory and at the McDonald Observatory seem to show that the regression of the north polar cap is different from year to year [7]. Interannual differences in the regression of the north polar cap were also observed by Iwasaki et al. [8–13]. James et al. [14] reported that the 1977 dust storms seemed to have a significant effect on the south polar retreat. Analysis of the regression of the martian south polar cap based on recent spacecraft and groundbased observations seems to reveal the existence of interannual differences in the regression of the south polar cap [15,16].

The 1996–1997 apparition was favorable for observing the receding phase of the north polar cap. The observations of Mars in 1996–1997 were carried out at Coral Gables, Florida, at the Hida Observatory, and at the Tumamoc Hill Observatory, University of Arizona. To investigate interannual differences in the regression of the north polar cap more fully, we are examining the data obtained in these observations in 1996–1997. In this paper, we describe the results of the measurements of the data obtained at Coral Gables, Florida, and compare them with other observations.

The observations of Mars in 1996–1997 were executed with the 41-cm reflector at Coral Gables, Florida, by Parker, using a Lynxx PC CCD camera and blue, green, and red filters. The dimensions of the north polar cap were measured on red-filter CCD images taken at the best seeing conditions from September 1996 to May 1997 (L_s = 11.1°–124.5°; L_s is the areocentric longitude of the Sun). To measure the extent of the north polar cap in the images of Mars, we used an image display routine (SAO image) in the IRAF (Image Reduction and Analysis Facility) to display images of Mars on the screen of the SUN workstations [17]. The contrast of the images can be changed easily in this routine, so we selected the best contrast for measuring the edge of the north polar cap. Sets of the longitude and the latitude of the edges of the north polar cap are calculated from the measured data on the same workstation. They are projected onto a plane tangent to the north pole of Mars using a polar stereographic projection method in which the planetary radius is set as 0.5 [18,19].

The measuring results of the regression of the north polar cap in 1996–1997 were compared with other results. Cantor et al. [20] measured the recession of the north polar cap in 1996–1997 using data obtained with the Hubble Space Telescope. Comparison shows that the agreement of the data of the Hubble Space Telescope with ours is almost perfect except L_s = 11° (Fig. 1). Hubble Space Telescope observations of Mars have a spatial resolution that is superior to groundbased observations, but these observations are less frequent than groundbased observations. Groundbased observations fill the time gaps left by infrequent HST Mars observations.

Measurements by Dollfus (1946, 1948, and 1950) [1], Baum (mean) [3], Briggs (1972) [17], James (1977–1978) [14], and Iwasaki et al. (1979–1980, 1994–1995) [8,13] were also compared with our measurements of the regression of the north polar cap in 1996–1997 (Fig. 2). The regression of the north polar cap in 1996–1997 is a little faster than the mean regression or the regression in 1979–1980 after L_s = 51° but is similar to those in 1946, 1948, 1950, 1972, 1977–1978, and 1994–1995. The data from 1996–1997 also support the proposition that year-to-year variations of the re-

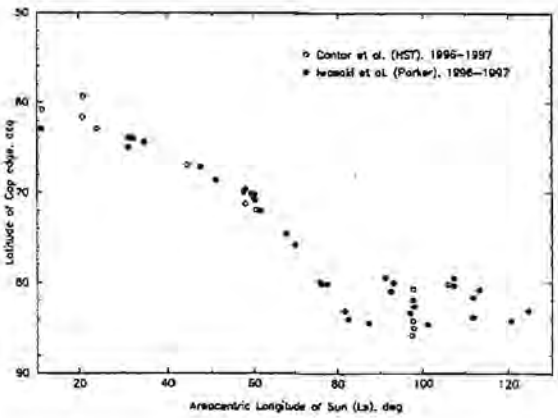

Fig. 1.

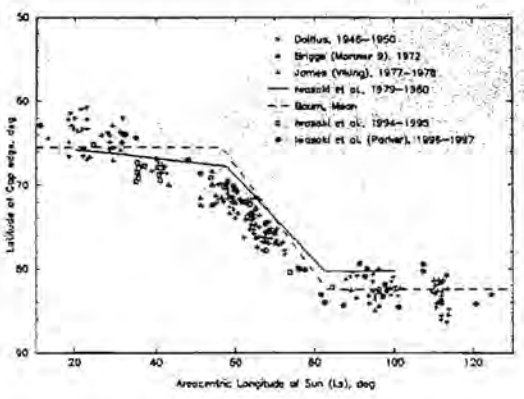

Fig. 2.

gression of the north polar cap may exist. Iwasaki et al. [8] demonstrated that the shape of the residual north polar cap for $L_s = 84°–101°$ in 1980 shows an asymmetric shape in relation to the pole and agrees very well with that for $L_s = 97°$ in 1972 obtained by Mariner 9. In our measurements, the residual north polar cap after $L_s = 82°$ in 1997 also shows an asymmetric shape and is similar to that observed by Viking.

The results of Baum [3] and Iwasaki et al. [8,13] show the temporary halt of the north polar cap retreat. The same tendency is seen in our measurements of this apparition data. On the other hand, Cantor et al. [20] reported the standstill in the north polar cap retreat was not observed in 1992–1997. However, they indicated the possibility that this result may be due to lack of sufficient coverage during the critical time period. The temporary halt of the north polar cap retreat is also seen in other datasets [6,11,14,21,22]. Miyamoto [6] claimed that the temporary stop of the north polar cap retreat may correspond to the epoch of transition, in the types of atmospheric general circulations, from the terrestrial type to the cross-equatorial type. Iwasaki et al. [8] also discussed the temporary stop of the north polar cap retreat with model circulations of seasonal variation of springtime circulation published by Haberle et al. [23]. Lindner et al. [24] reported that variations in terrain and surface roughness could easily account for the temporary halt of the regression of the north polar cap. More regular monitoring of the north polar cap would be desirable to establish the existence of the temporary halt of the north polar cap retreat.

References: [1] Dollfus A. (1973) *Icarus, 18,* 142. [2] Fischbacher et al. (1969) *Martian Polar Cap Boundaries*, Planetary Research Center, Lowell Observatory. [3] Baum W. A. (1974) in *Exploration of the Planetary System* (A. Woszczyk and C. Iwaniszewska, eds.), pp. 241–252, D. Reidel, Dordrecht. [4] Baum W. A. and Martin L. J. (1973) *BAAS, 5,* 296. [5] Miyamoto S. and Y. Nakai (1961) *Contr. Inst. Astrophys. Kwasan Obs., 105,* 1. [6] Miyamoto S. (1963) *Contr. Inst., Astrophys. Kwasan Obs., 124,* 1. [7] Capen C. F. and Capen V. W. (1970) *Icarus, 13,* 100. [8] Iwasaki K. et al. (1982) *JGR, 87,* 10265. [9] Iwasaki K. et al. (1984) *Publ. Astro. Soc. Japan, 36,* 347.[10] Iwasaki K. et al. (1986) *LPI Tech. Rpt. 87-01,* 57–59. [11] Iwasaki K. et al. (1993) *Proc. LPSC 26th,* 52–55. [12] Iwasaki K. et al. (1994) *Proc. LPSC 27th,* 43–46. [13] Iwasaki K. et al. (1995) *Proc. LPSC 28th,* 217–220. [14] James P. B. (1979) *JGR, 84,* 8332. [15] Iwasaki K. et al. (1991) *Proc. LPSC 24th,* 172–175. [16] James P.B. et al. (1990) *JGR, 95,* 1337. [17] Iwasaki K. and Ebisawa S. (1993) *Proc. LPSC 25th,* 1–5. [18] James P. B. and Lumme K. (1982) *Icarus, 50,* 368. [19] Iwasaki K. et al. (1986) *Publ. Astro. Soc. Japan, 38,* 267. [20] Cantor B. A. (1997) *BAAS, 29,* 963. [21] Iwasaki K. et al. (1979) *JGR, 84,* 8311. [22] Christensen P. R. and Zurek R. W. (1984) *JGR, 89,* 4587. [23] Haberle R. M. (1979) *Icarus, 39,* 151. [24] Lindner B. L. (1995) *BAAS, 27,* 828.

HUBBLE SPACE TELESCOPE OBSERVATIONS OF MARTIAN NORTH POLAR CAP, 1990–1997. P. B. James[1], B. A. Cantor[1], M. J. Wolff[1], S. W. Lee[2], R. T. Clancy[3], J. F. Bell III[4], and L. J. Martin[5], [1]Department of Physics and Astronomy, University of Toledo, Toledo OH 43606, USA (pbj@physics.utoledo.edu), [2]Laboratory for Atmospheric and Space Physics, University of Colorado, Boulder CO 80309, USA, [3]Space Science Institute, Boulder CO 80301, [4]Center for Radiophysics and Space Research, Cornell University, Ithaca NY 14853, USA, [5]Lowell Observatory, Flagstaff AZ 85721, USA (deceased).

Introduction: Hubble Space Telescope imaging of Mars from December 13, 1990, through October 13, 1997, has recorded four consecutive north polar cap regression cycles spanning $L_s = 335°–197°$ [1]. The period available for observation is controlled by the requirement that the elongation of Mars from the sun may not exceed 50°; this window progresses to a later range of L_s each year so that there is only partial overlap over the four martian years observed. The central meridians of the images also varied during the four years, although there were several "global" sequences obtained with three central meridians during one diurnal cycle from which mosaics were produced. The images have been used to study the regression of the polar cap, the photometric properties of the polar condensates, polar condensate, and dust clouds, and the formation of the north polar hood in late summer.

Cap Regression: The major objective of the study of the cap regression is a search for interannual variations and correlations with clouds, dust storms, and other phenomena. The inconstancy of the central meridian is a complication because the recession of the seasonal north polar cap is not symmetric about the geographic pole (i.e., it depends on longitude). The perceived recession also depends to some extent on the filter if clouds are present along the periphery of the cap. The general appearance of the polar cap is very

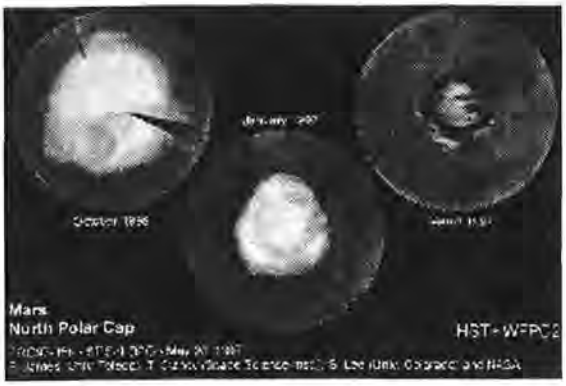

Fig. 1.

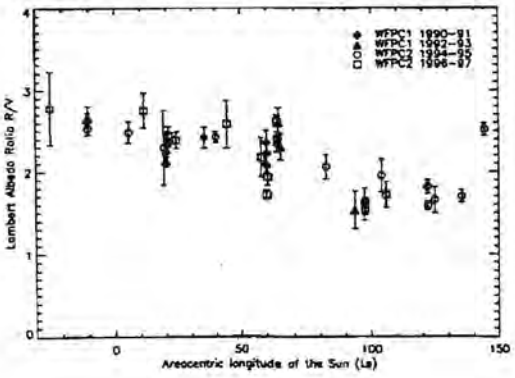

Fig. 3.

similar to the observations of Mariner 9 and Viking at similar dates. The cap is fairly symmetric about the geographic pole in early spring, but by $L_s = 60°$ the cap has become noticeably noncircular. In fact, the cap in 1997 was noticeably hexagonal at this time as observed previously by Mariner 9 and by HST in 1994–1995 [2,3]. The residual cap and outliers observed by HST are similar, within our more limited resolution, to Mariner 9 and Viking.

For interannual comparison, the regression curve in Fig. 2 is based only on data between 270° and 280° longitude using the 410-nm filter; except for the suggestion that the 1990–1991 recession was somewhat faster than the others in midspring, the data from the various years are consistent within the errors. There was little variation between filters except in the earliest sequences obtained before $L_s = 0°$. The four regressions observed by HST were very similar to the north polar regressions observed by Mariner 9 in 1972 and by Viking in 1977–1978 and 1980; however, comparison with groundbased data from other years suggests significant interannual variability [4].

Photometric Properties: The red (673 nm) and violet (410 nm) Lambert albedos of the polar condensate deposits were observed to increase secularly with L_s during all four years; there is a fair amount of scatter in the data, but the increases in both red and violet seem to be consistent with the hypothesis that the residual cap has higher albedo in both wavelengths than the seasonal CO_2 deposits. The mean (red, violet) Lambert albedos are (0.53, 0.23) and (0.66, 0.36) in spring (through $L_s = 65°$) and summer (after $L_s = 80°$) respectively. The color of the cap, measured by the ratio of red to violet reflectances, also changes in late spring as shown in Fig. 3. This ratio dips from ~2.3 in spring to 1.8 in summer (the high ratio in the last data point was caused by dust with an optical depth of 0.5–1.0 over the cap). The assumption that the surface phase function of the condensates is Lambertian in both red and violet wavelengths is known to break down at large emission angles, giving rise to different limb-darkening behaviors in the two wavelengths [5,6]; therefore, it is not possible to eliminate geometrical effects as a cause of the variation.

Circumpolar Clouds and Dust: Extensive condensate clouds were not seen in the regions surrounding the north

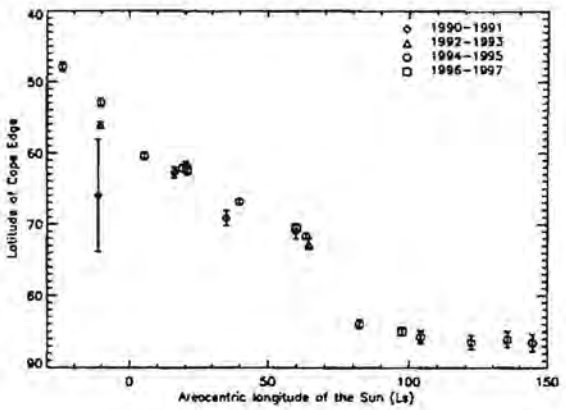

Fig. 2.

Fig. 4.

polar cap during spring and summer. Most of the circumpolar condensate clouds observed in spring were near the morning limb and probably reflect condensation of moisture released from the cap during the night. Once the entire cap is illuminated, these diurnally variable clouds tend to go away. The main exception is the Acidalia-Tempe region, in which extensive clouds were frequently seen; this is a region predicted by Hollingsworth et al. [7] to be exceptionally meteorologically active due to topography, though specifically in the winter rather than the summer.

On the other hand, dust was observed in the polar regions in several HST imaging sequences during 1995 and 1996. Rather diffuse dust that was present in midsummer in 1995 has been previously reported [8]. Several localized dust clouds were observed over the cap and near its edge during the subsequent spring. The scythe-shaped feature in the upper left image in Fig. 1 is one example, and the more substantial dust cloud in Fig. 4 is another. Possibly dust left on the cap surface as the CO_2 sublimes is levitated by winds associated with a front.

Polar Hood: The period between L_s = 150° and 180° is one of the less-documented seasons on Mars. The north polar hood, which is a major meteorological feature of the planet during fall and winter in the northern hemisphere, is known to form during this time. HST is observing this season at the present time, and observations will be reported.

Summary: Hubble Space Telescope has afforded a unique opportunity to observe the recession of the martian north polar cap during four consecutive martian years with the same resolution and with favorable viewing geometry. This has provided a dataset on a seasonal phenomenon, which may be sensitive to interannual variability in other phenomena such as the dust cycle. This dataset will be extended by the next generation of space missions as well as by future HST observations.

Acknowledgments: Support for this work was provided by NASA through grant No. 7276 from STScI, which is operated by AURA under NASA Contract NASS-26555.

References: [1] James P. B. et al. (1994) *Icarus, 109,* 79–101. [2] Soderblom L. A. et al. (1973) *JGR, 78,* 4197–4210. [3] James P. B. et al. (1996) *JGR, 101,* 18883–18890. [4] Cantor B. A. et al., *Icarus,* submitted. [5] Paige D. A. (1985) Ph.D. thesis, California Institute of Technology. [6] James P. B. et al. (1996) *Icarus, 123,* 87–100. [7] Hollingsworth J. L. et al. (1996) *Nature, 380,* 413–415. [8] Wolff M. J. et al. (1997) *JGR, 102,* 1679–1692.

VOLATILE SEARCHES IN MARTIAN NEAR-INFRARED SPECTRAL IMAGES FROM THE 1995 OPPOSITION.

D. R. Klassen[1], J. F. Bell III[1], R. R. Howell[2], and P. E. Johnson[2], [1]Center for Radiophysics and Space Research, Space Sciences Building, Cornell University, Ithaca NY 14853, USA, [2]Department of Physics and Astronomy, Box 3905, University of Wyoming, Laramie WY 82071, USA.

Near-infrared (NIR) multispectral images of Mars, taken at the NASA Infrared Telescope Facility (IRTF) near and at the 1995 opposition (January 14 and February 1, 1995), are used to identify and discriminate between CO_2 and H_2O frosts. Band-depth maps [1–3] of various diagnostic absorption features [4–6] identify polar volatiles as well as morning and evening frosts. These maps also act as a check for the techniques of principal components analysis (PCA) and linear mixture modeling (LMM). PCA and LMM are used to create maps that identify regions along the morning and evening limbs with a spectral signature similar to the north polar regions (and thus presumed to be volatile-enriched areas). This technique shows its power in that it requires no *a priori* spectral information to create the maps.

The volatile-bearing, so-called "blue" clouds have been seen on Mars for decades in planetary images. These clouds were assumed to be composed of condensed water. The first evidence for solid CO_2 was in Mariner 6 and 7 south polar spectra [7]. Viking IRTM measurements show both poles having 20-μm brightness temperatures less than the CO_2 condensation point of 150 K [8]. It is clear that CO_2 is condensing, but the question is whether it is condensing directly on the ground or in clouds and then falling out as grain sizes increase. Our band-depth map and PCA/LMM techniques are used to investigate that question.

The band-depth map technique is used to trace the variation of a particular absorption feature as a function of position. It is defined as the ratio of the image within the absorption feature of interest to a continuum level at that same wavelength. The continuum level is calculated from a linear interpolation between two local continuum images on either side of the absorption band. Band-depth maps at 3.33 μm have been shown to be a good tracer of CO_2 frosts [2,3]. Band-depth maps at 2.25 μm have been shown to be a good tracer of H_2O frosts [3]. In these maps areas with water ice

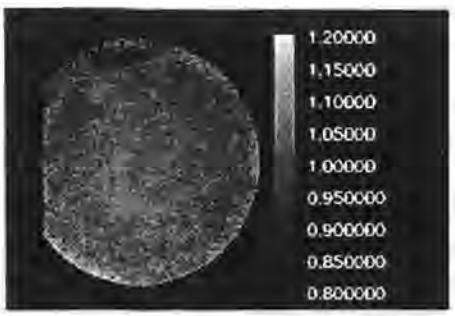

Fig. 1. Band-depth map centered at 3.33 μm using local continuum images at 3.27 μm and 3.4 μm. This map shows the adsorption collar around the north polar region indicating the recession of a cover from the seasonal north polar cap.

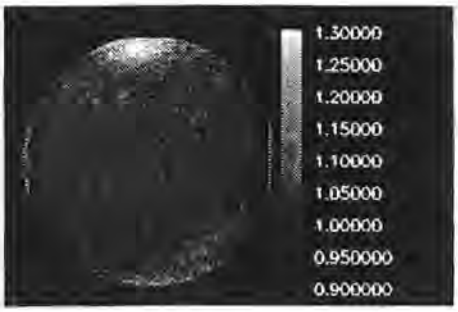

Fig. 2. Band-depth map centered at 2.254 μm using local continuum images at 2.136 μm and 2.337 μm. Only the north polar region can be seen.

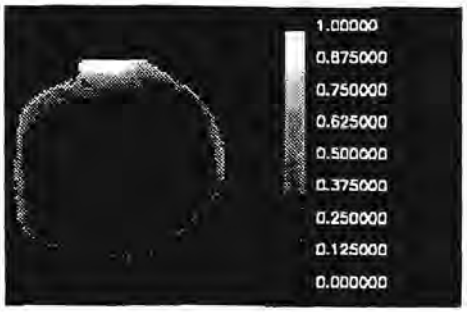

Fig. 4. North polar region endmember fractional abundance map. Morning and evening regions are shown to be modeled with up to 50% of this end member, indicating the existance of fine water frost in these regions.

will show as an "inverse absorption" feature as the water ice spectra have a local maximum at this wavelength. Band-depth maps at 3.69 μm have been shown to be able to differentiate between coarse and fine-grained water ices [3].

The PCA technique transforms the image set into a new vector space determined by minimization of the data variance/covariance matrix [3]. In our dataset, the fist two bases of this new vector space account for over 99% of the data variance. The first basis vector can be assigned to the physical trait of general albedo and the second to the degree of water frost coverage and low temperature.

The data are then plotted in the new vector space to determine which areas on Mars have the most extreme values of these new bases. These extreme value areas are end members, which are "pure" in the basis traits and are used in the LMM technique to model the remaining image pixels. Thus, each area on Mars can be described as a linear combination of a small number of end-member spectra. From the PCA the end members for the Mars spectral images are a bright, centrally located region, a dark, centrally located region, and the north polar region.

From the 3.33-μm band-depth maps (see Fig. 1) we see little, if any, evidence of CO_2 frosts. The variation across the disk is on the order of the image noise. We do see a ~15% feature in a collar around the north polar region in some of the later images. A region of pure CO_2 would have a feature on the order of 40–60%; thus, this region is not entirely composed of CO_2 frosts.

Evidence for water ices from the 2.25-μm band-depth maps show the north polar region as the only region with a major feature. There is little to no evidence of any morning or evening clouds. The 3.69-μm band-depth map indicates that these H_2O frosts are fine grained as opposed to coarser grained.

This fine-grain result is also seen with the PCA; however, pixels in both the morning and evening regions have high values of the frost/temperature basis vector, which would be a sign that there are water ice clouds there. The LMM also shows that morning and evening regions can be modeled with as much as 50% of the north polar region endmember.

We can conclude that our techniques show no evidence of CO_2 clouds on the two dates studied so far. There is evidence of the seasonal polar cap emerging from beneath some kind of fine-grained water ice covering. The spectral image sets, however, were registered using the albedo features to do the aligning. Since Mars was rotating over the time it takes to complete a spectral scan, this would cause some misalignment of the planetary disk. We are currently working on a method of registering the images based solely on the planetary disk, which will give results along the limbs that will be more trustworthy. Since there appears to be no trace of CO_2 frosts with the PCA/LMM techniques, we must rely entirely on the band-depth mapping.

We also conclude that all of the atmospheric volatiles seen on Mars can be modeled as fine-grained water frosts. This is seen with both the band-depth maps as well as the PCA/LMM. The PCA/LMM technique appears to be a better tracer of the frosts than the band-depth maps due to possible correlations of the bands with surface mineralogic absorptions.

With a combination of these techniques, it is possible to not only identify the martian clouds, but also to determine composition. Their application to the early northern spring images from the 1995 opposition, as well as images from the 1997 opposition, will be of great interest, as the temperature profile measured by the Pathfinder during its descent found a layer where the temperature was below the CO_2 frost

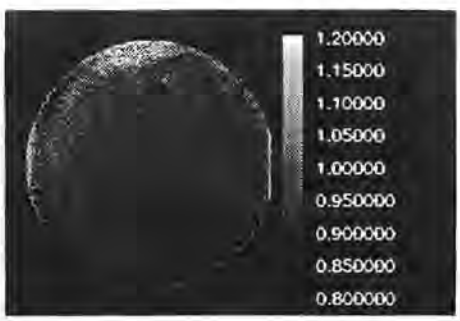

Fig. 3. Band-depth map centered at 3.69 μm using local continuum images at 3.40 μm and 3.80 μm. The value at the north polar region is greater than one, indicating a fine-grained frost.

condensation point [9], implying that CO_2 clouds could be expected.

References: [1] Bell J. F. III and Crisp D. (1993) *Icarus, 104,* 2–19. [2] Bell J. F. III et al. (1996) *JGR, 101,* 9227–9237. [3] Klassen D. R. (1997) Ph.D. dissertation, Univ. of Wyoming. [4] Fink U. and Sill G. T. (1982) in *Comets* (L. L. Wikening, ed.), pp. 164–202, Univ. of Arizona. [5] Calvin W. M. (1990) *JGR, 95,* 14743–14750. [6] Roush T. L. et al. (1990) *Icarus, 86,* 355–382. [7] Herr K. and Pimentel G. (1969) *Science, 166,* 469–499. [8] Kieffer H. et al. (1977) *JGR, 82,* 4249–4291. [9] Schofield T. et al., *Science,* submitted.

MARTIAN DUST AND CONDENSATE CLOUDS: 1996–1997 HUBBLE SPACE TELESCOPE OBSERVATIONS.

S. W. Lee[1], P. B. James[2], M. J. Wolff[2,3], R. T. Clancy[3], and J. F. Bell III[4], [1]Laboratory for Atmospheric and Space Physics, University of Colorado, Boulder CO 80309, USA (lee@syrtis.colorado.edu), [2]Department of Physics and Astronomy, University of Toledo, Toledo OH 43606, USA, [3]Space Science Institute, 1234 Innovation Drive, Suite 294, Boulder CO 80303-7814, USA, [4]Center for Radiophysics and Space Research, Cornell University, Ithaca NY 14853, USA.

Introduction: The Hubble Space Telescope began a long-term program of Mars observations on December 13, 1990, and has now accumulated observations over portions of four consecutive martian years. The most recent cycle of observations began on September 18, 1996, and has concentrated on characterizing the martian surface and atmosphere in the year leading up to the Pathfinder landing and the arrival of Mars Global Surveyor. During this period, a great deal of variability in the occurrence of dust and condensate clouds has been observed. This presentation will summarize Wide Field Planetary Cameras 2 (WFPC2) observations of such activity.

Fig. 1. Dust storm in Valles Marineris. Two full-disk HST images are shown (north is to the top); an extensive dust storm is evident in the June 27 image. A simple cylindrical projection map of the Valles Marineris region is shown at the bottom, extending from 25°S to 25°N latitude and 10° to 90° longitude. The Pathfinder landing site is marked by a +.

Fig. 2. Condensate clouds near opposition on March 30, 1997. This HST image was obtained through a 410-nm filter. The Tharsis volcanos can be seen protruding through the condensate clouds westward of the center of the disk. North is to the top; the sub-Earth point was about 93° longitude and 23°N latitude.

Dust Clouds: HST observations made in 1995 detected a number of regional dust storms in the vicinity of the north polar cap and in the Hellas basin [1]. In the observations beginning last September, dust clouds have been frequently observed on the border and interior of the receding seasonal north polar cap [2]. The most extensive dust cloud observed by HST to date was detected on June 27, 1997, one week prior to the Pathfinder landing. At that time, all of Valles Marineris was seen to be filled with dust (Fig. 1); the maximum estimated dust optical depth was about 2.8 [3]. This event appears to have been well confined to the canyon lands. A

Fig. 3. Development of condensate clouds over three consecutive days. Full-disk HST images are shown (north to the top), with the Pathfinder landing site denoted by a +. Polar projection maps are shown below; 0° longitude is to the bottom and latitude circles are drawn at 40°N, 60°N, and 80°N. Note the movement of the prominent cloud (located near 45° longitude on July 9).

MOC image obtained by Mars Global Surveyor on July 2 shows Valles Marineris still was filled with dust, but the dust storm had apparently dissipated when the next HST images were obtained on July 9. Subsequent HST observations in late August and September show renewed dust activity in the north polar region.

Condensate Clouds: The 1996–1997 HST observations have shown the occurrence of condensate clouds to be very extensive spatially, as well as highly variable both spatially and temporally [4]. Near opposition on March 30, 1997, high-altitude cirrus were present over much of the planet (Fig. 2). In early July, HST images were obtained on three consecutive days, an observing strategy not previously attempted in our HST program. These images (Fig. 3) allowed tracking of the movement and development of a cloud mass near the north pole; the apparent velocity of the cloud front was about 22 km/hr between July 9–10, and the cloud had dissipated by July 11.

Summary: During the past year, HST has provided abundant evidence for very dynamic occurrences of both condensate and dust clouds. These observations will provide the context for the state of the martian surface and atmosphere leading up to the early operations of both Pathfinder and Mars Global Surveyor.

Acknowledgments: Support for this work was provided by NASA through grant No. 7276 from STScI, which is operated by AURA under NASA Contract NASS-26555.

References: [1] Wolff M. J. et al. (1997) *JGR, 102,* 1679–1692. [2] James P. B. et al. (1997), this volume. [3] Wolff M., personal communication. [4] Wolff M. J. et al. (1997), this volume.

MARS PATHFINDER OBSERVATIONS OF WATER ON MARS.

M. T. Lemmon, M. G. Tomasko, P. H. Smith, and L. R. Doose, Lunar and Planetary Laboratory, University of Arizona, 1629 E. University Boulevard, Tucson AZ 85721-0092, USA.

Among the priorities for the Mars Pathfinder project, following the July 4, 1997, landing, was to measure and monitor atmospheric opacity. In addition to frequent measurements of the dust opacity, the Imager for Mars Pathfinder measured water vapor opacity on several occasions. The water vapor measurement is accomplished by taking several images of the Sun near 1-airmass in the 0.935-μm band and in adjacent continuum regions, taking a similar set of images near sunset or sunrise, and determining the additional opacity in the water band. The 1-airmass images are used to calibrate the measurement; the observations are done at elevation angles of 3.6°–6.5°, where the airmass is ~10. High airmasses are required, as we expect a feature of ~1% due to the weak water band even in these conditions.

To obtain the high airmasses, the observations are done in morning and the evening, within 15–25 min of sunrise/sunset. Evening observations were made on Sols 14, 25, and 32 (approximately July 17, July 29, and August 5) and morning observations were made on Sols 15, 18, and 21 (approximately July 18, 21, and 24).

We have done a preliminary analysis of the data from the evening of Sol 14. The variation of log (solar flux) with airmass factor is expected to be linear. At low elevation angles, the airmass factor depends on the scale height of the dust as well as on the elevation angle observed. We find that a dust scale height of 13 km causes the expected linear relationship. There is 1.5% more absorption in the water band than in the continuum. Accounting for the curve of growth for these filters under martian conditions, we determine the slant abundance of water to be 45–97 precipitable μm (changing as the path length increases as the Sun sets).

The vertical column abundance depends on the distribution of water. We consider two possibilities: first, the water is uniformly mixed with the dust (the latter is the dominant source of opacity), and second, the water is confined to a narrow layer near the surface, so that the airmass factor for water is simply 1/cos (zenith angle). In the first case, we find that the water abundance is 11 (–4, +6) precipitable μm, and that it appears to increase with time as the elevation of the Sun decreases. The latter is not a real effect, but it is also small compared to the error bars, so this case cannot be excluded. In the second case, we find the water abundance to be a constant 8 (–2, +4) precipitable μm. We expect this case to be more likely due to the large decline in temperature above from the surface. We will repeat the analysis for each of the days for which we have water data.

The primary source of random error is that we cannot locate the image of the Sun on the CCD (and thus the flat field). In the future we will take observations with a new scheme that is expected to allow recovery of the solar image. We also have not accounted for the possible variation of water vapor abundance with time of day. If the water abundance is twice as high at noon as at sunset, that will increase our estimates by ~10%.

In addition to observations of water vapor, IMP has obtained images of clouds in the predawn hours. We have sequences of images taken in the hour before sunrise on Sols 13, 14, 15, 16, 25, and 39. For each of the last four, we have two hours of predawn coverage. On Sols 13 and 14, we saw a red sky with only low contrast, color-neutral features. On Sol 15, and again on Sols 25 and 39, we saw streaks of clouds across a mostly featureless sky. On Sol 16, the sky was overcast.

On Sol 16, the clouds were observed to come from the northeast. We could not independently determine their altitude, but if we assume an altitude of 15 km, we determine the wind velocity to be ~10 m/s. The overcast sky was observed from 2 hr before sunrise until 40 min before sunrise, with the brightness exponentially increasing with time. The lack of an inflection indicating the Sun rising on the clouds suggests that either they are directly illuminated the entire time, or

that they are only diffusely illuminated by forward-scattered light the entire time. This requires that the cloud altitude be >120 km for the first case and <15 km for the second. It is likely that the lack of contrast 20 min before sunrise is not due to a real disappearance of the clouds, but rather to a loss of contrast associated with the changing illumination.

On each of the days, the contrast in the clouds was strongest in the blue. On Sol 39, the clouds were very blue: streaks with 50% contrast were observed in the blue filter that were <10% contrast in the red filter and not detectable in the infrared.

MIDINFRARED MAPPING OF MARTIAN CLOUDS. T. Z. Martin, Mail Stop 169-237, Jet Propulsion Laboratory, 4800 Oak Grove Drive, Pasadena CA 91109, USA (tzmartin@pop.jpl.nasa.gov).

Martian atmospheric dust strongly affects the planet's meteorological state and the transport of water. Although a number of major martian dust storms have now been observed, both from Earth and by spacecraft, the mechanisms for their inception are not known. It has also been suggested that the ambient state of the atmosphere may be much clearer in some years than others. Viking-era measurements [1,2] show a dustier atmosphere than that inferred recently in microwave observations by Clancy et al. [3]. Routine monitoring of dust content is not straightforward, however. Images reveal primarily thick storm activity. The Hubble Space Telescope cannot monitor frequently or when Mars is near the Sun. Regular measurements from the Earth or spacecraft are required to provide the essential clues to dust storm formation and to determine how martian years can vary so widely.

Dust also modifies the density at the altitudes of aerobraking spacecraft, such as Mars Global Surveyor. The advent of a global storm could strongly influence the progress of aerobraking; early warning is important. Future missions relying on aerocapture will be even more dependent on knowledge of the atmospheric state.

Imaging of Mars in and near the 9-μm silicate band provides the ability to map martian atmospheric dust opacity. This approach to opacity determination has promise both for its sensitivity and ability to operate when Mars is small and near the Sun.

The silicate band at 9 μm is optimal for determining dust opacity. Airborne dust absorbs emissions from the warmer surface below. The resulting broad spectral feature is readily distinguished from continuum at 8 and 12 μm, even with astronomical silicate filters. Experience with Viking IR Thermal Mapper data shows that the depth of the band relates directly to dust opacity, even as the atmospheric temperature profile is itself changed by the presence of dust. Infrared Thermal Mapper observations made during 1986–1988 showed that measurement at 7.8, 8.9, 9.5, 10.4, and 12.0 μm is sufficient to establish the shape and depth of the feature. Modern midinfrared array cameras now make the process of acquiring such data much more efficient, though the cameras are highly complex devices. Experience with Galileo support observations of Jupiter using several midinfrared camera systems has shown that imaging in selected bands can provide the accurate brightness temperatures needed to measure the broad dust and ice absorptions. A program to develop methods for the systematic mapping of atmospheric dust is under way, primarily at the IRTF.

As a bonus, water ice cloud absorption at 11–13 μm can also be mapped. Mars has recently been cold and clear enough that ice clouds have been more abundant. It is important to demonstrate the ability to measure these clouds for corroboration of microwave thermal measurements and HST-derived cloud parameters.

The first broad-scale dust opacity study of the martian atmosphere used the silicate band and spatial coverage of the Viking IR Thermal Mapper experiment [1]. The current effort follows directly from that approach. Martin is also using the MGS Mars Horizon Sensor (15-μm band) data for aerobraking monitoring and atmospheric characterization. The telescopic work meshes with periodic microwave measurements of the martian whole disk by R. T. Clancy that provide good atmospheric temperature profiles, but do not measure the dust amount directly.

Earth-based telescopic determination of martian dust and water ice cloud opacity, together with microwave measurements of atmospheric thermal state and the Viking thermal database, can be used to establish long-term climate variability, which is needed for modeling seasonal and interannual variation of thermal state and volatile transport. Such observations benefit martian dynamical studies and complement spacecraft mission experiments. The opacity derivation follows directly the successful Viking IRTM dust opacity mapping campaign and the similar ice cloud measurements done by Christensen and Zurek [4].

References: [1] Martin T. Z. (1986) *Icarus, 66,* 2. [2] Martin T. Z. and Richardson M. (1993) *JGR Planets, 98,* 10941. [3] Clancy R. T. et al. (1990) *JGR, 95,* 14543. [4] Christensen P. R. and Zurek R. W. (1984) *JGR, 89,* 4587.

TELESCOPIC MARTIAN DUST STORM ACTIVITY, 1971–1993. R. J. McKim, British Astronomical Association, Burlington House, Piccadilly, London, Great Britain W1V 9AG (mckim@oundle.northants.sch.uk).

Martian dust storms are among the most fascinating phenomena Mars has to offer to the telescopic observer [1–3]. In a major effort, the archives of national astronomical societies, observatories and private individuals were searched for new data [2,3]. In particular, much previously unpublished information was found in the archives of the British

Astronomical Association. These data have been combined with the results of a critical rereading of much of the original literature, coupled with discoveries from many new (especially non-English language) sources, as well as data from contemporary catalogs of storms, to create a complete narrative account of dust activity at every apparition from 1659 to 1993 [2–5]. A new summary catalog was also produced [5].

Several entries in existing lists are spurious, either being accounts of white diurnal clouds or duplicate records of a later stage of the same event. Some initiation sites of storms have also been wrongly stated in the past. For instance, the regional storm of November 1941 began not where de Vaucouleurs mapped it [6], but in northwest Hellas. Several intriguing regional events were logged during the 18th and 19th centuries. It was possible to demonstrate that the November 1924 Hellas storm at $L_s = 311°$ was truly a planet-encircling event, and at least one encircling storm has been overlooked in every list, although it was reported by the BAA [7], ALPO [8], SAF [9], and OAA, beginning south of Solis Lacus in July 1975, at $L_s = 270°$.

The epoch 1971–1993 was marked by an excess of planet-encircling storms in southern spring or summer (1971, 1973, and 1975, as well as 1977 and 1982 from Viking data). BAA data conclusively demonstrate that this epoch was unparalleled in this respect. All perihelic oppositions since 1877 have been well observed: the data have covered the appropriate L_s range, but there have only been a few encircling events. All perihelic apparitions from 1877 have exhibited at least one or more dust storms. The perihelic opposition series of the 1870s, 1890–1894, 1939–1943, and 1986–1990 contained no encircling events, but the series of 1907–1911, 1922–1926, 1954–1958, and 1971–1975 were notable for producing 1–3 telescopic encircling storms in each.

The general distribution of all dust events as a function of L_s varies on a timescale of decades. Successive 32-year epochs 1898–1929, 1930–1961, and 1962–1993 were chosen for comparison: in each time interval, Mars returned to the same place in the sky [3], and each contained a comparable number (51 ± 5) of events. All epochs showed more activity in southern spring and summer, but the first epoch had marked peaks of activity at approximately $L_s = 210°$ and 320°, the second a lower peak at $L_s = 240°$–270°, and the highest maximum of the third was at $L_s = 260°$. In the contemporary epoch the regional to local storm ratio was higher than in the first two, another indicator that Mars was more dusty in relatively modern times.

During 1971–1993, the most common emergence sites have varied both on the short and long terms. Thus, the Thaumasia/Solis Lacus/Valles Marineris region showed sporadic activity throughout the period, and was responsible for initiating all the encircling storms in 1973–1977 (Viking included). Libya was not active: it had produced local and regional events only between 1894 and 1958/1959 [2,3]. Hellas/Iapigia/E. Noachis was often active from 1971 to 1988, with a global event in 1971. Zephyria/Aeolis, the site of one regional storm each in 1704 and 1858, had again been active in 1969, but produced no telescopic events from 1971 to 1993.

Changes in classical albedo markings of Mars are additional indicators of dust activity and can give clues to emergence sites, even when the actual events have gone unobserved. Local activity in the Solis Lacus-Claritas region in July 1973 led to the development of an extensive low-albedo area, the "Claritas-Daedalia" darkening. It is highly likely that the new albedo differences coupled with the existing strong thermal inertia contrast in the region caused this site to be favored over northwest Hellas as the emergence source of the great encircling storms of 1973–1977. The region had returned to a high-albedo area by the mid-1980s and generated only local and regional events from then on. To the east of Syrtis Major, gradual dust deposition over Moeris Lacus and Nepenthes in the epoch of the 1960s (thus removing a source of albedo contrast) can be linked to the quiescence of the Libya site [3], formerly the most frequently active of all martian sites at the local and regional level [10].

By the late 1980s, Hellas was the most likely site for the emergence of a great storm, but in practice the latter region produced only some large regional events in the most recent series of perihelic oppositions (for example, in 1988) [11]. All the evidence of the last few apparitions seems to show that the martian atmosphere has become less dusty in southern spring and summer.

Of the purely telescopic events in the new catalog whose origins were well observed, 128 originated in or mostly affected the southern hemisphere, while 36 mostly affected the northern hemisphere (during 1704–1993). Telescopic detection of northern storms is difficult, for want of reference features. For example, Tempe exhibited activity in 1978 and 1982; historical parallels can be found in the 1930s, 1950s, and 1960s, but it was not active during every northern spring or summer. Polarimetry and multicolor CCD work could increase our knowledge of uncommon events such as the regional storm over Cebrenia/Elysium in 1993 [12].

Storm prediction is a very imprecise science. Examples of the repetition of some events from one apparition to another at closely similar L_s exist, but the pattern breaks down at the next. Dust deposition during the formation phase of the south polar cap, variable from apparition to apparition, must be of primary importance in controlling SPC regression, hence influencing the seasonal onset of great storms [3]. It may be the case that prediction of future major storms will long remain a matter of generalities based upon statistics.

References: [1] Kahn R. A. et al. (1992) in *Mars* (H. H. Kieffer et al., eds.), Arizona Univ. Press. [2] McKim R. J. (1996) *Sky & Telesccope, 92*, 8. [3] McKim R. J. (1993) *Bull. Soc. Astron. France, 107*, 312–315. [4] McKim R. J (1996) *J. Brit. Astron. Assoc., 106*, 185–200. [5] McKim R. J., unpublished data. [6] de Vaucouleurs G. (1954) *Physics of*

the Planet Mars, Faber & Faber. [7] Collinson E. H. (1978) *J. Brit. Astron. Assoc., 88*, 504–508. [8] Capen C. F. and Rhoads R. B. (1977) *J. Assoc. Lunar Planet. Obs., 27*, 63–76. [9] Dragesco J. (1978) *Bull. Soc. Astron. France, 92*, 3–17. [10] Slipher E. C. (1962) *The Photographic Story of Mars*, Northland Press. [11] McKim R. J. (1991) *J. Brit. Astron. Assoc., 101*, 265–283. [12] McKim R. J. (1995) *J. Brit. Astron. Assoc., 105*, 117–134.

WHAT HAPPENED TO CERBERUS? TELESCOPICALLY OBSERVED THERMOPHYSICAL PROPERTIES OF THE MARTIAN SURFACE.

J. Moersch, J. Bell III, L. Carter, T. Hayward, P. Nicholson, S. Squyres, and J. Van Cleve, Center for Radiophysics and Space Research, Cornell University, Ithaca NY 14853, USA (moersch@astro-sun.tn.cornell.edu).

Introduction: Historically, visible-wavelength telescopic, orbiter-based, and *in situ* lander observations of the martian near-surface environment have shown it to be a dynamic geologic setting. The most recent evidence of this comes from Hubble Space Telescope images taken during the 1995 [1,2] and 1997 [9] oppositions. These images reveal that several areas of the martian surface have undergone dramatic changes in appearance since the Viking landings. A striking example of current activity can be seen in the HST images showing Cerberus, a classically dark feature 1300 × 400 km in size, that has all but disappeared in recent years (Fig. 1). The most plausible explanation for the disappearance of Cerberus is that the region has been mantled with a high-albedo aeolian dust deposit. However, the thickness of the putative dust deposit is currently unknown.

When taken in time-series over the course of a martian day, thermal IR observations of Mars can be used to map the thermophysical properties (i.e., thermal inertia and albedo) of the surface. To date, this has only been done with one dataset, the Viking IRTM observations of the late 1970s [3–6]. In broad terms, areas of high thermal inertia and low albedo are interpreted to have a high rock-to-dust ratio, while areas of low thermal inertia and high albedo are thought to have a higher proportion of fines [7]. Viking IRTM maps of Cerberus indicate that it was an area of moderately high thermal inertia and low albedo in the 1970s. The recent HST observations clearly show that the albedo of Cerberus is now higher, although they offer no insight as to the present-day nature of the thermal inertia of the region. We seek to use our thermal infrared observations of Mars from the 1997 opposition to measure the current thermal inertia of Cerberus. In doing so, we hope to place limits on the thickness of the dust deposit that has masked the region in visible wavelengths.

Experiment: Using the SpectroCam-10 instrument on the Hale 200-in telescope at Palomar Observatory, we obtained an extensive set of images and spectra of Mars in the thermal infrared during the 1997 opposition. These observations were part of a several-year ongoing campaign to map the entire martian surface with SpectroCam [e.g., 8]. One specific goal of this year's observations was to collect a set of images of Cerberus, closely spaced in time, as it rotated from the morning limb to the evening limb. The near-perfect weather conditions at the observatory on the nights of March 5 and 6 (Universal Time) yielded image spatial resolutions of ~0.5 arcsec, the diffraction limit of the telescope at thermal IR wavelengths. Images were taken using a set of seven wide-band filters centered at 7.9, 8.8, 9.8, 10.3, 11.7, 12.5, and 17.9 μm at 18 times during the course of a local day at Cerberus. Images were flat-fielded, mosaicked, and map-projected to facilitate analysis.

Analysis: Figure 2 shows a time series of map-projected 11.7-μm thermal emission images of the Cerberus region from our March 1997 observations. Local times are given in the bottom right corner of each frame. The raw data have been ratioed to a featureless synthetic Mars image generated by a thermal model to remove much of the dawn-to-dusk contrast and enhance spatial inhomogeneities in the data. The dark "dot" in the upper left portion of most of the frames is Elysium Mons. South of Elysium Mons, running east-west

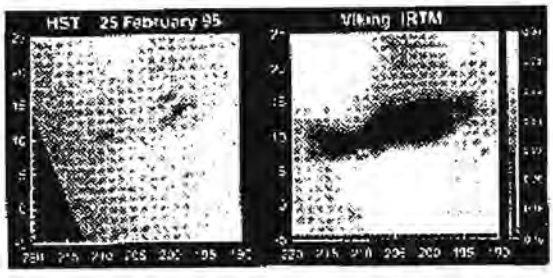

Fig. 1. Comparison of HST visible image and Viking albedo data for Cerberus. Taken from James et al. [1], courtesy S. Lee.

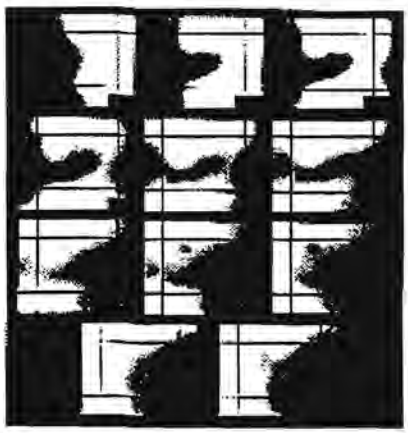

Fig. 2. Time series of 11.7-μm thermal emission images of the Cerberus region of Mars. The black rectangle in each frame shows the bounds of the Elysium quadrangle (0°–30°N and 180°–225°W).

across each of the frames, is Cerberus. Cerberus appears very dark compared to its surroundings in the morning hours and then gradually fades in contrast during the afternoon hours. Qualitatively, this is the signature of a relatively high thermal inertia region: it heats up more slowly in the morning than the surrounding low thermal inertia regions.

Discussion and Current Work: While the HST data show that Cerberus has disappeared as a visible-wavelength feature, our observations indicate that it remains clearly detectable as a high thermal inertia feature.

To obtain a more quantitative assessment of the current thermal inertia of Cerberus, we are currently resurrecting the Viking thermal model that was used to analyze the IRTM data. Heating/cooling curves from our observations of Cerberus will be compared to model-predicted heating/cooling curves for different albedo/thermal inertia combinations. The thermal inertia we derive for Cerberus will be compared to the Viking-era value, and a two-layer thermal model will be used to obtain a thickness (or, if the values are the same, an upper limit on the thickness) of the present day-dust mantle in the region.

References: [1] James P. B. et al. (1996) *JGR, 101,* 18883–18890. [2] Lee S. W. et al. (1995) *LPI Tech. Rpt. 95-04.* [3] Kieffer H. H. et al. (1977) *JGR, 82,* 4249–4291. [4] Palluconi F. D. and Kieffer H. H. (1981) *Icarus, 45,* 415–426. [5] Paige D. A. et al. (1994) *JGR, 99,* 25959–25991. [6] Paige D. A. et al. (1994) *JGR, 99,* 25993–26013. [7] Christensen P. R. (1986) *Icarus, 68,* 217–238. [8] Moersch J. et al. (1997) *Icarus, 126,* 183–196. [9] Bell J. F. III and Lee S. (1997), personal communication.

THERMAL EFFECTS OF THE NORTH POLAR HOOD OF MARS.

Y. Narumi, Kyushu-Tokai University, 9-1-1, Toroku, Kumamoto 862, Japan (narumi@skk-1.ktokai-u.ac.jp).

The purpose of this paper is to examine the thermal effects of the north polar hood on the heat balance of the martian polar region and compare these with the effects of the atmospheric dust cloud. We have calculated the diurnal variations of the atmospheric temperature, surface temperature, and subsurface temperature under the conditions of varying optical thickness of the polar hood and the atmospheric dust at the latitude of 60°N and at the season of the Solar Longitude $L_s = 180°$, which corresponds to the autumnal equinox of the northern hemisphere. In this calculation, we assumed that the polar hood is composed of H_2O ice particles. The main results are as following: (1) In the heavy dust case, the day-time atmospheric temperatures increase due to the absorption of the solar radiation. On the other hand, in the polar hood cases, the atmospheric temperature does not increase, because of little absorption of solar radiation by H_2O ice particles. (2) In the heavy dust case, the day-time surface

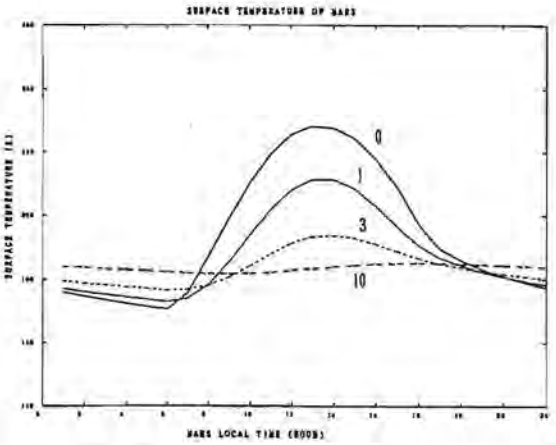

Fig. 1. Effect of dust particles. Latitude = 60°N; $L_s = 180°$. Optical thickness of dust = 0,1,3,10.

temperatures decrease greatly, because less solar radiation reaches the ground surface than in the no dust case (Fig. 1). In the polar hood case, the day-time surface temperatures are almost the same as those of the no cloud case. However, the nighttime surface temperatures are higher than those of the no cloud case (Fig. 2). This means that the polar hood has a conservative effect on the surface temperature (i.e., the greenhouse effect). (3) The above results may suggest that the development of the heavy polar hood over the north polar region works to delay the time of formation of the seasonal CO_2 cap during the fall and winter seasons.

The recession phases of the seasonal polar caps are well documented, while the deposition phases during fall and winter are almost unknown. The cap formation is obscured by the polar hoods, which makes observations difficult, particularly in the north. On the basis of the appearance of some albedo features beneath the polar hood clouds in red light, Iwasaki et al. suggested that the surface cap is only deposited at the vernal equinox [1]. To understand the sea-

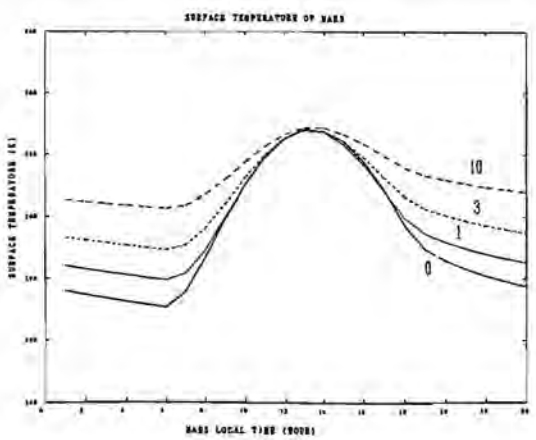

Fig. 2. Effect of polar hood. Latitude = 60°N; $L_s = 180°$. Optical thickness of H_2O ice = 0,1,3,10.

sonal behavior of the polar caps of Mars, it is important to consider correctly the thermal effect of the polar hood in the polar cap model. Furthermore, it is desirable to observe more precisely the polar region phenomena through the telescopic observations and the space probe exploration.

References: [1] Iwasaki et al. (1979).

TELESCOPIC OBSERVATIONS OF MARS, 1996–1997: RESULTS OF THE MARSWATCH PROGRAM PART II: CLOUDS. D. C. Parker, D. M. Troiani, D. P. Joyce, C. E. Hernandez, and J. D. Beish, Association of Lunar and Planetary Observers, P.O. Box 171302, Memphis TN 38187-130, USA.

A statistical analysis of data extracted from the ALPO records of 9650 visual and photographic observations of Mars made from 1969 to 1984 was undertaken by Beish. This Meteorology of Mars (MOM) study resulted in the publication of seasonal frequencies and trend analyses for each type of observed martian meteorology [1]. The study has now been extended through 1993 and includes 24,130 amateur and professional visual, photographic, and CCD observations covering a 29-year period. During the 1996–1997 Mars apparition, a significant percentage of the 2700 MarsWatch observations were of sufficient quality and spectral coverage for investigation of atmospheric phenomena. These data, extending through 155° L_s (11°–166°), will be compared with, and later included in, the MOM seasonal and trend analyses. A preliminary overview of these comparisons is presented here.

Discrete Clouds, Topographic and Orographic: As predicted for the seasons, the martian atmosphere exhibited numerous localized topographic and orographic clouds. These are identified by their shape, color, and general location. They tend to follow the diurnal rotation of the planet and are most often reported near historically cloudy regions and high mountainous areas [2]. Orographics over the Elysium shield were detected between 68° and 136° L_s, with peak intensities reported around 80° L_s. These clouds appeared somewhat later than they did during the 1994–1995 apparition and considerably later than in 1992–1993, when they appeared well formed by 28° L_s [3]. By northern midsummer no significant clouds were reported over Elysium. Orographic clouds over the Tharsis volcanos appear on HST images as early as 11° L_s. Groundbased images reveal these features intensifying after 70° L_s and becoming large and brilliant just before northern summer solstice. These clouds remained conspicuous throughout the bulk of the apparition and exhibited some confluence after 120° L_s. By 159° L_s the Tharsis region was free of clouds.

One remarkable example of a discrete topographic cloud is the Syrtis Blue Cloud, which circulates around the Libya Basin and across Syrtis Major, changing the color of this dark albedo feature to an intense blue. Originally named the Blue Scorpion by Fr. Angelo Secchi in 1858, this cloud usually makes its appearance during the early summer of Mars' northern hemisphere [4]. The cloud was prominent during the 1996–1997 apparition, but it made its appearance somewhat later than it had in 1995 [3]. It was extensively imaged by a number of observers between 66° and 115° L_s.

The Libya Basin was again the site of much localized cloud activity, with extensions westward across Syrtis Major and into Aeria being detected after aphelion by both groundbased observers and the HST. This is a likely cause of reported fading in Syrtis Major's intensity during the later stages of the apparition.

Hellas began to brighten after 67° L_s, becoming extremely bright, especially in the shorter wavelengths, by 80° L_s. Again, this appears to be slightly later than observed in 1994–1995. Hellas remained very bright until northern midsummer (143° L_s), when only thin hazes were reported over the basin.

Limb Clouds and Hazes: Both morning and evening limb/terminator clouds are most often observed in the martian tropical regions (± 20° areocentric latitudes). These clouds can be differentiated from limb/terminator hazes ("limb arcs") by their color and shape; they tend to have

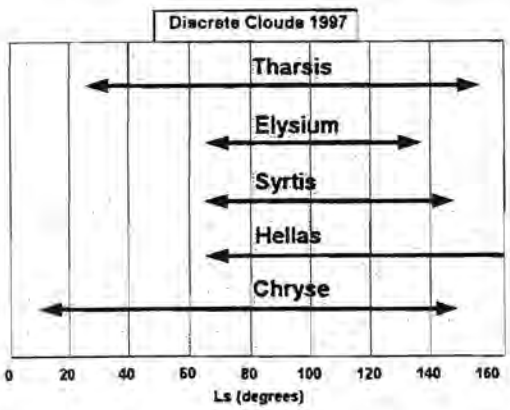

Fig. 1. Observed durations of discrete clouds, 1996–1997.

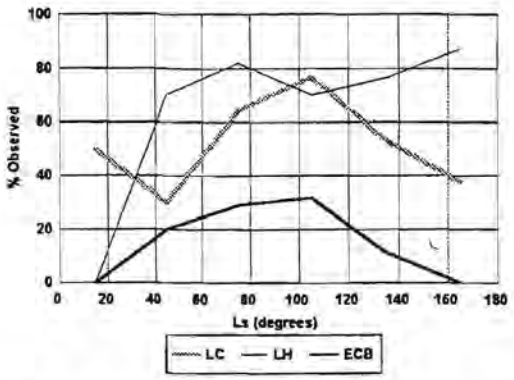

Fig. 2. Observed occurrences of limb clouds (LC), limb hazes (LH), and equatorial cloud bands (ECB), 1996–1997.

discrete boundaries, exhibit a variety of shapes that often conform to local topography and are usually brighter in shorter wavelengths. The size and frequency of limb clouds appear to be related to the regression of the northern, rather than the southern, polar cap [1]. In 1997 both limb arcs and limb clouds were prominent after aphelion, but the limb clouds rapidly decreased in frequency after 105° L_s, while the limb hazes became more numerous and conspicuous throughout the northern summer (Fig. 2). These trends are in agreement with the findings of the MOM study [1].

Equatorial Cloud Bands: Rarely observed are the Equatorial Cloud Bands (ECBs). ECBs appear as broad and diffuse hazy streaks usually observed within ± 20 degrees of the martian equator. Until recently, cloud bands were most often observed during the martian northern summer, but systematic tricolor CCD imaging and HST observations have revealed that these wisps may be more frequent than previously recognized and may occur in all martian seasons. These ephemeral clouds appeared to increase during the 1992–1993 and 1994–1995 apparitions [3,5]. It was not clear, however, whether this was due to a real prevalence or merely the result of better detection methods, such as CCD imaging. During the 1996–1997 apparition the ECBs were observed somewhat more frequently than during previous two apparitions, but the number of observations was insufficient for statistical analysis. Their incidence in 1997 appeared to parallel that of limb clouds (Fig. 2), raising the possibility that limb clouds are actually continuations of ECBs.

Arctic Clouds: Arctic clouds were less conspicuous than in the early 1980s. They were sighted as early as 48° L_s but became more prominent around aphelion, peaking around 90° L_s, and persisting into northern midsummer.

Summary: The martian cloud observations of 1996–1997 support the findings of the MOM studies that there is a marked proclivity for limb clouds and discrete clouds to appear during northern spring and summer. The much lower incidence of white clouds during southern spring and summer agrees with Mars' known asymmetry in water vapor abundance [6,7]. It should be pointed out, however, that the apparitions most favorable for studying these martian seasons were 1971 and 1973, years of global dust storm activity, which reduced the chances of observing other clouds throughout much of the southern spring and summer. However, reduction of the considerable data from the 1986 and 1988 apparitions [8] reveals that there is indeed much less discrete and limb cloud activity in southern spring and summer than there is during these seasons in the north. Even the orographic "W clouds" in 1986 (200°–220° L_s) were neither so numerous nor so long-lived that they would be able to alter the dominance of the "more usual" northern spring/summer meteorology in this survey. The 1988 apparition displayed even fewer clouds, despite a record number of experienced observers participating in the meteorological survey.

References: [1] Beish J. D. and Parker D. C. (1990) *JGR, 95,* 14657–14675. [2] Smith S. A. and Smith B. A. (1972) *Icarus, 16,* 509–521. [3] Troiani D. M. et al. (1996) *JALPO, 39(1),* 1–15. [4] Antoniadi E. M. (1930) *La Planete Mars, 1659–1929.* [5] Troiani D. M. et al. (1995) *JALPO, 38(3),* 97–113. [6] Farmer C. B. and Doms P. E. (1979) *JGR, 84,* 2881–2888. [7] Jakosky B. M. and Farmer C. B. (1982) *JGR, 87,* 2999–3019. [8] Parker D. C. et al (1989) *Sky and Telescope, 77(4),* 369–372.

DETECTABILITY LIMITS OF VOLATILE-BEARING MINERALS ON MARS: LABORATORY AND THEORETICAL CONSTRAINTS.

T. L. Roush[1,3], J. B. Orenberg[1], A. Banin[2], and S. White[3], [1]Mail Stop 245-3, San Francisco State University and Mail Stop 245-3, NASA Ames Research Center, Moffett Field CA 94035-1000, USA (roush@barsoom.arc.nasa.gov), [2]Department of Soil and Water Sciences, Hebrew University, P.O. Box 12, Rehovot 76100, Israel, [3]Mail Stop 234-1, NASA Ames Research Center, Moffett Field CA 94035-1000, USA.

Background: Characterization of the mineralogy and distribution of aqueous alteration products on Mars (for example, clays, carbonates, sulfates, nitrates, phosphates, etc.) provides direct information regarding the past and present climate [1,2]. Such information is crucial for addressing issues such issues as whether the martian environment was amenable to the development of life. Remote sensing spectroscopic observations can be used to determine surface mineralogy. However, in many cases the minimum detectability limits of minerals of interest remain poorly defined. Here we report the results of a study designed to investigate the detectability limits of various salts when contained in a nominal Mars soil analog matrix. Our study includes meas-urements of the reflectance of both physical and chemical mixtures covering the 0.25–25-μm wavelength region.

Laboratory Samples Studied: There are numerous analogs for the martian soils [3,4]. For the physical mixtures we use a matrix that consists of 85 wt.% palagonite (P), a weathering product of basaltic glass from the island of Hawai'i, and 15 wt.% Fe-substituted montmorillonite (FeM), where the interlayer cations have been chemically replaced with Fe [5,6]. To this matrix material we physically mixed low and high concentrations of $CaCO_3$ (1.5 and 3.0 wt.%), $MgSO_4$ (4.8 and 13.0 wt.%), $NaNO_3$ (0.5 and 1.0 wt.%), and KPO_4 (0.25 and 0.5 wt.%) both individually and collectively. The salt concentrations were selected based upon results of previous Viking analyses and spectroscopic studies [3,7]. For the chemical mixtures, we began with a Hawai'ian palagonite and added varying amounts of sulfuric, hydrochloric, and nitric acids. The palagonite was allowed to react with the acids for 7 days and the mixtures were then air-dried for 15

days at room temperature. Final drying was done at 40°–60°C for 1–2 days[7].

Experimental Spectral Measurements: Reflectance spectra were obtained using two different spectrometers. A Perkin-Elmer Lambda 9 spectrometer, equipped with a Labsphere DRTA-9 integrating sphere, was used to obtain data in the 0.25–2.5-μm wavelength region (vis-near-infrared) and a Nicolet Model 550 Fourier transform infrared spectrometer, with a Praying Mantis diffuse reflectance attachment, was used to obtain data in the 2.15–25-μm wavelength region (fir). In the vis-near-infrared region, samples were placed in a stainless-steel planchet, covered with a quartz window, and mounted vertically in the integrating sphere; the reflectance standard was spectralon. In the fir the samples were placed into the horizontal sample cup and the reflectance standard was a diffuse Al surface. Because of the distinctively different instrumental geometries, no attempt has been made to scale the vis-near-infrared data to the fir data.

Theoretical Mixtures: Using reflectance measurements [8,9], a linear mixing model was used to investigate detectability limits of salts, calcite, siderite, anhydrite, and jarosite when mixed with major phases, palagonite, montmorillonite, and FeM.

Results, Physical Mixtures: In the vis-NIR wavelength region, visual inspection of the resulting spectra indicates a subtle increase of the overall reflectance at the highest concentrations of sulfate and all the salts mixed together. In the fir distinctive spectral features are visually observed for carbonate and sulfate salts at all concentrations when they are present, but no distinctive spectral features are seen for the nitrate or sulfate. Additional spectral analyses are planned to investigate whether subtle spectral features will help identify the presence of the nitrates and sulfates.

Chemical Mixtures: We are currently collecting the vis-near-infrared data for analysis. In the fir, the reflectance spectra of the acid-leached samples exhibit spectral signatures of sulfate and carbonate created during the acidification processes.

Theoretical Mixtures: These calculations indicate that the presence of 10% of the salts can be readily identified in the spectrum in both the vis-NIR and fir wavelength regions.

Summary: Our results for the theoretical and physical mixtures suggest that concentrations of carbonate and sulfate, consistent with limits imposed by previous telescopic spectroscopic, chemical, and petrologic analyses, can be detected. For the nitrate and phosphate samples studied here it appears that the concentrations, consistent with previous chemical and analytical studies used, do not give rise to readily observed spectral features. Although we have not performed calculations that consider the influence of thermal emission from Mars' surface, our results for carbonates are consistent with previous studies [10]. More complete analyses of the acid-leached samples are required to characterize the abundance and phases of the reaction products prior to defining detectability limits of these samples.

Acknowledgments: This research is supported by NASA's Exobiology Program via RTOP 185-52-62-07.

References: [1] Fanale F. et al. (1992) in *Mars* (H. Kieffer et al., eds.), Univ. of Arizona. [2] McKay C. et al. (1992) in *Mars* (H. Keiffer et al., eds.), Univ. of Arizona. [3] Banin A. (1996) *Adv. Space Res., 18,* 12233. [4] Roush T. et al. (1993) in *Remote Geochemical Analyses: Elemental and Mineralogical Composition* (C. Pieters and A. Englert, eds.), Cambridge Univ. [5] Orenberg J. and Handy J. (1992) *Icarus, 96,* 219. [6] Roush T. and Orenberg J. (1996) *JGR, 101,* 26111. [7] Banin A. et al. (1997) *JGR, 102,* 13341. [8] Clark R. et al. (1993) *USGS Digital Spectral Library, Open File Report 93-592.* [9] Salisbury J. et al. (1991) *Infrared (2.1–25 μm) Spectra of Minerals,* Johns Hopkins Univ. [10] Wagner C. and Schade U. (1996) *Icarus, 123,* 256.

PATHFINDER IMAGING. P. H. Smith, Lunar and Planetary Lab, University of Arizona, 1629 E. University Avenue, Tucson AZ 85721, USA (psmith@lpl.arizona.edu).

On July 4, 1997, the Mars Pathfinder lander bounced onto the Ares Vallis flood plain, opened its petals, and began taking pictures and returning them to Earth. A live TV link broadcast the images to millions of viewers around the world and, for the first time since the two Viking missions in July 1976, an enthusiastic public was able to explore the surface of Mars. The spacecraft, sitting in a slight depression, was surrounded by ridges toothed with rounded boulders beyond which a rock-strewn plain stretched to two low hills on the horizon. Toward the south a low ridge signified the rim of an impact crater. Low ridges and valleys both parallel and perpendicular to the known flow direction of the ancient catastrophic flood were easily seen in the stereoscopic views available from the Imager for Mars Pathfinder (IMP).

The first IMP goal was to help the Sojourner Rover egress off the lander petal. These images were gathered in the stowed position that IMP was locked into during the cruise to Mars. A complete stereoscopic panorama and a so-called insurance pan were obtained from this perspective (about 1 m above the surface). The insurance pan was stored in the spacecraft computer memory in case the IMP failed on deployment. Although it was originally expected to be erased on successfully deploying, the higher-than-expected data rate allowed it to be returned. Now it is being used as part of a low-high stereo view to give accurate distances to objects further than 30 m.

After deploying the mast, the IMP was nominally at a height of 1.8 m above the local surface and a monster pan was obtained that gave four-color panoramas of the middle tiers

around the lander and a high-quality red stereo view. This was augmented later by a gallery pan that extended the color to all four tiers. The resolution of these panoramas is 1 mrad/pixel and the field of view is 14° square. The details of the camera design and calibration have been reported [1], and the actual performance on Mars seems to be within the expected ranges.

At the end of the nominal 30-day mission, there was an unexpectedly high data volume for the next 60 days. The science team has decided to do a complete super pan, or a compressed set of hyperspectral cubes that includes images from each of the 15 filters that can be used for surface imaging. Three of these filters are left-right pairs that give the stereoscopic information and allow for the construction of true-color stereo panoramas. By September 10, 1997, three-quarters of this super pan was available on the ground, with the final portions expected by the time of the meeting in early October.

Early results from the spectral imaging show that four spectrally separable types of soil and three types of rock have been identified. One surprise is the absence of clear hematite signatures anywhere on the scene; these have been seen from space. In addition, pyroxene bands are not in evidence, although slight dips near 0.9 μm are sometimes seen.

Looking up with IMP has given us an excellent view of the haze layers and clouds. Eight low-transmission, narrow-band filters are used for imaging the Sun. Preliminary results show that the daytime opacity is about 0.5 optical depths with about a 10% variation between days. Tracking stars at night has shown that the early morning opacity is about 0.25 larger. Sunrise sequences reveal clouds in the predawn that were never seen by Viking. These thin clouds "burn" off by noon and sunset images are cloudless.

Observations of the sky near the Sun and at increasing angles away from the Sun give us the ability to measure the scattering properties of the haze and to model the sizes of the aerosols. The best models show sizes near 1 μm, much less than the value of 1.85 μm measured from Viking [2].

References: [1] Smith P. H. et al. (1997) *JGR, 102,* 4003–4025. [2] Pollack J. B. et al. (1995) *JGR, 100,* 5235–5250.

SPECTROSCOPIC MEASUREMENTS OF WATER VAPOR IN MARS' ATMOSPHERE.

A. L. Sprague, R. E. Hill, D. M. Hunten, and B. Rizk, Lunar and Planetary Laboratory, University of Arizona, Tucson AZ 85721-0092, USA.

We report partial results of systematic measurements of water vapor abundance in the martian atmosphere. As in our previous work [1,2] measurements are made with the LPL echelle spectrograph on the 1.5-m telescope at the Catalina Observatory, a short distance north of Tucson (see Table 1). For this report we include observations made between October 4, 1996, and July 12, 1997, just eight days after the landing of Mars Pathfinder (see Table 2). It is a happy state of affairs that we have two independent, Earth-based datasets of water vapor measurements at the Pathfinder landing site for July [2,3]. The two groups have agreed upon similar data-reduction methods. This decision was in part facilitated by the Mars Telescopic Observations Workshop II. Both groups will use the FORTRAN program written by Rizk and Hunten (colabunh2.f) for converting equivalent widths to zenith column abundances. A uniform method of weighting the airmass by the measured intensity profile is now being used. Several measurements were made, including measurements of the Pathfinder landing site. These are clearly indicated in the tables. Measurements at the Pathfinder site do not coincide with the IMP measurements in local time or calendar date.

Table 3 gives a comparison of water vapor measurements for July 12, 1997, using two slightly different methods of calculating the airmass corrections. In the analysis of Sprague et al. [2] and the preliminary abstracts for this workshop, airmasses were weighted by the full extent of intensity profile. This included most of the seeing smeared "wings" (Method 1). Following the Mars Telescopic Observations Workshop II, a simple improvement was made in the technique and was adopted by both Barker and Sprague et al. (Method 2). As an

TABLE 1. Observations of martian water vapor abundance.

Date	Time h	Time m	L_s	Slit Geometry	MPF Site?	Arcsec Diam.	Doppler Shift (Å)
1996							
Oct. 4, #44	11	34	18.5	EW	no	4.9	−0.32
#45	11	55		NS	no		
Dec. 3, #38	10	30	45.9	EW	YES	6.5	−0.44
#49	11	42		NS	YES		
1997							
Jan. 2, #29	09	45	59.1	NS offset +2"	YES	8.3	−0.45
#42	11	44		NS offset −2"	no		
Feb. 1, #35	09	58	72.3	EW	no	10.7	−0.38
#46	11	55		NS	no		
Feb. 15, #33	08	56	78.4	EW	YES	12.1	−0.31
#48	10	48		NS	YES		
May 5, #21	05	09	113.7	NS	no	11.1	0.32
May 29, #7	04	34	124.9	NS	no	9.3	0.35
#16	06	08		EW	no		
June 22, #14	03	20	137	NS	no	7.9	0.35
#19	04	04		EW	no		
July 12, #14	03	19	146.4	NS offset −1"	YES	7.9	0.33
#15	03	32		EW	YES		

TABLE 2. Water vapor abundances in the martian atmosphere: October 4, 1996–July 12, 1997.

Date		L_s	Slit	MPF	Equiv.
Abun.		Direc.	Site?	Width	ppt μm
1996					
Oct. 4					
#44	18.5	EW—E	no	3.8	19
		a.m.		2.7	16
				3.7	20
		W, p.m.		4.7	9
#45		NS—N	no	<1	< 3
				2.7	15
				<1	<5
		S		1.5	6
Dec. 3					
#38	45.9	EW—E	**YES**	2.0	4
		a.m.		1.2	7
				1.5	7
		W, p.m.		2.7	10
#49		NS—N	**YES**	1.1	4
				2.2	12
				1.1	6
		S		1.2	5
1997					
Jan. 2					
#29	59.1	NS—N	no	4.2	8
		offset+2"		3.6	12
				2.7	10
				1.3	4
		S		< 1	1
#42		NS—N	**YES**	4.3	18
		offset-2"		3.5	20
				2.3	13
				2.2	12
		S		2.5	9
Feb. 1					
#35	72.3	EW—E	no	1.8	8
		a.m.		1.5	9
				3.5	22
				3.1	17
				3.2	13
		W, p.m.		3.0	4
#46		NS—N	no	6.7	29
				5.9	34
				2.9	17
				3.3	19
				2.6	13
		S		2.6	8
Feb. 15					
#33	78.4	EW-E	**YES**	2.5	10
		a.m.		2.0	11
				3.2	20
				3.1	19
				3.7	21
				3.8	16
		W, p.m.		4.4	7
continued					
#48		NS-N	YES	7.3	31
				8.0	49
			4.6	28	
			1.5	9	
			0.5	3	
			0.4	2	
		S		<<1	<<2.7
May 5					
#21	113.7	NS-N	NO	11.3	51
				8.4	48
				4.7	28
				3.4	20
				2.3	13
				1.6	7
		S		3.5	10
May 29					
#7	124.9	NS-N	NO	8.5	35
				6.1	33
				2.4	13
				1.3	7
				1.2	5
				2.1	7
#16		EW-E	NO	5.5	4
		a.m.		3.1	10
				3.2	17
				1.1	7
				2.7	16
		W, p.m.		4.1	19
June 22					
#14	137	NS-N	NO	8.6	33
				6.2	32
				4.4	25
				3.3	18
				1.6	8
				1.3	4
#19		EW-E	NO	5.2	4
		a.m.		4.2	14
				3.7	19
				3.6	21
			5.0	32	
		p.m.		4.9	23
July 12					
#14	146.4	NS-N	YES	5.4	12
		offset-1"		4.7	19
				5.6	28
				4.3	19
		S		2.8	8
#15		EW-E	YES	4.2	4
		a.m.		3.9	15
				5.8	27
				4.7	32
		W,p.m.		5.6	23

TABLE 3.

Pathfinder Site Comparison			Method 1 Prior to Workshop			
July 12	L_s	Slit Direc.	Eq. Width	Column Abund ppt μm	Avg. lat.	Avg. long.
#14	146.4	NS—N	5.4	12	-22	39
		offset	4.7	19	3	37
		-1"	5.6	28	25	39
			4.3	19	45	45
		S	2.8	8	66	69
#15		EW—E	4.2	4	16	76
		a.m.	3.9	15	23	48
			5.8	27	25	23
			4.7	32	23	359
		W p.m.	5.6	23	17	334
Pathfinder Site Comparison			Method 2 Uniform: Barker/Sprague et al.			
July 12	L_s	Slit Direc.	Eq. Width	Column Abund ppt μm	Avg. lat.	Avg. long.
#14	146.4	NS—N	3.2	8	-24	39
		offset	4.5	20	2	37
		-1"	5.5	27	25	39
			5.3	22	46	45
		S	5.9	12	67	73
#15		EW—E	4.9	4	15	79
		a.m.	4.2	16	23	49
			4.8	29	25	24
			5.1	32	23	358
		W p.m.	4.7	23	16	332

example for study and comparison, we chose two frames from July 12, 1997, following the landing of Pathfinder. The landing site is in the images chosen, but the sector averages are somewhat large for an accurate portrayal of the column abundance localized at the site itself. Future reduction will allow a better estimate for the smaller, more localized region. An important result of this comparison between methods is that differences are small, allowing intercomparison with earlier datasets of Sprague et al. and Barker.

References: [1] Rizk B. et al. (1991) *Icarus, 90,* 205–213. [2] Sprague A. L. et al. (1996) *JGR, 101,* 23229–23241. [3] Barker.

TELESCOPIC OBSERVATIONS OF MARS, 1996–1997: RESULTS OF THE MARSWATCH PROGRAM I: SURFACE AND DUST.

D. M. Troiani, D. P. Joyce, D. C. Parker, C. E. Hernandez, and J. D. Beish, Association of Lunar and Planetary Observers, P.O. Box 171302, Memphis TN 38187-1302, USA.

MarsWatch '97: The MarsWatch program was reinitiated in electronic form through the collaboration of astronomers at Cornell University, the JPL Mars Pathfinder Project, and the Mars Section of the Association of Lunar and Planetary Observers (ALPO) as a vehicle through which Mars astronomers worldwide could upload their observations to a World Wide Web home page and archive site at JPL. To date, MarsWatch and the Mars Section of ALPO have received more than 2700 observations from 70 observers in 14 countries. Some of this research is already in place on the MarsWatch Web site. Approximately 41% of these observations are CCD images made through standard filters covering a spectral range from 330 to 820 nm. In addition, a large number of quality visual observations were performed through standard color filters, permitting more accurate assessments of atmospheric phenomena. The apparition coverage extended through 155° L_s (11°–166°), permitting monitoring of the northern hemisphere spring/summer meteorological activity, north polar cap (NPC) behavior, and albedo feature changes.

Surface Features: Cerberus-Trivium Charontis (197°W, 12°N) remained very weak throughout the apparition. This feature, once very conspicuous, has been indistinct since 1984, with occasional variations in intensity. On the northwest side of the Elysium shield, the "Hyblaeus Extension" (225°–255°W, 42°N) was prominent, as it has been since first detected by ALPO astronomers in 1977. Toward the end of the 1996–1997 apparition (L_s = 153°), however, this feature appeared to increase in both breadth and intensity.

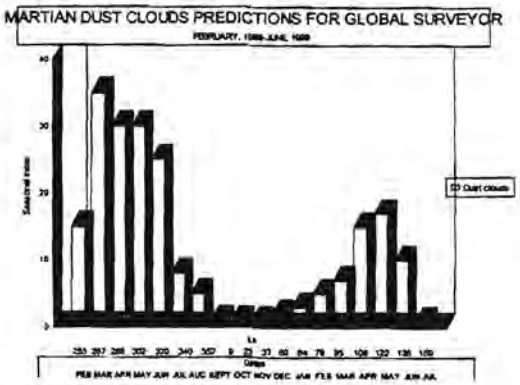

Fig. 1. The above chart shows the ALPO Mars section dust clouds prediction for NASA Global Surveyor. When the spacecraft commences regular imaging next March, Mars will be at the height of its dust season. While dust storms can occur during any martian season, there are two main peaks of activity as shown in the above chart. High dust activity just a month before the prime mission starts imaging Mars is predicted. This is reminiscent of the Mariner 9 global dust storm. The 1973 dust started at L_s = 300° and in March 1998 we will be at L_s = 285°. Global dust is very rare, but we do expect to see a few strong dust storms at this time. The seasonal index is a simple index and graphically indicates the average departure from the "normal" for any given martian subseason. It is arbitrarily set so that the average value for all 12 subseasons is 1. Thus, a subseason with a seasonal index of less than unity has fewer clouds than "normal," and a index >1 reveals a higher than expected number. This index was calculated for both the raw numerical values and for the probabilities (the number of cloudy/dust degrees L_s observed relative to the total degrees L_s observed). Chart prepared by D. M. Troiani.

The Syrtis Major (290°W, 10°N) remained dark and conspicuous throughout the apparition, although some observers reported a weakening around 130° L_s. CCD images in blue and violet light revealed the presence of cloud bands across Syrtis Major, even at local noon, as early as 82° L_s. Classically, Syrtis Major broadens after 90° L_s, but no evidence of this was detected. This agrees with data obtained from the 1992–1993 and 1994–1995 apparitions [1–3].

The Thoth-Nepenthes complex, which lies east of the Syrtis, remained virtually undetectable, as it has since 1980.

Solis Lacus (85°W, 26°S) remained dark and elongated in the east-west direction. Despite more foreshortening, it appeared much as it had during the previous apparition, while in 1990 this feature exhibited a north-south orientation, even when corrections were made for the smaller De.

The North Polar Region: The regression of the north polar cap (NPC) has been determined from numerous red-light CCD images and is presented in this symposium [4]. The Rima Tenuis was not detected during this apparition, despite Mars' favorable earthward tilt. This could be because at first there was rapid cap regression, but it reverted back to normal by December. The Rima Tenuis is usually visible when there is a consistently rapid regression of the NPC.

With the recent revelations from the HST images that show several dust streaks crossing the cap, we may have to rethink our theories for the Rima Tenuis. The variations in the C. M., shape, and the aberrant sightings of the Rima Tenuis over the years make a good case for polar dust activity. Can it be that the Rima Tennis is a NPC dust event? The Rima does vary in C. M. from 330°–336°. It has been detected with conventional photography, CCD imagery, and CCD-chip video. Both HST and Parker images of the NPC dust in the fall of 1996 show dust cutting across the cap. When the Rima Tenuis is first observed, it is usually just a notch in the cap that later develops into a fissure across the cap. This is very similar to what the fall 1996 NPC dust event appears like in the pertinent images. Also it is best to image the Rima Tenuis in integrated light, but it has been imaged through red light a few times. Because it is an inconspicuous object, it is best not to use a filter with small telescopes.

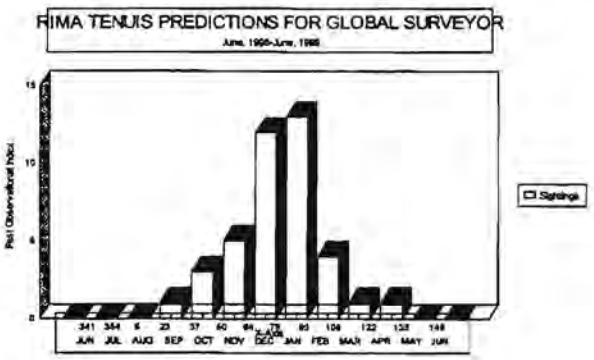

Fig. 2. This chart shows the ALPO Mars section predictions for when the Rima Tenuis might next be visible. Both the G. S. and HST have the opportunity, along with groundbased observers, to look for it. This will be the last chance to hunt for it until 2007. If we can confirm that the Rima Tenuis is an NPC dust event, then we can go back to look at past observations and study the long-term variation of NPC dust clouds. Chart prepared by D. M. Troiani.

The classic NPC outliers, Ierne, Lemuria, and Cecropia, were reported by a number of observers, but these features were less conspicuous than in 1995.

Dust: Groundbased observers did not report any definite dust cloud activity during most of the apparition. There were sporadic reports of brightening in Chryse, but these are fairly normal for the season and exhibited no characteristics of significant dust events.

Chryse has been very bright in red light from time to time since the early 1980s. No major dust storms have occurred, though some dust interspersed with white clouds possibly have. Evening and morning clouds apparently injected with dust may be the cause of a number of false reports of dust storms. The dust devil activity observed by Pathfinder may be at least a partial source of this dust. Chryse has been heavily saturated with this fine dust for the last two decides.

The dust storm of June 27, 1997, detected over the Valles Marineris by the HST, bore a striking resemblance to two localized dust storms of early October 1990 (309° L_s) and early November 1990 (326° L_s) [5]. While the 1990 storms happened at $L_s = 320°$, at the height of the Mars dust season, the 1997 storm occurred at $L_s = 126°$, which is near the end of the secondary, less intense dust season. During the 1996–1997 apparition, MarsWatch astronomers detected no discernible changes in surface morphology after this dust event.

References: [1] Troiani D. M. et al. (1995) *JALPO, 38(3),* 97–113. [2] Troiani D.M. et al. (1996) *JALPO, 39(1),* 1–15. [3] Lee S. W. et al. (1995) *LPI Tech. Rpt. 95-01,* 19. [4] Iwasaki K. et al. (1997) NPC regression papers to be presented at MTO-II. [5] McKim R. (1992) *JBAA, 102(5),* 248-264.

INFRARED SPECTROSCOPY OF MINERALS: WHAT COULD OUR LAB CONTRIBUTE TO THE INTERPRETATION OF MARTIAN SPECTRA?

C. Wagner, Institute of Planetary Exploration, German Aerospace Research Establishment (DLR), Rudower Chaussee 5, D-12489 Berlin, Germany (christoph.wagner@dlr.de).

Spectroscopy in the infrared region is a well-established method for investigating the mineralogical composition of planetary surfaces. The spectral information derived from telescopic observations usually must be interpreted on the basis of spectral measurements in the laboratory, because of the complex processes that control the photons' interaction with the surface layer material. A lot of pioneering work in lab spectroscopy has been done in the United States and is still

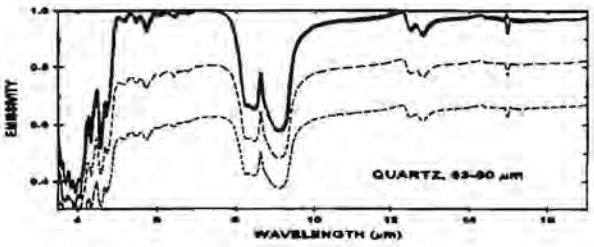

Fig. 1. The temperature-corrected spectra (dotted curves) of the two thick samples (1.636 and 0.248 gcm^{-2}) coincide with the spectrum of the thin sample (0.049 gcm^{-2}, solid line). The dashed line is the spectra of the thick samples, as measured. The feature at 15 µm is artificial and should be omitted in all figures.

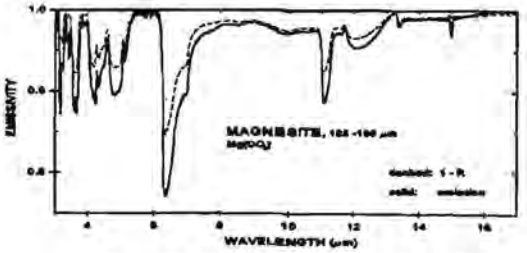

Fig. 3. Emission spectrum compared to 1-R.

continued there. Nevertheless, there are still many unresolved problems, and the wealth of new data from space missions will also require much supporting experimental work to answer new questions. Thus, in the hope of future cooperation, our experimental techniques and a few results are presented.

Reflectance Spectra: We use a FT-spectrometer (Bruker IFS88) operating in the wavelength range from 0.5 to 50 µm. It is purged with dry air. For measuring reflectance spectra, a commercial reflectance attachment is used. It realizes a symmetric biconical geometry (i = e = 18...50°, cone angle $\Omega = 0.087$ sr). The illumination spot at the sample is 1–2 mm in diameter. For coarse grain fractions, a rotating sample cup is used for "averaging," i.e., to avoid the incident radiation being reflected by only a single or a few sample grains. The sample is measured at room temperature and atmospheric pressure. Our work is aimed at (1) collecting spectra of well-characterized minerals and rocks and (2) understanding spectral differences as a result of (a) grain size or porosity influence and (b) mineral mixing.

Emission Spectra: For measuring emission spectra, the particulate sample is located in an Al-cup and heated from below to a constant temperature of 90°C. The radiation emitted by the sample (or a calibrated blackbody, respectively) normal to the surface is collected by a parabolic off-axis mirror and reflected to the entrance port of the spectrometer. The emissivity of the sample is obtained by ratioing the background-corrected signals obtained for the sample, and for the reference blackbody [e.g., 1]. For a thick sample of particulate minerals, however, the vertical temperature gradient is larger than for the blackbody (a 6-mm-thick Cu disk with a Nextel Velvet Coating). Therefore, a systematically too-low emissivity would be obtained. According to the common practice [1–7], this systematic error is corrected by a fit procedure. It is assumed that the sample approaches a known maximum emissivity (usually 1.0) somewhere in the measured spectral range. At this wavelength, a Planck curve is fitted to determine the actual sample temperature, and then the emissivity of the sample is scaled to that of the blackbody [5]. Fortunately, for many minerals the assumption $\varepsilon = 1$ is justified at the materials' Christiansen wavelength, i.e., where $n(\lambda) = 1$. Another approach to get the true emissivity is keeping the temperature gradient low within the sample by using a very small sample thickness.

The results of both methods practically agree, as Fig. 1 shows for a quartz sample. Using a thin sample may be advantageous if only a small quantity of material is available, or when no fitting point is known. Erroneous spectra due to an insufficient optical depth are possible, but they result only if the sample thickness falls below a minimum value, as is evident from Fig. 2, which shows emission spectra of a carbonate for varying sample thickness. Only for the thinnest sample (0.029 gcm^{-2} or 0.19 mm, dashed curve) is a differing

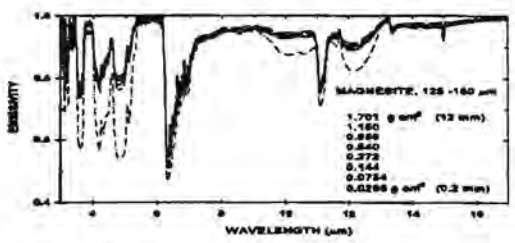

Fig. 2. Emission spectra for varying sample thickness.

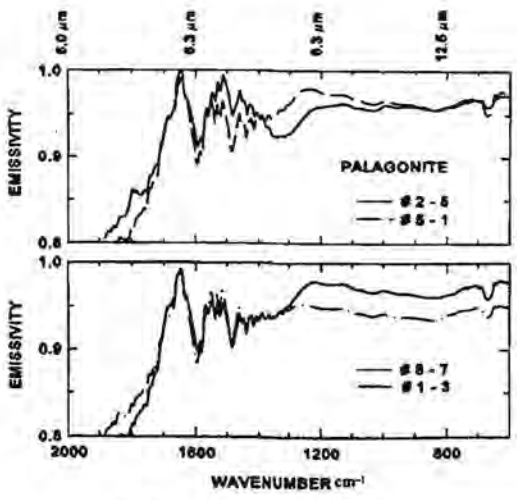

Fig. 4. Emission spectra of four palagonites.

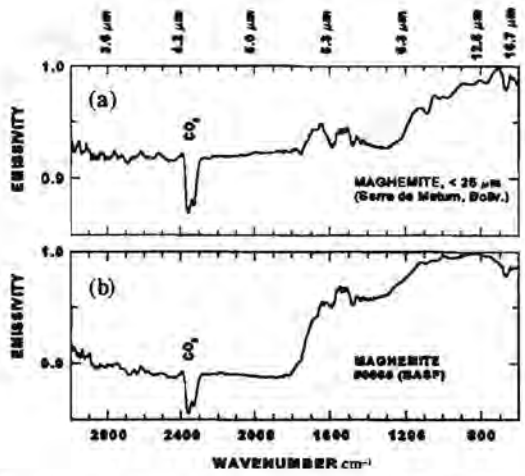

Fig. 5. Emission spectra of (a) a natural and (b) a synthetic maghemite sample.

spectrum obtained, whereas the spectra of the thicker samples practically agree. A comparison of the measured emission spectra with the spectra computed from our reflectance data via Kirchhoff's law, $\varepsilon = 1\text{-}R$, is questionable because not the entire reflected flux is collected [5,8]. Whereas Clark et al. [9] found good agreement for comparison with biconical data "within the sample set limitations," our measurements show a significant difference in the stronger bands (cf. Fig. 3), which we found being "deeper" for the emission spectra than for 1-R. It should be noted, however, that the biconical measurements of Clark et al. [9] integrated about 50% of the hemisphere, compared to less than 2% in our biconical measurements. A tentative explanation for the observed difference is the vertical temperature gradient in our samples, combined with the wavelength-dependent opacity. As known [4,10], the measured emission spectrum is controlled not only by the variation in emissivity, but additionally also by the brightness temperature, which varies with the wavelength as well. But a quantitative treatment for this special case is missing still.

Figure 4 shows emission spectra of four palagonites (Pahala ash, HI), grain size <25 µm, after heating the samples for 70 hr at 90°C, and Fig. 5 shows emission spectra of a natural and a synthetic maghemite. Moreover, measurements were carried out for several further silicates, carbonates, and a few sulfates, partially for various grain sizes. Although our present equipment does not allow measurements at low pressure, as is actually required for a realistic simulation of the martian environment [11,12], we believe that it still may be useful for some supporting investigations concerning Mars.

Acknowledgments: I thank R. Wäsch for providing and preparing the mineral samples and A. L. Sprague for the invitation to present our results at the MTO-II workshop.

References: [1] Henderson B. G. et al. (1996) *JGR, 101,* 14969–14975. [2] Conel J. E. (1969) *JGR, 74,* 1614–1634. [3] Kahle A. B. et al. (1980) *Appl. Opt., 19,* 2279–2290. [4] Nash D. B. et al. (1993) *JGR, 98,* 22535–23552. [5] Christensen P. R. and Harrison S. T. (1993) *JGR, 98,* 19819–19834. [6] Salisbury J. W. et al. (1994) *JGR, 99,* 11897–11911. [7] Moersch J. E. and Christensen P. R. (1995) *JGR, 100,* 7465–7477. [8] Nicodemus F. E. (1965) *Appl. Opt., 4,* 767–773. [9] Clark R. N. et al. (1993) *Bull. AAS, 25,* 1033. [10] Henderson B. G. and Jakosky B. M. (1997) *JGR, 102,* 6567–6586. [11] Logan L. M. et al. (1973) *JGR, 78,* 4983–5003. [12] Henderson B. G. and Jakosky B. M. (1994) *JGR, 99,* 19063–19073.

SPECTRAL IRRADIANCE STANDARDS FOR OBSERVATIONS FROM 3 TO 30 MICRONS.

F. C. Witteborn[1] and M. Cohen[2], [1]Space Science Division, M/S 245-6, NASA Ames Research Center, Moffett Field CA 94035, USA, [2]Radio Astronomy Laboratory, 601 Campbell Hall, University of California at Berkeley, Berkeley CA 94720, USA.

Spectroscopic observations of astronomical objects aimed at determining compositional information require reference irradiance standards. The judicious use of widely distributed, well-understood celestial objects as standards permits simultaneous correction for optics absorption, diffraction, atmospheric absorption, and effects of foreground emission on detector response. In answer to requests from scientists planning observations from the Infrared Space Observatory (ISO) and the Midcourse Space Experiment (MSX), we have provided celestial spectral irradiance standards throughout the 3–30-µm wavelength range. Three approaches were used to characterize primary standards:

1. Emergent spectral fluxes from stellar models of the hot stars Vega (AOV) and Sirius (AIV) were calculated by Kurucz [1]. His predicted spectra agree very well with absolutely calibrated spectra in the visible and did not need to account for molecular absorptions, which appear only in cooler stars. Airborne and groundbased spectra of a variety of K and early

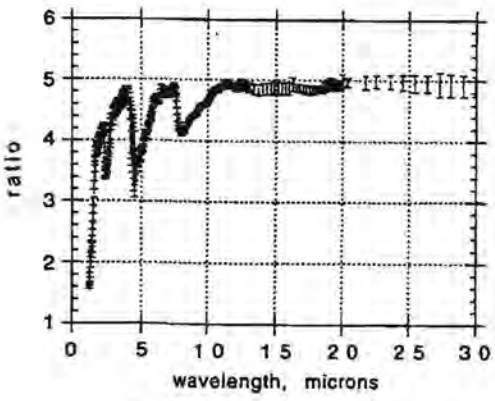

Fig. 1. Ratio of a τ to a CMa.

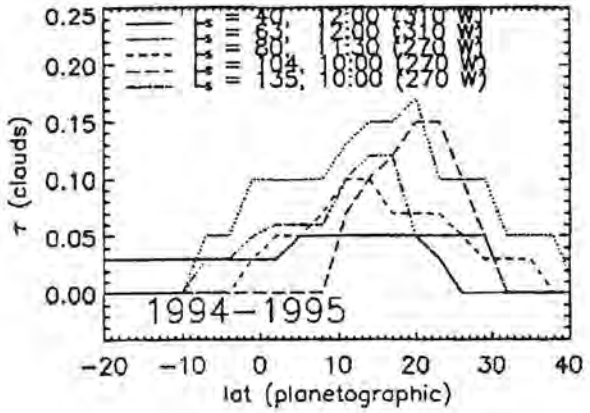

Fig. 1.

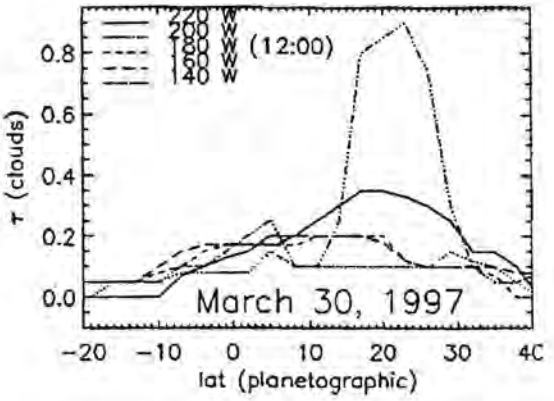

Fig. 3.

M giants, one G dwarf, and a bright asteroid (Ceres) were obtained, each on the same night and with the same instrument as one of the primary standards. The ratios of spectra of secondary standards to primary standard multiplied at each wavelength increment by the calculated primary star's irradiance provide the calibrated spectral irradiance. This method provides high precision and is the basis of our tabulated data that have been presented in a series of papers on irradiance standards [2–5]. A conceivable drawback to this approach is that assumptions used in the stellar models might be incorrect. For example, the presence of dust around Vega [6] limits its usefulness as an easily modeled standard to wavelengths <15 μm. Sirius, on the other hand, shows no evidence of unusual infrared characteristics.

2. Models of asteroid spectra that allow for effects of varying distances from the Earth and Sun, phase angle and effects of surface texture, and temperature distribution have been developed [7,8]. These provide a totally independent set of standards. The extent to which the Ceres spectrum based upon calibration against stellar models agrees with the Ceres spectral models provides confidence in both types of standard. Our recent measurements [9] show that there is rough agreement (10%) with a model in which the beaming factor has been set to unity, but with significant differences, believed to be caused by mineral features that are not incorporated in the models.

3. Direct comparisons of stellar and asteroid spectra to laboratory standards provide calibrations free of any assumptions involved in theoretical models of remote objects. However, difficulties in determining the telescope absorption spectrum, verifying the equivalence of the detector response function in the laboratory and observatory environments, and determining the diffraction effects on the laboratory source combine to make calibration by this method very difficult and ultimately less precise than by using stellar models. Even so, this method has been used to determine the spectra of Ceres and Arcturus (α Boo) from 3 to 30 μm on the basis of airborne spectra and laboratory blackbody spectra. These results (in preparation) give us no reason to doubt the veracity of the standards that we have published using stellar models to characterize our primary standards. The following stars make up the set of celestial standards that is published and available in electronic form: β Peg, β And, β Gem, α Hya [3], α Boo, γ Dra, α Cet, γ Cru, μ UMa [5], α CMa, α Lyr [3,10], α Tau [2], α^1Cen, α TrA, and ε Car [4]. Access to electronic files for the irradiance spectra is indicated after the corresponding reference. Figure 1, the ratio of the spectrum of α Tau to that of a CMa, shows deep absorptions caused by CO and SiO present in the cooler star but not in the primary standard.

The absolute uncertainties in irradiance arise from the uncertainties in absolute photometry used in scaling the calculated spectra of the primary stars (1.45%) convolved with measurement errors in relative fluxes. This yields absolute, 1-sigma errors in secondary standards of typically 3% or better at wavelengths below 25 μm. The set of standards now available provides a useful tool for planetary surface spectroscopy.

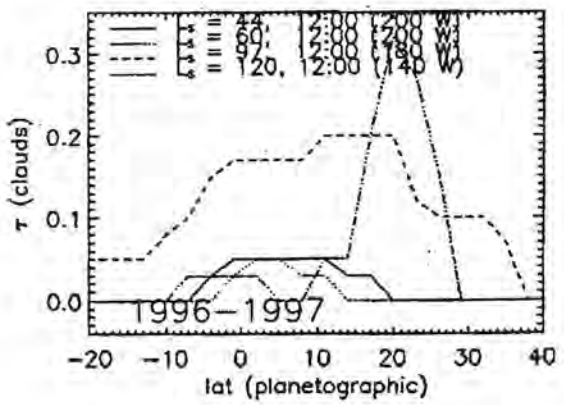

Fig. 2.

References: [1] Kurucz R. L. (1991) in *Precision Photometry: Astrophysics in the Galaxy* (A. G. Davis Philip et al., eds.), p. 27, Davis, Schenectady. [2] Cohen M. et al. (1992) *AJ, 104,* 2030–2044 (ftp://cma.arc.nasa.gov/pub/cohen or ftp://ssa1.arc. nasa.gov/pub/cohen will get all standards men-

tioned in this article). [3] Cohen M. et al. (1995) *AJ, 110,* 275–289 (ftp://adc.gsfc.nasa.gov/pub/adc/archives/journal_tables/AJ/110/275/). [4] Cohen M. et al. (1996) *AJ, 112,* 241–251 (ftp://adc.gsfc.nasa.gov/pub/adc/archives/journal_tables/AJ/112/241/). [5] Cohen M. et al. (1996) *AJ, 112,* 2274-2285 (ftp://adc.gsfc.nasa.gov/pub/adc/archives/journal_tables/AJ/112/2274/). [6] Aumann H. H. et al. (1984) *ApJ, 278,* L23-L27. [7] Morrison D. (1973) *Icarus, 19,* 1–14. [8] Lebofsky L. A. et al. (1986) *Icarus, 68,* 239–251. [9] Cohen M. et al. (1997), in review. [10] Cohen M. et al. (1992) *AJ, 104,* 1650–1657.

OF MARTIAN WATER ICE CLOUDS: NEW INSIGHTS USING THE HUBBLE SPACE TELESCOPE.

M. J. Wolff[1,2], R. T. Clancy[1], P. B. James[2], S. W. Lee[3], and J. F. Bell III[4], [1]Space Science Institute, 1234 Innovation Drive, Suite 294, Boulder CO 80303-7814, USA (wolff@colorado.edu), [2]Department of Physics and Astronomy, University of Toledo, Toledo OH 43606, USA, [3]Laboratory for Atmospheric and Space Physics, University of Colorado, Boulder CO 80309, USA, [4] Center for Radiophysics and Space Research, Cornell University, Ithaca NY 14853, USA.

Introduction: A fundamental problem in the current understanding of the martian atmosphere and climate is the role of water ice clouds. The long absence of spacecraft missions appears to have led some workers to blindly embrace the Viking dataset as indicative of the current state of the martian climate. However, recent microwave temperature and water profiling measurements indicate that the warm, dusty period observed by Viking was atypical. More specifically, Clancy et al. [1] find that the current atmosphere is approximately 15–20 K cooler than the Viking temperature measurements obtained for the same seasons. A natural consequence of a drier, cooler martian climate would be the presence of a global midlatitude cloud belt, which has in fact been observed in the limited analysis of several HST images by Clancy et al. (but not seen in analysis and discussion of the Viking data published to date). The key to enhancing our knowledge is to better characterize the spatial and temporal variability of atmospheric cloud (and dust) processes, including interannual variations, through long-term synoptic monitoring of atmospheric phenomena. The Hubble Space Telescope provides an ideal platform for such an endeavor. This abstract briefly highlights some of the results that will be presented at the workshop.

Observations: The Hubble Space Telescope has observed Mars periodically since the 1990 opposition. These data have been primarily obtained by two instruments: the Wide Field/Planetary Camera (WFPC) and its successor, WFPC2. In addition, the Faint Object Spectrograph (FOS) and Space Telescope Imaging Spectrograph (STIS) have been used to monitor atmospheric activity such as changes in ozone abundance. Our efforts in this presentation will concentrate on the data acquired since the installation of the COSTAR corrective optics (i.e., the 1994–1995 and 1996–1997 observing seasons), particularly those from WFPC2.

The reduction and analysis techniques are described in Wolff et al. [2] and James et al. [3]. Briefly, a multiple-scattering radiative transfer code is used for multiple WFPC2 bandpasses to constrain the optical depth of cloud and dust particles. Primary inputs (and hence, sources of errors) include particle single scattering albedo and surface reflectance. The background aerosol loading in the reference albedo images are estimated using ultraviolet FOS spectra.

Initial Results: Our analysis of the 1994–1995 and 1996–1997 images show that the low-latitude cloud belt develops in early spring and peaks near aphelion, as discussed by Clancy et al. This can be clearly seen in Figs. 1 and 2, which show the cloud optical depth as a function of longitude for several epochs each season. The longitude and local time for each cross section are given in the figure legend. The longitudes displayed represent either the subearth or subsolar points.

As one would expect, the cloud optical depths vary across the disk, due in part to diurnal heating and topography. Such variation can be seen in Fig. 3. Note the cross section for 140°W, which passes through the well-known cloud formation west of Olympus Mons. The subsolar point for the observations in Fig. 3 is 180°W and the areocentric longitude (L_s) is 97°.

The dust loading was handled in a simplistic manner. We assumed a spatially uniform, well-mixed component. Our choice of parameters was guided by the desire to derive *upper limits*. For the 1996–1997 season, analysis of the WFPC2 images indicates an optical depth of 0.1 in October ($L_s = 21°$), increasing to 0.3 by May ($L_s = 120°$). An additional 0.1 of optical depth may be present in reference albedo maps, as measured by UV spectroscopy.

Additional Work To Be Presented: We intend to present additional results, including our analysis of the Pathfinder region (before and after touchdown).

References: [1] Clancy R. T. et al. (1995) *Icarus, 122,* 36. [2] Wolff M. J. et al. (1997) *JGR, 102,* 1679. [3] James P. B. et al. (1997) *Science,* submitted.

List of Workshop Participants

Tokuhide Akabane
Hida Observatory
Kyoto University
Kamitakara
Gifu 506-13
Japan
Phone: 81-578-6-2311
Fax: 81-578-6-2118
E-mail: akabane@kusastro.kyoto-u.ac.jp

Edwin S. Barker
RLM 15.308
McDonald Observatory
University of Texas
Austin TX 78712-1083
Phone: 512-471-3432
Fax: 512-471-6016
E-mail: esb@pecos.as.utexas.edu

James Bell
Center for Radiophysics and Space Research
Cornell University
424 Space Sciences Building
Ithaca NY 14853-6801
Phone: 607-255-5911
Fax: 607-255-9002
E-mail: jimbo@cuspif.tn.cornell.edu

Diana L. Blaney
Mail Stop 183-501
Jet Propulsion Laboratory
4800 Oak Grove Drive
Pasadena CA 91109
Phone: 818-354-5419
Fax: 818-354-0966
E-mail: blaney@scn1.jpl.nasa.gov

Stephen Bougher
Space Science Building
Lunar and Planetary Laboratory
University of Arizona
P.O. Box 210092
Tucson AZ 85721-0092
Phone: 520-621-4900
Fax: 520-621-4933
E-mail: sbougher@lpl.arizona.edu

R. T. Clancy
Space Science Institute
1234 Innovation Drive
Boulder CO 80303
Phone: 303-492-6998
Fax: 303-492-3789
E-mail: clancy@isidis.colorado.edu

Joshua P. Emery
Lunar and Planetary Laboratory
University of Arizona
1629 E. University Boulevard
Tucson AZ 85721-0092
Phone: 520-621-1594
Fax: 520-621-4933
E-mail: josh@lpl.arizona.edu

Mark Gurwell
Mail Stop 42
Harvard-Smithsonian Astrophysics
60 Garden Street
Cambridge MA 02138
Phone: 617-495-7292
Fax: 617-495-7345
E-mail: mgurwell@cfa.harvard.edu

Robert M. Haberle
Space Science Division
Mail Stop 245-3
NASA Ames Research Center
Moffett Field CA 94035
Phone: 650-604-5491
Fax: 650-604-6779
E-mail: bhaberle@mail.arc.nasa.gov

Richard Hill
Lunar and Planetary Laboratory
University of Arizona
P.O. Box 910092
Tucson AZ 85721-0092
Phone: 520-621-4077
Fax: 520-621-4933
E-mail: rhill@lpl.arizona.edu

Don Hunten
Lunar and Planetary Laboratory
University of Arizona
P.O. Box 210092
Tucson AZ 85721-0092
Phone: 520-621-4002
Fax: 520-621-4933
E-mail: dhunten@lpl.arizona.edu

List of Workshop Participants

Tokuhide Akabane
Hida Observatory
Kyoto University
Kamitakara
Gifu 506-13
Japan
Phone: 81-578-6-2311
Fax: 81-578-6-2118
E-mail: akabane@kusastro.kyoto-u.ac.jp

Edwin S. Barker
RLM 15.308
McDonald Observatory
University of Texas
Austin TX 78712-1083
Phone: 512-471-3432
Fax: 512-471-6016
E-mail: esb@pecos.as.utexas.edu

James Bell
Center for Radiophysics and Space Research
Cornell University
424 Space Sciences Building
Ithaca NY 14853-6801
Phone: 607-255-5911
Fax: 607-255-9002
E-mail: jimbo@cuspif.tn.cornell.edu

Diana L. Blaney
Mail Stop 183-501
Jet Propulsion Laboratory
4800 Oak Grove Drive
Pasadena CA 91109
Phone: 818-354-5419
Fax: 818-354-0966
E-mail: blaney@scn1.jpl.nasa.gov

Stephen Bougher
Space Science Building
Lunar and Planetary Laboratory
University of Arizona
P.O. Box 210092
Tucson AZ 85721-0092
Phone: 520-621-4900
Fax: 520-621-4933
E-mail: sbougher@lpl.arizona.edu

R. T. Clancy
Space Science Institute
1234 Innovation Drive
Boulder CO 80303
Phone: 303-492-6998
Fax: 303-492-3789
E-mail: clancy@isidis.colorado.edu

Joshua P. Emery
Lunar and Planetary Laboratory
University of Arizona
1629 E. University Boulevard
Tucson AZ 85721-0092
Phone: 520-621-1594
Fax: 520-621-4933
E-mail: josh@lpl.arizona.edu

Mark Gurwell
Mail Stop 42
Harvard-Smithsonian Astrophysics
60 Garden Street
Cambridge MA 02138
Phone: 617-495-7292
Fax: 617-495-7345
E-mail: mgurwell@cfa.harvard.edu

Robert M. Haberle
Space Science Division
Mail Stop 245-3
NASA Ames Research Center
Moffett Field CA 94035
Phone: 650-604-5491
Fax: 650-604-6779
E-mail: bhaberle@mail.arc.nasa.gov

Richard Hill
Lunar and Planetary Laboratory
University of Arizona
P.O. Box 910092
Tucson AZ 85721-0092
Phone: 520-621-4077
Fax: 520-621-4933
E-mail: rhill@lpl.arizona.edu

Don Hunten
Lunar and Planetary Laboratory
University of Arizona
P.O. Box 210092
Tucson AZ 85721-0092
Phone: 520-621-4002
Fax: 520-621-4933
E-mail: dhunten@lpl.arizona.edu

Kyosuke Iwasaki
Lunar and Planetary Laboratory
University of Arizona
P.O. Box 210092
Tucson AZ 85721-0092
Phone: 602-621-4861
Fax: 602-621-4933
E-mail: kiwasaki@pirl.lpl.arizona.edu

Bruce Jakosky
Laboratory for Atmospheric and
Space Physics
Campus Box 392
University of Colorado
Boulder CO 80309-0392
Phone: 303-492-8004
Fax: 303-492-6946
E-mail: jakosky@argyre.colorado.edu

Philip James
Department of Physics and Astronomy
University of Toledo
Toledo OH 43606
Phone: 419-530-4906
Fax: 419-530-2723
E-mail: pbj@physics.utoledo.edu

Daniel P. Joyce
Cernan Space Center
Triton College
2000 N. 5th Avenuenue
River Grove IL 60171
Phone: 708-456-0300 x3372
Fax: 708-583-3121
E-mail: djoyce@triton.cc.il.us

David R. Klassen
Department of Astronomy
Space Sciences Building
Cornell University
Ithaca NY 14853-6801
Phone: 607-255-6910
E-mail: drk14@cornell.edu

Steve W. Lee
Laboratory for Atmospheric and
Space Physics
Campus Box 392
University of Colorado
Boulder CO 80309
Phone: 303-492-5348
Fax: 303-492-6946
E-mail: lee@syrtis.colorado.edu

Mark T. Lemmon
University of Arizona
Lunar and Planetery Laboratory
1629 E University Boulevard
Tucson AZ 85721-0092
Phone: 520-621-3994
Fax: 520-621-2994
E-mail: lemmon@lpl.arizona.edu

Terry Z. Martin
Mail Stop 169-237
Jet Propulsion Laboratory
4800 Oak Grove Drive
Pasadena CA 91109
Phone: 818-354-2178
Fax: 818-393-4619
E-mail: tzmartin@pop.jpl.nasa.gov

Richard McKim
British Astronomical Association
9 Monson Way
Oundle
Peterborough PE8 4QG
United Kingdom
Phone: 44-1832-274553
Fax: 44-1832-284-052
E-mail: mckim@oundle.northants.sch.uk

Mike Mellon
Laboratory for Atmospheric and Space Physics
Campus Box 392
University of Colorado
Boulder CO 80309-0392
Phone: 303-492-1711
Fax: 303-492-6946
E-mail: mellon@argyre.colorado.edu

Jeffrey E. Moersch
427 Space Sciences Building
Cornell University
Ithaca NY 14853
Phone: 607-255-4709
Fax: 607-255-5907
E-mail: moersch@astrosun.tn.cornell.edu

Yasunori Narumi
Kyushu-Takai University
9-1-1, Toroku
Kumamoto 862
Japan
Phone: 81-96-382-1141
Fax: 81-96-381-7956
E-mail: narumi@skk-1.ktokai-u.ac.jp

Donald Parker
ALPO Mars Section
12911 Lerida Street
Coral Gables FL 33156
Phone: 305-665-1438
E-mail: dparker@gil.net

Gary Rosenbaum
Steward Observatory
University of Arizona
933 N Cherry Avenue 350C
Tucson AZ 85721
Phone: 520-621-5136
E-mail: garyr@as.arizona.edu

Ted L. Roush
Space Sciences Division
Mail Stop 245-3
NASA Ames Research Center
Moffett Field CA 94035-1000
Phone: 650-604-3526
Fax: 650-604-6779
E-mail: roush@barsoom.arc.nasa.gov

Sumisaburo Saito
Noda 3-9-14
Takatsuki
Osaka 569
Japan
Phone: 81-726-74-0169
Fax: 81-726-74-0169
E-mail: saitocmb@qa2.so-net.or.jp

William Schmitt
Lunar and Planetary Laboratory
University of Arizona
P.O. Box 210092
Tucson AZ 85721-0092
Phone: 520-621-4077
Fax: 520-621-4933
E-mail: schmitt@lpl.arizona.edu

Peter Smith
Lunar and Planetary Laboratory
University of Arizona
P.O. Box 210092
Tucson AZ 85721-0092
Phone: 520-621-2725
Fax: 520-621-2994
E-mail: psmith@lpl.arizona.edu

Ann L. Sprague
Lunar and Planetary Laboratory
University of Arizona
P.O. Box 210092
Tucson AZ 85721-0092
Phone: 520-621-2282
Fax: 520-621-4933
E-mail: sprague@lpl.arizona.edu

Daniel M. Troiani
Association of Lunar and Planetary Observers
629 Verona Court
Schaumburg IL 60193
Phone: 847-524-1716
E-mail: dtroiani@triton.cc.il.us

Christoph Wagner
Institute for Planetary Exploration
DLR
Rudower Chaussee 5
D-12484 Berlin
Germany
Phone: 49-30-67055-413
Fax: 49-30-67055-385
E-mail: christoph.wagner@dlr.de

Fred C. Witteborn
2071 Madelaine Court
Los Altos CA 94024
Phone: 415-968-5442
Fax: 415-604-6779
E-mail: witteborn@aol.com

Michael J. Wolff
Space Science Institute
2039 Pheasant Creek Drive
Martinez GA 30907
Phone: 706-651-1356
Fax: 706-651-8052
E-mail: wolff@colorado.edu

Aaron Zent
Mail Stop 245-3
NASA Ames Research Center
Moffett Field CA 94035
Phone: 415-604-5517
Fax: 415-604-6779
E-mail: zent@barsoom.arc.nasa.gov